UNCLASSIFIED

SECURITY CLASSIFICATION OF THIS PAGE

REPORT DOCUMENTATION PAGE

Form Approved OMB No. 0704-0188

1a. REPORT SECURITY CLASSIFICATION: UNCLASSIFIED	1b. RESTRICTIVE MARKINGS
2a. SECURITY CLASSIFICATION AUTHORITY	3. DISTRIBUTION/AVAILABILITY OF REPORT: Approved for public release; distribution unlimited.
2b. DECLASSIFICATION/DOWNGRADING SCHEDULE	
4. PERFORMING ORGANIZATION REPORT NUMBER(S): N00014-85-C-0141-TR10	5. MONITORING ORGANIZATION REPORT NUMBER(S)
6a. NAME OF PERFORMING ORGANIZATION: Washington State University; 6b. OFFICE SYMBOL (If applicable)	7a. NAME OF MONITORING ORGANIZATION: Office of Naval Research
6c. ADDRESS (City, State, and ZIP Code): Department of Physics, Washington State University, Pullman, WA 99164-2814	7b. ADDRESS (City, State, and ZIP Code): Physics Division Code 1112, Arlington, VA 22217-5000
8a. NAME OF FUNDING/SPONSORING ORGANIZATION; 8b. OFFICE SYMBOL (If applicable)	9. PROCUREMENT INSTRUMENT IDENTIFICATION NUMBER: N00014-85-C-0141
8c. ADDRESS (City, State, and ZIP Code)	10. SOURCE OF FUNDING NUMBERS: PROGRAM ELEMENT NO. 61153N; PROJECT NO. 4126934; TASK NO; WORK UNIT ACCESSION NO.

11. TITLE (Include Security Classification)
Quantitative Ray Methods for Scattering of Sound by Spherical Shells.

12. PERSONAL AUTHOR(S)
Kargl, S. G.

13a. TYPE OF REPORT	13b. TIME COVERED	14. DATE OF REPORT (Year, Month, Day)	15. PAGE COUNT
Technical	FROM 870516 TO 900731	910801	xiii + 174 = 187

16. SUPPLEMENTARY NOTATION
This is the Ph.D. dissertation of Steven Gregory Kargl. The contract P. I. was P. L. Marston, Telephone (509) 335-5343 or 335-9531.

17 COSATI CODES		
FIELD	GROUP	SUB-GROUP
20	01	

18. SUBJECT TERMS (Continue on reverse if necessary and identify by block number)
Acoustical Scattering, Lamb Waves, Resonances

19. ABSTRACT (Continue on reverse if necessary and identify by block number)

The application of ray methods to the scattering of high-frequency plane waves from evacuated elastic spherical shells is investigated. The investigation of ray methods for spherical shells is a precursor to the application of such methods to shells having more complicated shapes. The scattered pressure in the farfield of the shell is $p_{sc} = p_i(a/2r)f(\theta)\exp(ikr)$ where p_i is the plane wave amplitude. The outer radius of the shell is a, $h = a - b$ is the shell's thickness, and r is the distance to an observation

20. DISTRIBUTION/AVAILABILITY OF ABSTRACT	21. ABSTRACT SECURITY CLASSIFICATION
☒ UNCLASSIFIED/UNLIMITED ☐ SAME AS RPT ☐ DTIC USERS	UNCLASSIFIED

22a. NAME OF RESPONSIBLE INDIVIDUAL	22b. TELEPHONE (Include Area Code)	22c. OFFICE SYMBOL
L. E. Hargrove	(703) 696-4221	ONR Code 1112

DD Form 1473, JUN 86 — Previous editions are obsolete. — SECURITY CLASSIFICATION OF THIS PAGE

UNCLASSIFIED

19. ABSTRACT (continued)

point. Ray models are developed to synthesize the form function $f(\theta, ka)$ where k is the wavenumber of the incident wave and θ is the scattering angle. The forward scattering amplitude, $f(\theta = 0)$, is related to the extinction cross section, σ_e by the optical theorem. If the absorption by the scatterer is negligible, the σ_e is equal to the total scattering cross section σ_t. A ray synthesis partitions $f(\theta = 0)$ into a component for ordinary forward diffraction about the shell, f_{FD}, and contributions from surface guided elastic waves. For high-frequency scattering, the relevant surface guided elastic waves are leaky Lamb waves. A similar ray synthesis of the backscattering amplitude $f(\theta = \pi)$ contains a specular reflection component, $f_{sp}(\theta = \pi)$, and leaky Lamb wave contributions. A generalization of the geometrical theory of diffraction is employed to synthesize $f_l(\theta = 0, ka)$ and $f_l(\theta = \pi, ka)$ for the *lth* leaky Lamb wave contribution. The syntheses for forward and backwards scattering correctly describe the leaky Lamb wave contributions and are expressible in a Fabry-Perot resonator form. While the ray description of backscattering ordinarily accurately reproduces exact computations and experiments with tone burst, certain anomalies are discussed. A ray synthesis of f_{sp} demonstrates a significant longitudinal resonance effect when $k_L h = n\pi$, $n = 1, 2, ...$, where $k_L = \omega/c_L$ is the longitudinal wavenumber within the shell. The analysis of f_{sp} is for an elastic material with vanishing shear velocity. The relevant range of ka is $7 \leq ka \leq 100$. The shell is surrounded by water and is composed of 440c stainless steel with inner-to-outer radii ratio $b/a = 0.838$. While portions of this report have been published in the Journal of the Acoustical Society of America [**85**, 1014-1029 (1989); **88**, 1103-1113 (1990); **88**, 1114-1122 (1990); **89**, 2462 (1991); **89**, 2545-2558 (1991)], appendices give unpublished analytical and computational results.

QUANTITATIVE RAY METHODS FOR SCATTERING OF SOUND BY SPHERICAL SHELLS

By

STEVEN GREGORY KARGL

A dissertation submitted in partial fulfillment of

the requirements for the degree of

DOCTOR OF PHILOSOPHY

WASHINGTON STATE UNIVERSITY

Department of Physics

AUGUST 1990

Technical Report, Contract N00014-85-C-0141

To the Faculty of Washington State University:

The members of the Committee appointed to examine the dissertation of STEVEN GREGORY KARGL find it satisfactory and recommend that it be accepted.

_____
Chair

_____

_____

_____

ACKNOWLEDGMENTS

First, I am sincerely thankful for the opportunity to study physics under the guidance of the faculty of Washington State University. From their insight and knowledge of nature, the faculty enriched my graduate studies and stimulated my own curiosity about physical phenomena. I am particularly indebted to my Advisor, Professor Philip L. Marston, who developed and instilled in me a deep appreciation for experimental physics. The work in this dissertation would not have been possible without his encouragement and encyclopedic knowledge of acoustics and optics.

For the past five years, I have had the pleasure of interacting both academically and socially with past and present graduate students. I thank those individuals who have had some influence on my life. In particular, I am grateful to W. Patrick Arnott and Carl K. Frederickson with whom I shared an office.

Finally, I am grateful for the financial support from the Office of Naval Research which provided the funding throughout my graduate studies.

QUANTITATIVE RAY METHODS FOR SCATTERING OF SOUND BY SPHERICAL SHELLS

Abstract

by Steven Gregory Kargl, Ph. D.
Washington State University
August 1990

Chair: Philip L. Marston

The application of ray methods to the scattering of high-frequency plane waves from evacuated elastic spherical shells is investigated. The investigation of ray methods for spherical shells is a precursor to the application of such methods to shells having more complicated shapes. The scattered pressure in the farfield of the shell is $p_{sc} = p_i(a/2r)f(\theta)exp(ikr)$ where p_i is the plane wave amplitude. The outer radius of the shell is a, $h = a - b$ is the shell's thickness, and r is the distance to an observation point. Ray models are developed to synthesize the form function $f(\theta, ka)$ where k is the wavenumber of the incident wave and θ is the scattering angle. The forward scattering amplitude, $f(\theta = 0)$, is related to the extinction cross section, σ_e, by the optical theorem. If the absorption by the scatterer is negligible, then σ_e is equal to the total scattering cross section σ_t. A ray synthesis partitions $f(\theta = 0)$ into a component for ordinary forward diffraction about the shell, f_{FD}, and contributions from surface guided elastic waves. For high-frequency scattering, the relevant surface guided elastic waves are leaky Lamb waves. A similar ray synthesis of the backscattering amplitude $f(\theta = \pi)$ contains a specular reflection component, $f_{sp}(\theta = \pi)$, and leaky Lamb wave contributions. A generalization of the geometrical theory of diffraction is employed to synthesize $f_l(\theta = 0, ka)$ and $f_l(\theta = \pi, ka)$ for the *lth* leaky Lamb wave contribution. The syntheses for forward and backwards scattering correctly describe the leaky Lamb wave contributions and are

expressible in a Fabry-Perot resonator form. While the ray description of backscattering ordinarily accurately reproduces exact computations and experiments with tone burst, certain anomalies are discussed. A ray synthesis of f_{sp} demonstrates a significant longitudinal resonance effect when $k_L h = n\pi$, $n = 1, 2, ...$, where $k_L = \omega/c_L$ is the longitudinal wavenumber within the shell. The analysis of f_{sp} is for an elastic material with vanishing shear velocity. The relevant range of ka is $7 \leq ka \leq 100$. The shell is surrounded by water and is composed of 440c stainless steel with inner-to-outer radii ratio $b/a = 0.838$.

TABLE OF CONTENTS

LIST OF TABLES

LIST OF ILLUSTRATIONS

Chapter 1

Chapter 2

Chapter 3

Chapter 4

Dedication

This work is dedicated to my parents and family whose spiritual support provided me with the inspiration to continue my education.

Chapter 1

Introduction

1.1 Review of the exact partial wave series for the form function

The application of acoustic ray methods to scattering problems can provide a simple understanding of the physical interaction of an incident pressure wave and a scatterer. When a scatterer has an arbitrary shape, direct solution of the appropriate boundary value problem is not usually possible. While numerical solutions can be performed for a scatterer of known composition and shape, physical insight into the underlying interaction between an incident wave and a scatterer is often obfuscated. Ray methods may be directly applied to describe the scattering from an object of arbitrary shape and the physical mechanisms involved in the scattering process may easily be identified and understood. When developing new ray techniques, it is advantageous to test these techniques by comparison to a canonical problem where an exact solution is known. The comparison of a ray model with an exact solution should allow one to identify regions where the simple ray model is useful. This dissertation investigates novel ray techniques, based on an elastic generalization of the geometrical theory of diffraction,[1,2] which describe the forward and backwards scattering from evacuated elastic spherical shells. It is anticipated that these new ray techniques may be easily generalized to elastic objects with smooth convex shapes.

Before developing quantitative ray techniques for the scattering of a plane wave from a submerged evacuated elastic spherical shell, it is appropriate to review the exact solution to this canonical problem. A plane wave in the surrounding water propagates in the positive z-direction and is incident on an elastic spherical shell situated at the origin of a coordinate system. The physical parameters that describe the shell are the inner-to-outer radii ratio b/a, the longitudinal sound speed c_L, the shear sound speed c_t, and the density

ρ_e. The parameters for water are the speed of sound c and density ρ. After scattering, the total pressure in the water is $p = p_{inc} + p_{sc}$ where $p_{inc} = p_i exp(ikz)$ is the incident plane wave and p_{sc} is the scattered pressured. The pressure amplitude of p_{inc} is p_i and $k = 2\pi/\lambda$ is the wavenumber of p_{inc} in water where λ is the wavelength. The harmonic time dependence, $exp(-i\omega t)$, has been suppressed and ω is the angular frequency. Using elasticity theory, Goodman and Stern derived an exact expression for the steady-state pressure as a partial wave series.[3,4] Their analysis considered an elastic spherical shell with a fluid interior which gave an expression similar to (see Eqs. (4a) and (6) of Ref. 3)

$$p = p_i \sum_{n=0}^{\infty} i^n (2n+1)\left[j_n(kr) + \frac{B_n(ka)}{D_n(ka)} h_n^{(1)}(kr)\right] P_n(\cos(\theta)) , \qquad (1)$$

where j_n and h_n are spherical Bessel and Hankel functions of the first kind and P_n is a Legendre polynomial. The functions B_n and D_n of the dimensionless size parameter ka are 6×6 determinants for a shell with a fluid interior and 5×5 determinants for an evacuated shell. The elements of these determinants are contained in Refs. 3 and 5. The first term in the square brackets of Eq. (1) is the partial wave expansion of p_{inc} while the second term is p_{sc}. In the farfield of the elastic shell, p_{sc} has the spherically diverging form[1,5]

$$p_{sc} = p_i (a/2r) f(\theta) e^{ikr} , \qquad (2)$$

where the distance from the center of the shell to a distant observation point is r and $f(\theta)$ is the scattering form function or scattering amplitude. [In general, f is a function of the spherical coordinates θ and ϕ, but the azimuthal symmetry of the spherical shell implies that f is independent of ϕ.] Inspection of Eq. (2) reveals that any structure evident in $|p_{sc}|$ must be a result of structure in $|f(\theta)|$. An *exact* partial wave series representation of $f(\theta)$ in the farfield can be obtained from Eq. (1) by introducing the asymptotic form

$h_n \rightarrow i^{-(n+1)}exp(ikr)/kr$, $kr >> 1$. Comparing the asymptotic form of the second term in Eq. (1) with Eq. (2) gives

$$f(\theta) = \frac{2}{ika}\sum_{n=0}^{\infty}(2n+1)\frac{B_n(ka)}{D_n(ka)}P_n(\cos(\theta)) \; . \qquad (3)$$

It is well known that a partial wave series tends to be slowly converging for large *ka* (see Secs. 2.5 and 4.3 and Appendix B of Chapter 3). Also, from inspection of Eq. (3), it is evident that the underlying physical interaction of p_{inc} with the scatterer is obfuscated. That is, the complicated partial wave series representation of f is not amenable to a simple physical interpretation of the scattering process.

In 1964, Hickling calculated the form function for backscattering, $f(\theta = \pi)$, from iron and aluminum shells.[6] The range of frequencies investigated corresponds to $0 < ka < 30$ and the thickness of these shells varied from $0.05 \leq h/a \leq 0.8$. These form function calculations contain complicated structure that was attributed to the elastic response of the shell. Using Fourier transform techniques, Hickling then constructed the backscattered pressure for short sine-wave tone bursts incident on the shells. [Equations (1) and (3) describe the steady-state pressure. As discussed by Hickling, these equations may be used to give a Fourier synthesis of the scattering of tone bursts.[6]] The computed backscattered echoes contained a contribution due to a specular reflection. The specular reflection is essentially the reflection of the incident burst from the outer surface of the shell. Also, evident in the computed backscattered pressures are echoes that are delayed in time with respect to the specular reflection. Hickling concluded that these observed echoes were due to a flexural type wave within the shell that propagated around the shell re-radiating energy into the water. Later, Diercks and Hickling gave experimental confirmation of the computed echoes for backscattering from air- or water-filled aluminum shells.[7] Their

experiments involved several shells of various thicknesses and tone bursts of varying duration with a frequency corresponding to $ka = 20$.

Subsequently, for high-frequency scattering the waves that circumnavigate within an elastic shell have been classified as leaky Lamb waves.[5,8,9] [Franz waves (creeping waves) may be guided by the shell's surface. Franz waves circumnavigate the shell, but for these types of waves the strain is primarily in the surrounding water and the waves are usually heavily radiation damped.] Leaky Lamb waves may be thought of as a generalization of Lamb waves in a flat elastic plate in vacuum[10,11] to the case of a fluid-loaded curved plate. That is, the particle displacements for leaky Lamb waves in a fluid-loaded shell of thickness $h = a - b$ are analogous to the displacements associated with the equivalent Lamb waves in a flat plate of the same thickness. Figure 1 illustrates the surface displacements of the lowest antisymmetric and symmetric Lamb waves in a plate in vacuum. While the amplitudes have been exaggerated, the values of $k_l h = ka(c/c_l)(1 - b/a)$ used for Fig. 1 are indicative of those encountered in the experiments of Ref. 5 and those reviewed below.

1.2 Backscattering of short tone bursts from a shell

This section briefly reviews a ray model for backscattering from an elastic sphere or shell and supporting experiments from Ref. 5. The scattering process is illustrated in Fig. 2. Ray diagrams similar to Fig. 2 are described in detail in Refs. 1, 2, and 5. The center of a sphere or shell of outer radius a is located at the origin of a coordinate system. [The inner radius of the shell is b and for the solid sphere $b = 0$.] The total scattered pressure is a superposition of a specular reflection from the region near point C' and contributions due to the circumnavigation of the l*th* class of surface guided elastic waves around the shell. For high-frequency scattering from elastic spheres, Rayleigh and Whispering Gallery

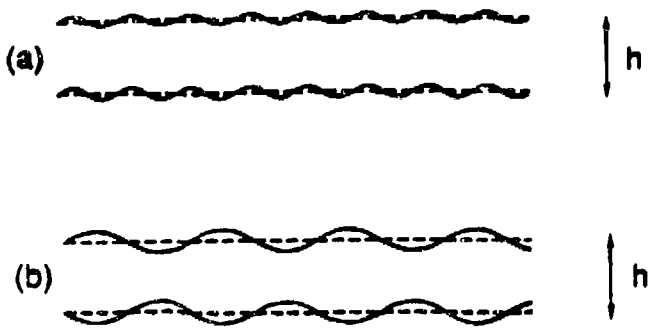

Fig.1 Surface displacements of the a_0 antisymmetric (a) and s_0 symmetric (b) Lamb wave on a flat elastic plate of thickness h in vacuum. The dashed lines indicate the equilibrium position for the surfaces of the flat plate.

waves[1,2] are the relevant surface guided elastic waves while leaky Lamb waves[5,8,9] are the appropriate elastic waves for a shell. The incident plane wave excites a surface guided elastic wave near point B in Fig. 2 that propagates about the shell radiating energy back into the water. In the vicinity of point B', the radiation is directed in the backscattered direction. The points B and B' are determined from the phase velocity trace matching condition $sin(\theta_l) = c/c_l$ where θ_l is the local angle of incidence and c_l is the surface guided elastic wave phase velocity.[1,2,5] The contribution to the form function due to the backscattering of a surface guided elastic wave can be synthesized by considering the propagation path length relative to an exit plane perpendicular to the z-axis through C' in Fig. 2 and it can be expressed in a Fabry-Perot resonator form[1,2,12]

$$f_l = [-G_l e^{-2(\pi - \theta_l)\beta_l} e^{i\eta_l}]/[1 + e^{-2\pi\beta_l} e^{i2\pi kac/c_l}], \qquad (4)$$

where η_l is a propagation phase delay. A complex coupling coefficient G_l describes the efficiency of the coupling between the acoustic wavefield in water and the surface guided elastic wave and β_l is the radiation damping parameter (in *Np/rad*) for the surface guided elastic wave. A virtually *exact* expression for G_l is available for elastic spheres, but its dependence on the physically relevant parameters c_l/c and β_l is non-trivial.[2] Marston has developed an approximation for G_l that appears to give excellent results for elastic spheres as well as shells (see Appendix I).[1,13]

In backscattering and near backscattering experiments described in Ref. 5, a 3 or 4 cycle sine-wave tone burst was incident on a sphere or shell with frequency $\omega/2\pi$. Figure 3a contains hydrophone output voltage versus time records for the backscattering of a burst from a solid tungsten carbide sphere; while Figs. 3b - d are for the backscattering from a hollow 440c stainless steel shell. The radius of the tungsten carbide sphere is $a_{WC} = 12.7$ *mm* and the outer radius of the 440c stainless steel shell is $a_{SS} = 19.05$ *mm* while the shell's

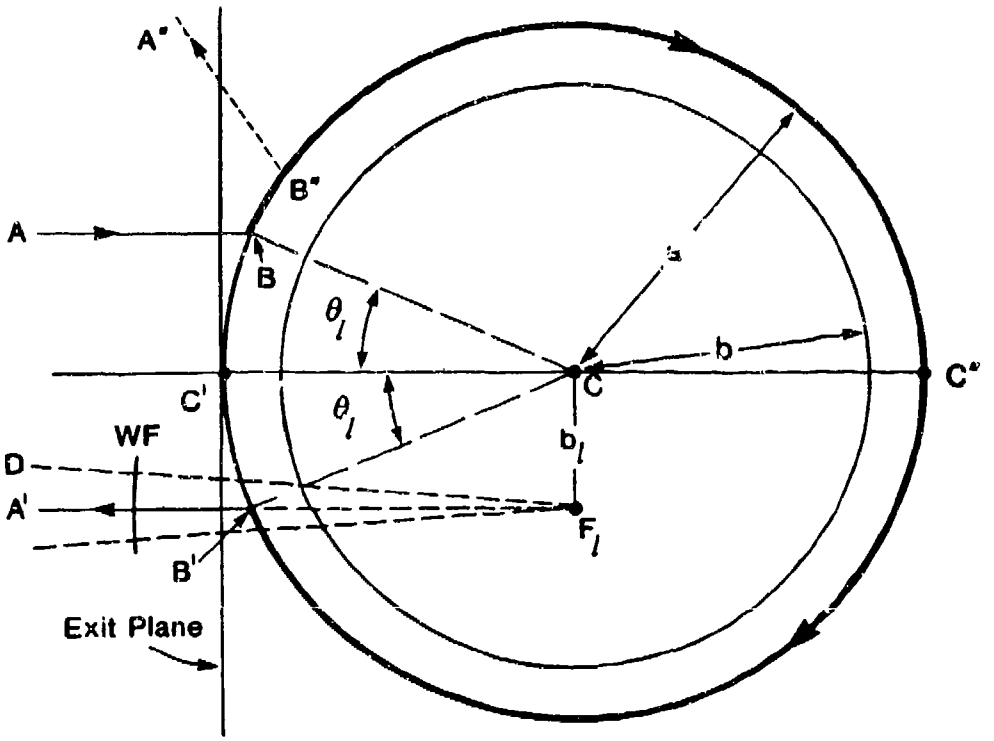

Fig. 2 Ray diagram of a surface guided elastic wave contribution to backscattering from a sphere ($b = 0$) or shell of inner-to-outer radii ratio b/a. The incident plane wave launches a surface guided elastic wave on shell at B. The surface wave repeatedly circumnavigates the sphere or shell continually shedding energy back into the water. At B', the radiated energy is directed in the backscattered direction and appears to originate from a virtual ring-like source generated by rotating the point F_l about the CC' axis. The ring-like source describes a toroidal wave front associated with the axial focusing or glory scattering of the surface wave. There are also contributions to backscattering associated with the specular reflection and repeated internal reflections in the vicinity of C'.

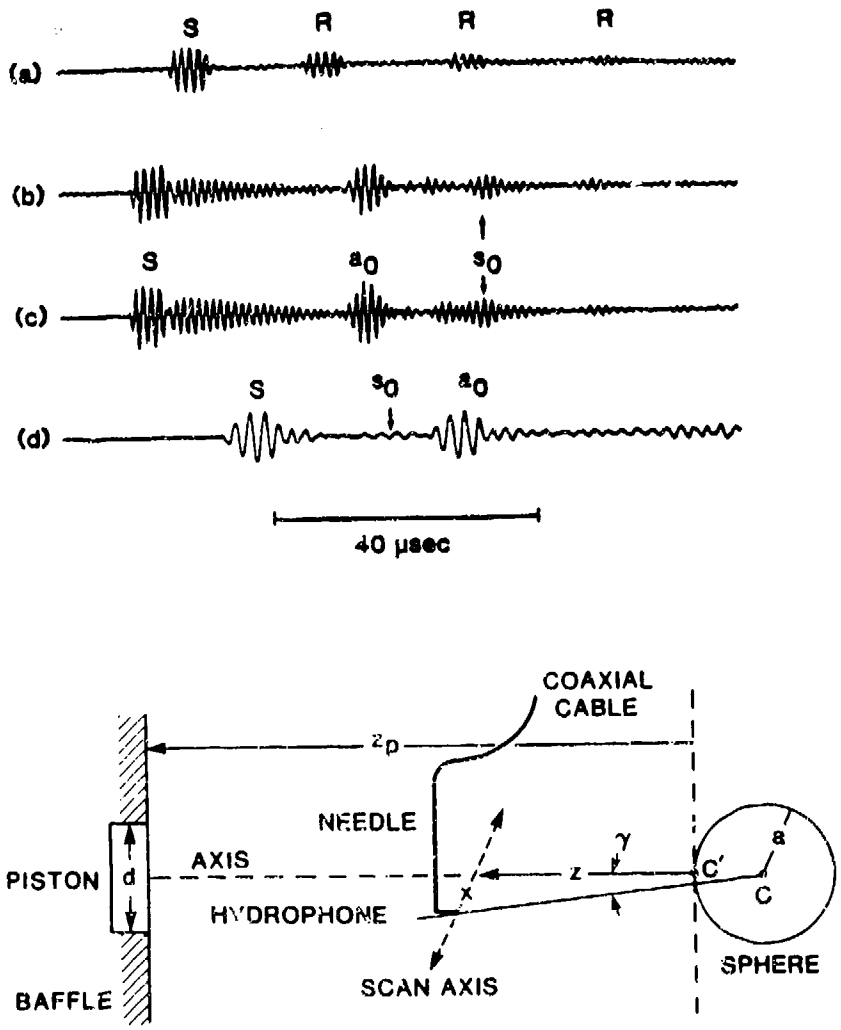

Fig. 3 (Upper) Measured echoes for backscattering a 3 or 4-cyle sine-wave tone burst from a solid tungsten carbide sphere (a) and an evacuated spherical shell composed of 440c stainless steel (b - d). The specular reflection is labeled *S*. Rayleigh wave and lowest antisymmetric and symmetric leaky Lamb waves echoes are denoted by *R*, a_0, and s_0, respectively. The tail immediately following the specular reflection in (b) and (c) is partially due to a longitudinal resonance. (Lower) Schematic of the experimental apparatus employed for backscattering and near backscattering experiments.

thickness is $h = a_{ss} - b = 3.09$ *mm*. The size parameter, $ka = \omega a/c$, for each trace is as follows: (a) 43.2, (b) 64.7, (c) 68.8, and (d) 36.4. In Fig. 3, the specular reflection from the sphere or shell is labeled S. The Rayleigh wave contributions radiated from the tungsten carbide sphere are labeled by $l = R$ while the lowest antisymmetric and symmetric leaky Lamb wave contributions radiated from the shell are designated $l = a_0$ and s_0, respectively. The identification of a specific surface guided elastic wave with an echo in Fig. 3 is in accordance with their arrival time relative to the specular reflection. Detailed analyses of backscattering records from a tungsten carbide sphere similar to Fig. 3a are given in Refs. 12 and 14. Although, Figs. 3a and 3d are similar to the scattered pressure computed by Hickling for an incident tone burst,[6,15] the records in Figs. 3b and 3c contain a feature not evident in Hickling's computations for shells. Inspection of Figs. 3b and 3c shows a long decaying pulse train immediately following the specular reflection. This decaying echo appears to be partially associated with the "ringing down" of a bulk, longitudinal resonance that is investigated in detail in Chapter 4.

Distinct echo contributions are enumerated $m = 0, 1, \ldots$, by considering the number of complete circumnavigations associated with each echo. The backscattered pressure amplitude for the *mth* distinct contribution from the *lth* class of surface guided elastic wave has the predicted form

$$|p_{ml}| = |p_i| A_{ml}\, a/2r, \qquad A_{ml} = |G_l|\, e^{-2(\pi - \theta_l)\beta_l - 2\pi m\beta_l}\, |J_0(u) - i\beta_l\gamma J_1(u)|, \qquad (5a,b)$$

where the functions $J_0(u)$ and $J_1(u)$, $u = ka\gamma c_l/c_l$, are cylindrical Bessel functions and γ is the local backscattering angle, $\gamma = \pi - \theta$. The normalization in Eq. (5a) is such that the specular reflection from a large immovable rigid sphere is a wave whose amplitude is $|p_i|(a/2r)$. For exact backscattering $\gamma = 0$ and $|J_0(u) - i\beta\gamma J_1(u)| = 1$. Figure 4 contains the normalized on-axis amplitudes of the $m = 0$ echo for the $l = a_0$ (solid line) and s_0

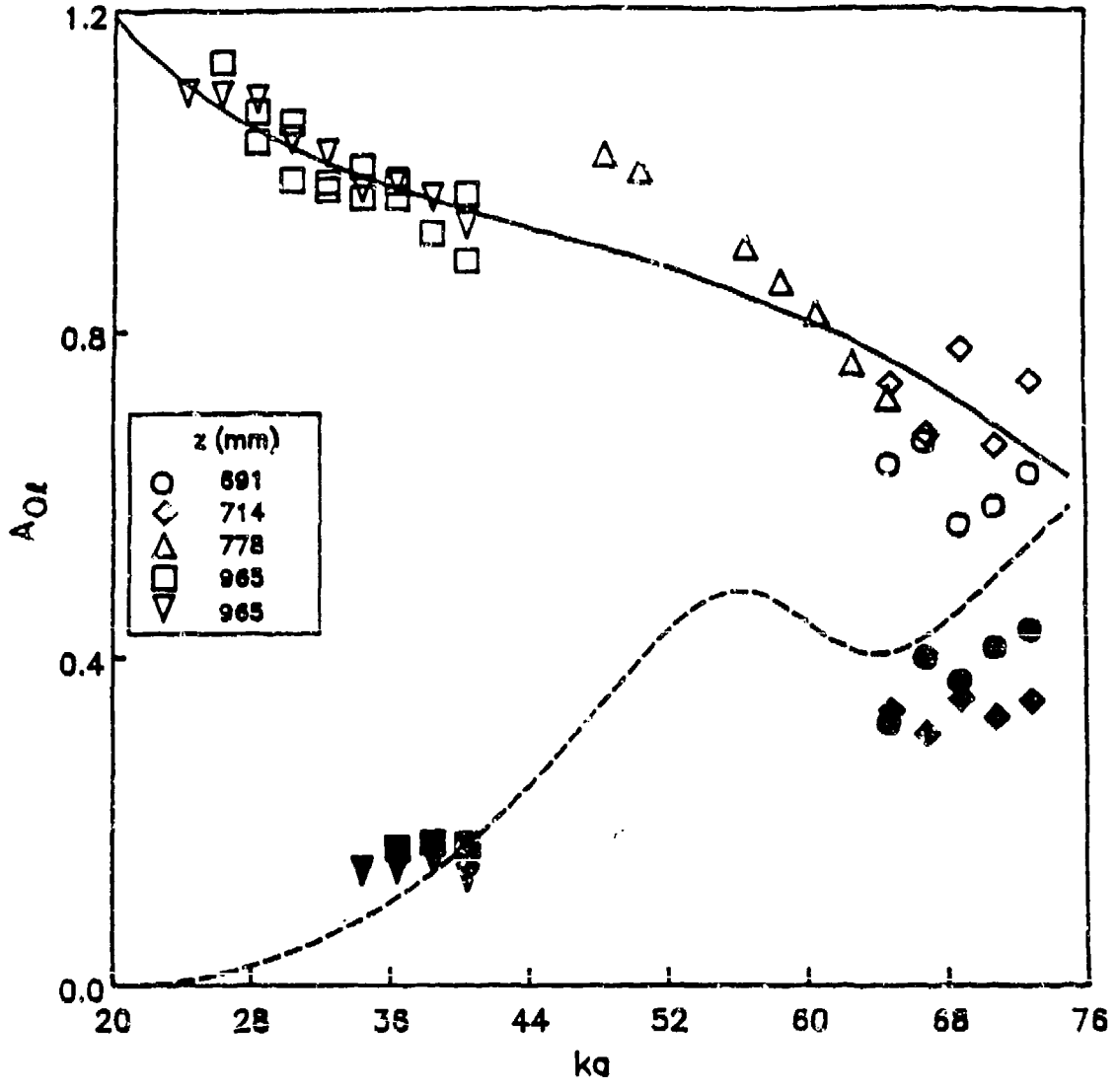

Fig. 4 Theoretical normalized backscattering amplitudes for a_0 (solid line) and s_0 (dashed line) leaky Lamb wave echoes are compared with experimental data. The normalization is with respect to a tungsten carbide sphere. The on-axis hydrophone distances for each data set from the point C' in Fig. 2 is indicated. The data points were obtained from voltage measurements on traces similar to those in Fig. 3.

(dashed line) leaky Lamb waves. Since absolute pressure amplitude measurements could not be achieved over the entire range of frequencies, both the theoretical and experimental amplitudes of the backscattering from the 440c stainless steel shell were normalized by the specular reflection from the tungsten carbide sphere. The normalized measured A_{0l} are given by $(V_{0l}/V_{swc})(a_{wc}|f_{swc}|/a_{ss})$ where V_{0l} and V_{swc} are the measured peak-to-peak voltages of the ($l = a_0, s_0$) leaky Lamb wave echo and specular reflection from tungsten carbide, respectively. The magnitude of the specular reflection form function for the tungsten carbide sphere is $|f_{swc}|$ and the ratio of radii appears because of the difference in the size of the sphere and shell used. [For the frequency range of interest $|f_{swc}| = (\rho_e c_L - \rho c)/(\rho_e c_L + \rho c) \approx 0.969$.] The agreement for $ka < 44$ between Eq. (5b) and experiment is good, but for the $ka > 44$ the measured values deviate substantially from the predicted amplitudes. One plausible cause for this discrepancy is the possible excitation of the $l = a_1$ and s_1 leaky Lamb waves for $ka > 41$ and 65, respectively. These waves were neglected in the original analysis in Ref. 5. A second probable cause of the disagreement between the measured and predicted values is that the a_0 and s_0 echoes overlap in time for $50 < ka < 70$ and the long decaying pulse train for $ka > 65$ may also interfere with the a_0 echo.

Equation (5b) indicates that A_{ml} should have a maximum for $\gamma = 0$ and it decreases when the observation point is moved away from the axis (so that $\gamma \neq 0$). The localization of the pressure amplitude near the backward axis is a manifestation of the acoustical glory.[5,14] The $m = 0$ amplitude for the $l = a_0$ leaky Lamb wave was studied to verify this prediction. Again, the theory and measurements were normalized by the on-axis specular reflection from a tungsten carbide sphere. From Eqs. (2) and (5a), the normalized pressure is

$$\frac{|p_{ml}(r_0,\gamma)|}{|p_{swc}(r_0)|} = \frac{a}{a_{wc}|f_{swc}|} \frac{A_{ml}}{[1 + \tan^2\gamma]^{1/2}} . \qquad (6)$$

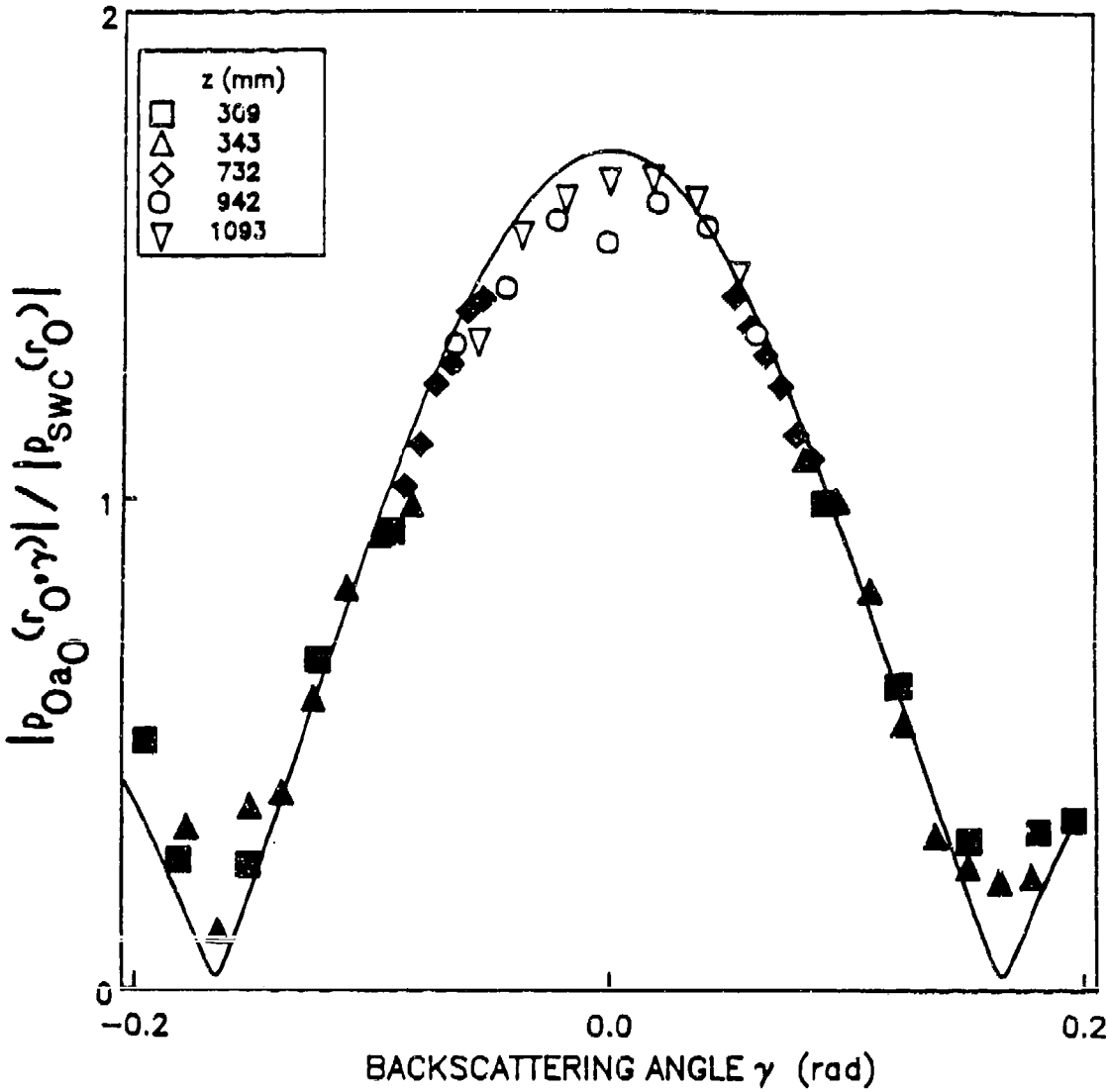

Fig. 5 Experimental confirmation of the axial focusing predicted by Eq. (6). The $m = 0$ amplitude of the a_0 leaky Lamb wave echo was measured as the hydrophone was shifted away from backscattering ($\gamma = 0$). For the 440c stainless steel shell studied, the frequency of the incident 4-cycle sine-wave tone burst corresponds to $ka = 24.3$

The on-axis distance of the hydrophone from point C' in Fig. 2 is z and $r_0 = z + a$. Figure 5 compares the theoretical prediction from Eq. (6) with experimental data for $ka = 24.3$. Inspection of Eqs. (5b) and (6) reveals that $|p_{ml}(r_0,\gamma)|/|p_{swc}(r_0)|$ depends only on γ (note $r_0/r = [1 + tan^2\gamma]^{-1/2}$) and that it contains *no adjustable parameters*. The agreement between theory and experiment is excellent for a measurement of this type. A detailed discussion of the theory and experimental methods used in obtaining Figs. 4 and 5 is contained in Ref. 5 as well as other theoretical and experimental results. The importance of these results is that a qualitative ray model of the backscattered pressure described the experimental observations.

The remainder of this dissertation gives a more detailed analysis of the forward and backwards scattering of a plane wave from an evacuated spherical shell. Chapter 2 develops quantitative ray methods used in synthesizing the forward scattering amplitude and, ultimately, the total scattering cross section via the optical theorem. Chapters 3 and 4 investigate quantitative ray methods for the modeling of the form function for backscattering. The contents of chapters 2 and 3 have been accepted for publication in the Journal of the Acoustical Society of America. The present form of chapter 4 has been submitted for publication in the Journal of the Acoustical Society of America. Since these chapters are independent papers, they may be read separately. As such, each chapter contains its own abstract, introduction, sections, appendices, and references. The numbering of equations, figures, and tables are unique to a given chapter. Mathematical symbols may differ slightly between chapters, however, each symbol is clearly defined within the appropriate chapter. It is suggested that chapter 3 be read prior to chapter 4, since some results from chapter 3 are used in chapter 4. Two appendices follow the main text. Each appendix contains material germane to the ray synthesis of the forward and backwards scattering from an evacuated elastic spherical shell. This material could not be

adequately presented within chapters 2 - 4, but it is deemed important for completeness of the analysis. Appendix I discusses Marston's approximation for the complex coupling coefficient and comparison to an apparent exact complex coupling coefficient for each leaky Lamb wave is presented. The dependence of the leaky Lamb wave resonance spacing on the phase and group velocities is also discussed in Appendix I. Finally, Appendix II contains tables of the leaky Lamb wave parameters necessary for the ray synthesis. These parameters were generated by extending certain results of the Sommerfeld-Watson transformation of the partial wave series for backscattering from a solid elastic sphere to the shell.

References

1. P. L. Marston, "GTD for backscattering from elastic spheres and cylinders in water and the coupling of surface elastic waves with the acoustic field," J. Acoust. Soc. Am. 83, 25 - 37 (1988).

2. K. L. Williams and P. L. Marston, "Backscattering from an elastic sphere: Sommerfeld-Watson transformation and experimental confirmation," J. Acoust. Soc. Am. 78, 1093 - 1102 (1985).

3. R. R. Goodman and R. Stern, "Reflection and transmission of sound by elastic spherical shells," J. Acoust. Soc. Am 34, 338 - 344 (1962).

4. M. C. Junger, "Sound scattering by thin elastic shells," J. Acoust. Soc. Am. 24, 366 - 373 (1952). The expression for p_s in Eq. (38) is equivalent to the second term in Eq. (1) here except Junger has introduced the concept of a scattering phase shift. Junger's analysis appears to be the first to consider the scattering from an elastic spherical shell. The method employed correlating the solution to the Helmholtz wave equation with the Lagrange equations for a thin elastic shell.

5. S. G. Kargl and P. L. Marston, "Observations and modeling of the backscattering of short tone bursts from a spherical shell: Lamb wave echoes, glory, and axial reverberations," J. Acoust. Soc. Am. 85, 1014 - 1028 (1989).

6. R. Hickling, "Analysis of echoes from a hollow metallic sphere in water," J. Acoust. Soc. Am. 36, 1124 - 1137 (1964).

7. K. J. Diercks and R. Hickling, "Echoes from hollow aluminum spheres in water," J. Acoust. Soc. Am. 41, 380 - 393 (1967).

8. G. C. Gaunaurd and M. F. Werby, "Lamb and creeping waves around submerged spherical shells resonantly excited by sound scattering," J. Acoust. Soc. Am. 82, 2021 - 2033 (1987).

9. G. S. Sammelmann, D. H. Trivett, and R. H. Hackman, "The acoustic scattering by a submerged, spherical shell. I: The bifurcation of the dispersion curve for the spherical antisymmetric Lamb wave," J. Acoust. Soc. Am. 85, 114 - 124 (1989).

10. H. Lamb, "On waves in an elastic plate," Proc. R. Soc. London Ser. A **93**, 114 - 128 (1917).

11. I. A. Viktorov, *Rayleigh and Lamb waves: Physical theory and applications*, (Plenum, New York, 1967).

12. K. L. Williams and P. L. Marston, "Synthesis of backscattering from an elastic sphere using the Sommerfeld-Watson transformation and giving a Fabry-Perot analysis of resonances," J. Acoust. Soc. Am. 79, 1702 - 1708 (1986).

13. P. L. Marston, S. G. Kargl, and K. L. Williams,"Rayleigh, Lamb, and Whispering Gallery wave contributions to backscattering from smooth elastic objects in water described by generalization of GTD," in *Elastic Wave Propagation and Ultrasonic Nondestructive Evaluation*, edited by S. K. Datta, J. D. Achenbach, and Y. S. Rajapakse [Elsevier Science, Amsterdam 1990] pp. 211 - 216.

14. K. L. Williams and P. L. Marston, "Axially focused (glory) scattering due to surface waves generated on spheres: Model and experimental confirmation using tungsten carbide spheres," J. Acoust. Soc. Am. 78, 722 - 728 (1985).

15. R. Hickling, "Analysis of echoes from a solid elastic sphere in water," J. Acoust. Soc. Am. 34, 1582 - 1592 (1962).

Chapter 2

Ray synthesis of Lamb wave contributions to the total scattering cross section for an elastic spherical shell

Abstract

The optical theorem relates the extinction cross section, $\sigma_e(ka)$, to the forward scattering amplitude, $f(\theta = 0, ka)$. Here θ denotes the scattering angle, k is the wavenumber of the incident sound, and a is the radius of the scatterer. If the absorption by the scatterer is negligible so that the scatterer is elastic, σ_e is equal to the total scattering cross section σ_t. By applying this theorem to the partial wave series for $f(0,ka)$, we can obtain an expression for σ_t for an elastic spherical shell in water. However, the series representation of σ_t does not facilitate a direct understanding of the rich structure caused by the shell's elastic response. In particular, the elastic response is attributable to leaky Lamb waves. We employ a generalization of the geometrical theory of diffraction [P. L. Marston, J. Acoust. Soc. Am. 83, 25-37 (1988)] to synthesize $f(0, ka)$. This simple ray acoustic synthesis contains a component for ordinary diffraction by the shell and distinct contributions for the individual Lamb waves that can be excited on the shell. A comparison of numerical computations for σ_t utilizing the exact partial wave series and the ray synthesis shows good agreement in the description of the resonance structure. The relevant range of ka for this comparison is $7 < ka < 100$. The elastic material of the shell is 440c stainless steel and the inner-to-outer radius ratio is $b/a = 0.838$. Dispersion curves and radiation damping for Lamb waves were calculated by Watson transform methods. The structure in $\sigma_t(ka)$ due to Lamb waves may also be depicted as a manifestation of forward glory scattering and experimental evidence for the forward glory is noted.

2.1 Introduction

Several articles have concentrated on the *surface elastic wave* contributions to backscattering from solid elastic spheres[1, 2, 3] and cylinders[4] as well as spherical[5, 6, 7] and circular cylindrical shells.[8, 9] The surface elastic waves on solid spheres and cylinders are leaky Rayleigh and whispering gallery waves; while the surface elastic waves on spherical and cylindrical shells are a generalization of Lamb waves. (Although the strains due to Lamb waves are not strictly confined to the surface of the shell, it may be appropriate to label Lamb waves as surface elastic waves, since the surface of the shell *guides* the Lamb wave propagation.) In particular, some of these authors have considered the significance of surface elastic wave resonances to the backscattering form function, $f(\theta = \pi)$ defined in Eq. (1) below. Since the structure found in the backscattering form function is attributed to the presence of surface elastic wave resonances, then these resonances should also contribute to the scattering in the forward direction. In this article, we are concerned with the manifestation of such contributions to the total scattering cross section for an elastic spherical shell.

When a scatterer is placed in an incident acoustic plane wave of intensity $I(W/m^2)$, the total power in the scattered wave is $I\sigma_t$ where σ_t denotes *the total scattering cross section.*[10] The *extinction cross section,* denoted as σ_e, expresses the total power removed (scattered or absorbed) from the incident plane wave as $I\sigma_e$. From the conservation of energy $\sigma_e = \sigma_t + \sigma_{abs}$ where $I\sigma_{abs}$ is the power absorbed by the scatterer and σ_{abs} is known as the *absorption cross section.* The extinction cross section is related to the *forward scattering amplitude* by the *optical theorem* reviewed in Sec. 2.2 below.[11,12] (This theorem has also been referred to as the extinction theorem.) Some early examples of the application of the optical theorem to acoustical problems are given in Refs. 13 - 15. For a scatterer with no absorption, $\sigma_{abs} = 0$, so that $\sigma_e = \sigma_t$ and the optical theorem may be used

to calculate σ_t directly. (Even for nonabsorbing scatterers, however, some authors[16-18] resorted to integration of differential cross section over 4π sr to obtain σ_t.) The scatterer considered in the present paper is modeled as perfectly elastic.

In this paper, the forward scattering amplitude is obtained from the exact partial wave series and from a synthesis in terms of ray contributions. The synthesis is partially facilitated by the elastic generalization of the geometrical theory of diffraction given in Ref. 9.

This paper is organized as follows. In Sec. 2.2, the optical theorem is stated for the case of scattering from spheres. Using the optical theorem and partial wave series representation for the forward scattering amplitude, σ_t for an elastic spherical shell is obtained. The basis of the ray synthesis of σ_t is outlined at the end of Sec. 2.2. In Sec. 2.3, the component of σ_t due to ordinary forward diffraction is developed for the ray model. Individual Lamb wave contributions to the ray representation of the forward scattering amplitude are determined in Sec. 2.4. Section 2.5 compares the results of the exact partial-wave series calculation with the ray model. The pertinent conclusions from the comparison in Sec. 2.5 are contained in Sec. 2.6 along with a discussion of relevant aspects of forward glory scattering for spheres. Section 2.6 also summarizes an experimental observation pertinent to the forward glory of shells and comments on the cause of certain frequency dependent structure in σ_t. Appendix A discusses the Lamb wave parameters used in the synthesis as given by Watson transform methodology.[1,3,5,9]

2.2 The optical theorem for acoustic scattering

A. Partial wave series analysis

A unit amplitude plane wave, propagating in the positive z-direction, in water is incident upon an elastic spherical shell. The total pressure in the water can be expressed as

a superposition of the incident plane wave and a scattered wave. In particular, in the farfield of the shell, the total pressure is [1, 5]

$$p_t = e^{ikz} + (a/2r)f(\theta)e^{ikr}. \tag{1}$$

The first term is the incident plane wave with wavenumber $k = \omega/c$. The second term is a spherically diverging scattered wave. The outer radius of the shell is denoted by a and $f(\theta)$ is the complex dimensionless scattering amplitude. The harmonic time dependence, $exp(-i\omega t)$, has been and, henceforth, will be suppressed.

The optical theorem provides a fundamental relationship between the scattering amplitude and σ_e. Several authors give various expressions for the optical theorem (see, e.g., Refs. 11, 12, 19, and 20). For the amplitude normalization used in Eq. (1), it follows that

$$\sigma_e = (2\pi a/k)\ \mathrm{Im}\{f(\theta = 0)\}, \tag{2}$$

where $Im\{\}$ means the imaginary part of the enclosed quantity. The significance of Eq. (2) is that the only scattering amplitude needed is the one for forward scattering. It is convenient to normalize σ_e by the geometrical cross section of the shell, πa^2,

$$(\sigma_e/\pi a^2) = (2/x)\ \mathrm{Im}\{f(\theta = 0)\}. \tag{3}$$

This normalization introduces the dimensionless size parameter, $x = ka$, into Eq. (3). In the discussion which follows we consider perfectly elastic scatters so that $\sigma_t = \sigma_e$.

The *partial wave series* (PWS) representation of the *exact* forward scattering amplitude for an evacuated elastic spherical shell is

$$f(\theta = 0) = (2/ix) \sum_{n=0}^{\infty} (2n + 1) \frac{B_n(x)}{D_n(x)}, \tag{4}$$

where n is the partial wave index. The functions B_n and D_n are 5×5 determinants whose elements are complicated combinations of spherical Bessel functions of the first and second kind.[5] Using Eqs. (3) and (4), the normalized total scattering cross section for the shell becomes

$$(\sigma_t/\pi a^2) = (-4/x^2) \sum_{n=0}^{\infty} (2n + 1)\, \mathrm{Re}\left\{\frac{B_n(x)}{D_n(x)}\right\}, \qquad (5)$$

where $Re\{\}$ denotes the real part of the enclosed quantity. The dashed curve in Fig. 1, that contains the complicated structure, is the normalized σ_t for a 440c stainless steel shell as computed from Eq. (5) with the material parameters given in Sec. 2.5. There are two important features in Fig. 1. First, σ_t is approaching the expected value of twice the geometrical cross section of the shell as $x \rightarrow \infty$. This asymptotic result for σ_t is known as the *extinction paradox*. Physical interpretations of the extinction paradox have been discussed by various authors.[20-22] Second, and perhaps more important, the structure observed in σ_t for a 440c stainless steel shell is a manifestation of the elastic nature of the scatterer. That is, a comparison of σ_t for an elastic shell and a rigid sphere of radius a in Fig. 1 shows that the elastic properties of the shell are important.

The expression for the normalized cross section in Eq. (5) has properties which would make a geometrical representation worthy of investigation. First, a simple physical interpretation of the structure in σ_t is not easily obtained directly from the PWS representation. Although, it is known that the incident plane wave can excite Lamb wave resonances in a shell, the quantitative description for this coupling is not immediately apparent from the PWS expression. Second, it is well-known, that for large ka, the PWS is a slowly converging series; the number of terms required exceeds ka. See Eq. (16) below. We examine below a simple expression for σ_t based on a generalization[9] of the geometrical theory of diffraction[23]. It should be possible to modify this ray representation

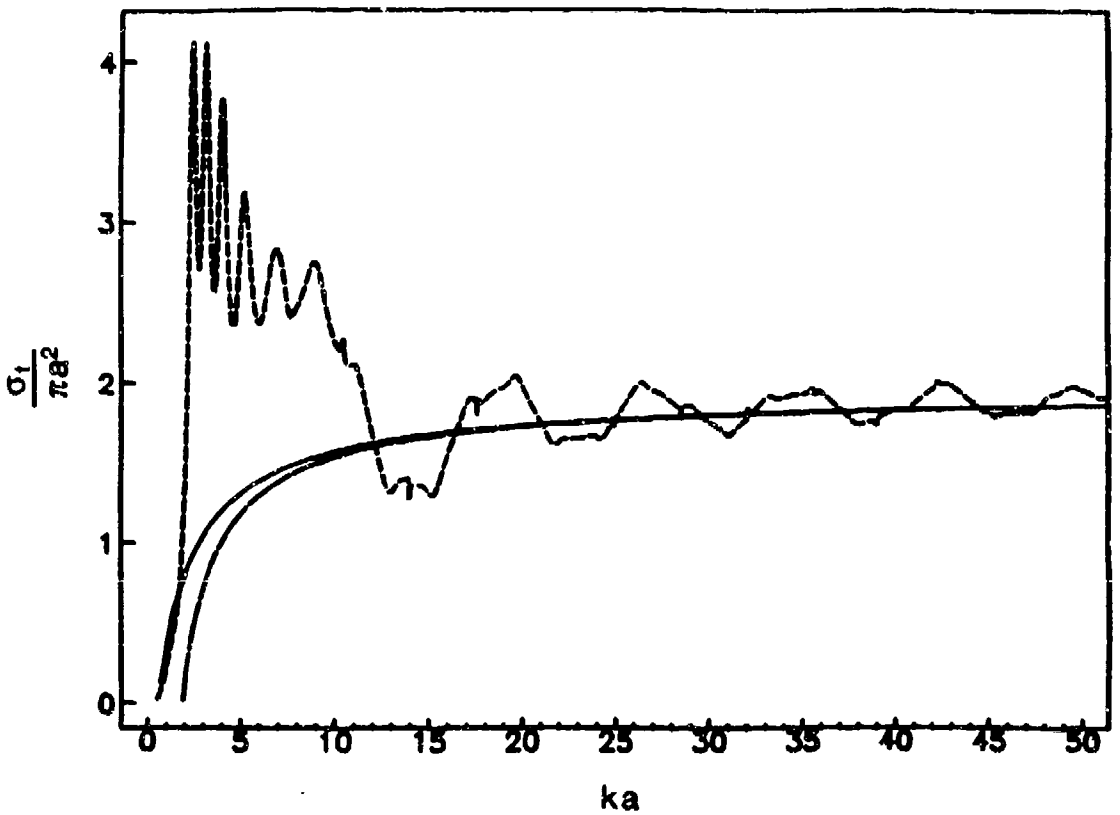

Fig. 1 Normalized total scattering cross sections for empty elastic spherical shell in water and a rigid sphere, each of outer radius a. The short dashed line is the exact partial wave series result for the shell, Eq. (5), with the stainless steel parameters listed in Sec. 2.5 and an inner to outer radius $b/a = 0.838$. The solid, monotonic curve corresponds to the rigid sphere, where the partial wave series, Eq. (9), is calculated. The long dashed line is the first three terms of Beckmann and Franz's approximation, Eq. (10), for the normalized cross section for the rigid sphere

of the total scattering cross section for objects of other shapes where the cross section is not easily obtained from a PWS.

B. Ray synthesis of the total scattering total scattering cross section

It has been proposed, that the form function describing the steady-state high-frequency backscattering amplitude from spheres can be approximated by three ordinarily distinct classes of contributions.[1,3,9] These contributions are: a specular reflection, transmitted bulk wave contributions, and surface elastic wave contributions. A superposition of these components gives the scattered pressure term of the total pressure in the backward direction. (If *ka* is smaller than about 15, a contribution to backscattering from Franz-type creeping waves can also become significant for some materials or shell thicknesses but such contributions were not separately analyzed.) By superposing the appropriate contributions, the forward scattering amplitude may be synthesized as discussed below.

To construct the geometrical synthesis of the forward scattering amplitude for the spherical shell, the specular reflection term for backscattering is replaced by a contribution that describes the ordinary forward diffraction about the shell (see Sec. 2.3 below). The transmitted bulk wave contributions, that backscattering form functions may contain, do not occur in the forward scattering amplitude of a thin elastic air-filled or evacuated shell. That is, there is no mechanism for the transmission of a bulk wave through the interior of the shell. Since surface elastic waves leak energy continuously back into the surrounding water, then these contributions must also be included in the forward scattering amplitude. Hence, the forward scattering amplitude has the approximate form

$$f(\theta = 0) \approx f_{FD} + \sum_{l} f_{l} , \qquad (6)$$

where the summation is over all possible surface elastic wave contributions. Since the operator, $Im\{\}$, is linear, then by inspection of Eqs. (2) and (6) the total scattering cross section is

$$\sigma_t \approx \sigma_{FD} + \sum_l \sigma_l \,. \tag{7}$$

The forms of the individual components in Eqs. (6) and (7) are considered in Secs. 2.3 and 2.4.

2.3 Forward diffraction term for the total scattering cross section

The specific form of the contribution to σ_t due to ordinary forward diffraction about an *elastic spherical shell* is not currently available from a Watson transformation.[1] The simplest approximation would be the total scattering cross section of a rigid disk of radius a. That is, the total scattering cross section for a rigid disk (computed from the optical theorem) can only be attributed to ordinary forward diffraction. The asymptotic value (i.e., $ka >> 1$) for the normalized total scattering cross section of the rigid disk[24] is 2. As noted previously, $(\sigma_t / \pi a^2) \rightarrow 2$ as $ka \rightarrow \infty$ is known as the extinction paradox. Although forward diffraction from a rigid disk gives the expected asymptotic value, this approximation is inappropriate for the ka range of interest, $7 < ka < 100$.

A more suitable approximation for the normalized ordinary forward diffraction contribution $(\sigma_{FD}/ \pi a^2)$ is the total scattering cross section for a fixed rigid or *acoustically hard* sphere. To obtain $(\sigma_{FD}/ \pi a^2)$, we employ the optical theorem, as given by Eq. (3), and the forward scattering amplitude for the rigid sphere. The forward scattering amplitude for the rigid sphere is given by the PWS[7, 25]

$$f_{FD} = (-2/ix) \sum_{n=0}^{\infty} (2n + 1) \frac{j_n'(x)}{h_n^{(1)'}(x)} \,, \tag{8}$$

where j_n and h_n are spherical Bessel functions of the first and third kind, respectively. The prime in Eq. (8) denotes differentiation with respect to the argument of the function. The result of inserting Eq. (8) into Eq. (3) is

$$(\sigma_{FD}/\pi a^2) = (4/x^2) \sum_{n=0}^{\infty} (2n + 1)\, \mathrm{Re}\left\{ \frac{j_n'(x)}{h_n^{(1)'}(x)} \right\} . \qquad (9)$$

The solid, monotonically increasing curve in Fig. 1 is $\sigma_{FD}/\pi a^2$ for a rigid sphere of radius a. From Fig. 1 one observes that the cross section for the rigid sphere asymptotically approaches 2. Although Eq. (9) is a suitable candidate for $(\sigma_{FD}/\pi a^2)$, its dependence on x is complicated and , hence, not a simple parameterization of the ordinary forward diffraction contribution to σ_t of an elastic sphere.

Beckmann and Franz performed a *modified* Watson transformation on a rigid sphere result similar to Eq. (9).[26, 27] The Watson transformation transforms the slowly converging PWS into a more rapidly converging series. The result of their calculation is a series in inverse powers of x,

$$(\sigma_{FD}/\pi a^2) = 2 - 1.7284\, x^{-2/3} - 2.0104\, x^{-4/3} + O(x^{-2}) . \qquad (10)$$

The first three terms in Eq. (10) are plotted as the long-dashed line in Fig. 1. From inspection of Fig. 1, we observe that the Beckmann and Franz result is, perhaps, the simplest approximation of the ordinary forward diffraction term in Eq. (7) throughout the region of interest $7 < x < 100$. Thus, for the numerical computations given in Sec. 2.5, we use the first three terms in Eq. (10) for the contribution of ordinary forward diffraction to σ_t.

It may be argued that the second term in Eq. (10) represents approximately the x dependence of contributions of grazing rays (also known as edge rays) to $Im[f(\theta = 0)]$ for a rigid sphere. In addition, there could be distinct ray contributions which wrap completely

around a rigid sphere. The waves associated with those rays are creeping waves having phase velocities close to the speed in the outer media (water). The damping of such waves is sufficiently large that contributions from a complete circumnavigation to *forward* scattering are generally thought to be negligible for impenetrable spheres.[15,28]

2.4 Leaky surface wave contributions to the forward scattering amplitude

In this section, we use the methodology of geometrical theory of diffraction generalized to elastic objects[9] to derive an expression for an individual surface elastic wave contribution, f_l, to the forward scattering amplitude. The acoustic ray diagram in Fig. 2 facilitates an understanding of this ray synthesis of f_l. The ray diagram is similar to those discussed in Refs. 1, 5 and 9. An acoustic plane wave propagates along the ray AB in the positive z-direction. At the point B the acoustic wavefield in water couples to the elastic shell and launches a surface elastic wave. The surface elastic wave propagates from B to B' shedding energy continuously back into the water. At B' the radiated energy is directed along the forward scattering direction (parallel to the $+z$-axis). The surface elastic wave repeatedly circumnavigates the shell radiating energy each time in the forward direction. The points B and B' are determined by the phase velocity trace-matching condition,

$$\theta_l = \arcsin(c/c_l), \qquad c_l \geq c, \tag{11}$$

where θ_l is the local angle of incidence and c/c_l is the ratio of the speed of sound in water, c, and the phase velocity *along the shell's outer surface* of the Lamb wave, c_l. The phase velocity is assumed to be supersonic.

The form of the individual surface elastic wave contribution to the forward scattering amplitude is

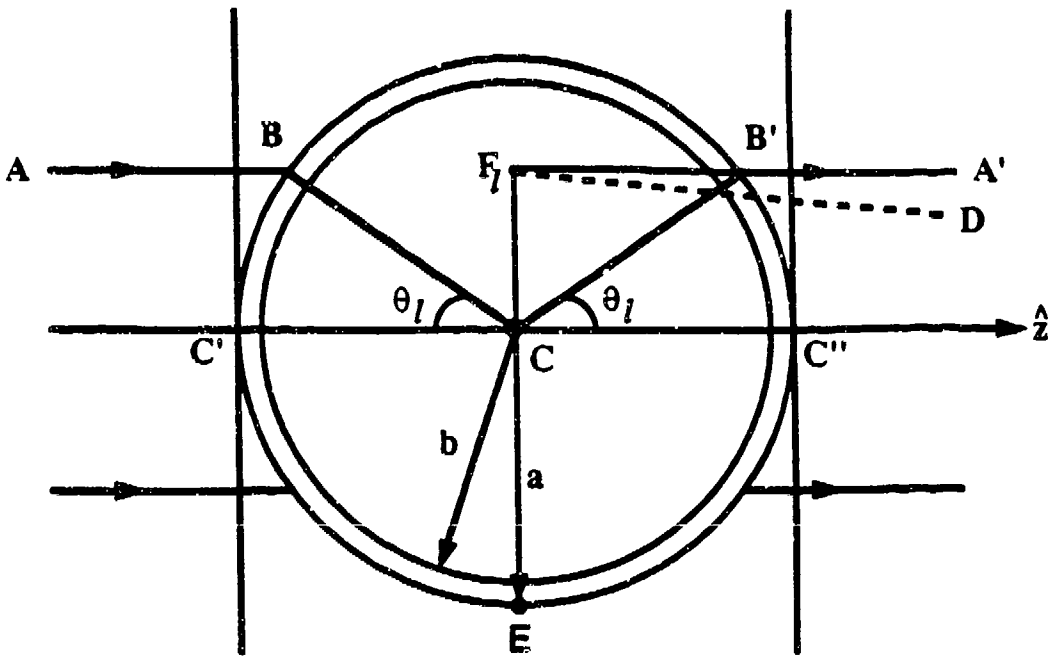

Fig. 2 Acoustic ray diagram for Lamb wave contributions to the forward scattering amplitude for Lamb waves having $c_l > c$. The outer radius of the shell is a and the inner radius is b. The incident acoustic plane wave launches a Lamb wave in the vicinity of point B. The Lamb wave propagates along the shell and radiates in the forward direction at point B'. The points B and B' are determined by Eq. (11). The qualitative features of the ray diagram are made quantitative through Eqs. (12) - (14) to describe the scattering. The ray synthesis also contains a contribution due to diffraction about the shell. That includes contributions due to rays which touch the shell near E at the edge.

$$f_l = - G_l e^{i\eta_l} e^{-(\pi - 2\theta_l)\beta_l} \sum_{m=0}^{\infty} e^{im\pi} e^{-2m\pi\beta_l} e^{i2m\pi xc/c_l} . \qquad (12)$$

The coupling efficiency of the acoustic wavefield in water with the elastic shell at the points B and B' in Fig. 2 is characterized by a complex coupling coefficient G_l. The geometrical phase shift,

$$\eta_l = x(c/c_l)(\pi - 2\theta_l) - 2x\cos(\theta_l) \qquad (13)$$

accounts for the difference in phase of a surface elastic wave traveling from B to B' along the shell and a plane wave in water traveling from B to B' as if the shell were not present. The factor $exp[-(\pi - 2\theta_l)\beta_l]$ is associated with the radiation damping of the surface elastic wave propagating along the arc BB'. The radiation damping parameter is denoted by β_l and has the units of np/radian. The summation occurs in Eq. (12) from the circumnavigations of the surface elastic wave. The $m = 0$ term is the first partial circumnavigation of the shell; while $m = 1, 2,...$ is for each successive complete circumnavigation. The terms $exp(-2m\pi\beta_l)$ and $exp(i2m\pi xc/c_l)$ are the additional radiation damping and phase shift. Finally, the term $exp(im\pi)$ arises from the passage of the surface elastic wave through the caustics at the points C' and C''.

It is observed that the summation in Eq. (12) is a geometric series and may be expressed in a simple analytic form.[3] Summing the series in Eq. (12), we have

$$f_l = [- G_l e^{i\eta_l} e^{-(\pi - 2\theta_l)\beta_l}]/[1 + e^{-2\pi\beta_l} e^{i2\pi xc/c_l}] . \qquad (14)$$

The form of the denominator in f_l is that of a Fabry-Perot resonator.[3,9] Equation (14) is the desired ray synthesis for f_l.

The coupling coefficient, G_l, for the elastic *solid* sphere was determined from the Sommerfeld-Watson transformation on the appropriate PWS.[1, 9] At the time of this writing, an expression for the coupling coefficient for the elastic spherical shell is not

available directly from the Watson transformation. However, Marston has derived approximations for G_l for an elastic sphere and cylinder.[9,29] The approximations were supported by various numerical results for solid spheres and cylindrical shells.[9] The relevant result for spheres may be written

$$G_l = 8\pi\beta_l \, (c/c_l) \, e^{i\phi_l} \tag{15}$$

where ϕ_l denotes the phase of G_l and it may be argued[29] that $\phi_l \approx 0$. For the calculation in Sec. 2.5, ϕ_l for the *lth* surface elastic wave is taken to be identically equal to zero. It is noteworthy that the magnitude of G_l depends on only the damping parameter and the ratio of the velocities. This result for $|\, G_l \,|$ was confirmed in Ref. 5 for the stainless steel shell considered here by use of measured backscattering amplitudes. The computations discussed in Sec. 2.5 give additional support for Eq. (15) with $\phi_l = 0$ as does a synthesis of the steady state backscattering amplitude for the shell considered.[30]

The ray synthesis of the contribution of a particular surface elastic wave is given by Eqs. (11), (13) and (14) with the approximation, Eq. (15), used for the coupling coefficient. Inspection of Eqs. (11) - (15) shows that a particular surface elastic wave contribution depends on only the damping parameter and the phase velocity ratio. The method used for determining β_l and c/c_l is described in Appendix A.

2.5 Numerical results and discussion

The calculations shown in Figs. 3 - 8 are for a 440c stainless steel shell immersed in water. For these computations, the material parameters for 440c stainless steel were selected because of previous work with a shell composed of this material.[5] The longitudinal velocity, c_L, for 440c stainless steel is 5.854 $mm/\mu s$ and the shear wave velocity, c_s, is 3.150 $mm/\mu s$. The density is $\rho_S = 7.84\ g/cm^3$. The shell's outer radius is

$a = 19.05\ mm$ and the ratio of the inner-to-outer radius is $b/a = 0.838$. The speed of sound for the water is $c = 1.479\ mm/\mu s$; while the density is $\rho = 1.00\ g/cm^3$.

For the PWS computations, we use Eq. (5), where the determinants B_n and D_n are given in Ref. 5. The PWS calculation for $(\sigma_t/\pi a^2)$ is performed over the range $0 < x < 100$. In Figs. 3 - 8, the dashed curves are the exact PWS results. When summing PWS, the following maximum values for the partial wave index were tested and found to ensure convergence:

$$\begin{aligned} n_{max} &= 2 + [\, x + 4.0\, x^{1/3}\,], \qquad x < 8, \\ n_{max} &= 3 + [\, x + 4.05\, x^{1/3}\,], \qquad x \geq 8, \end{aligned} \tag{16}$$

where the square brackets imply the integer part (i.e., rounded up or down) is to be used. These values are similar to ones used when evaluating the Mie PWS for light scattering.[31] That the maximum partial wave index in the optical and acoustical cases should be similar may be argued from the localization principle.[12] (The proper convergence of the PWS for the shell considered was verified by substantially increasing n_{max}. Equation (16) should be used with caution, however, for thin shells having significant subsonic wave contributions.) Since a Lamb wave resonance can contain sharp peaks, the increment of x needs to be small. Hence, it is apparent that the implementation of Eq. (5) can be relatively computationally intensive.

The particular Lamb waves, that can be coupled to a shell with the above material properties and in the range $7 < x < 100$, are the two lowest antisymmetric or flexural modes a_0 and a_1 and the two lowest symmetric or dilatational modes s_0 and s_1. The present ray synthesis is restricted to $x > 7$ for two reason. First, the numerical procedure used to obtain Lamb wave damping parameters and phase velocities begins to breakdown as noted in Appendix A. That is, the numerical accuracy of the results become suspect. Second, the

a_0 mode becomes *subsonic* for $x < 7$. The present ray synthesis is limited to supersonic surface elastic waves as evident from Eq. (11) and the related analysis given in Refs. 1 and 3.

The solid curves in Figs. 3 - 8 are the ray synthesis, where $(\sigma_{FD}/\pi a^2)$ is given by the first three terms in Eq.(10) (a monotonic function of x) and the appropriate Lamb wave contributions are included. In Fig. 3, the ray result has only two terms. These terms are the ordinary forward diffraction component and the lowest antisymmetric Lamb mode contribution, σ_{a0}. It is apparent that the course structure, for $7 < x < 25$, is attributed entirely to the a_0 flexural Lamb wave. The sharp resonances in Fig. 3, that are not modeled, are from the σ_{s0} contribution. Figure 4 includes σ_{s0}. The agreement of the ray synthesis and the exact PWS for $(\sigma_t/\pi a^2)$ is good considering the ray model is based on high-frequency methods. Observe that the above synthesis appears to be accurate down to $x \approx 9$. It is noteworthy, however, that the s_0 resonances near ka of 17.60, 21.28, and 24.95 may not have been fully resolved due to the narrowness of their line widths.

The region $25 < x < 50$ is plotted in Figs. 5 and 6. The vertical axis has been magnify to enhance the visibility of narrow resonance features and to better illustrate the agreement between the ray and PWS results. In Fig. 5, the ray model contains the ordinary forward diffraction term and the a_0 and s_0 Lamb wave contributions. Again, the broad structure is associated with the a_0 Lamb wave while the sharp resonances are attributable to the s_0 Lamb wave. However, as noted in Appendix A, the a_1 antisymmetric mode can be excited on the shell for $x > 40$. In particular, the resonance features at $x \approx 43$, 44, 46 and 50 are not associated with either the a_0 or s_0 modes. By adding the a_1 contribution in this region, we recover all the resonance features of the PWS result in the ray synthesis of the cross section.

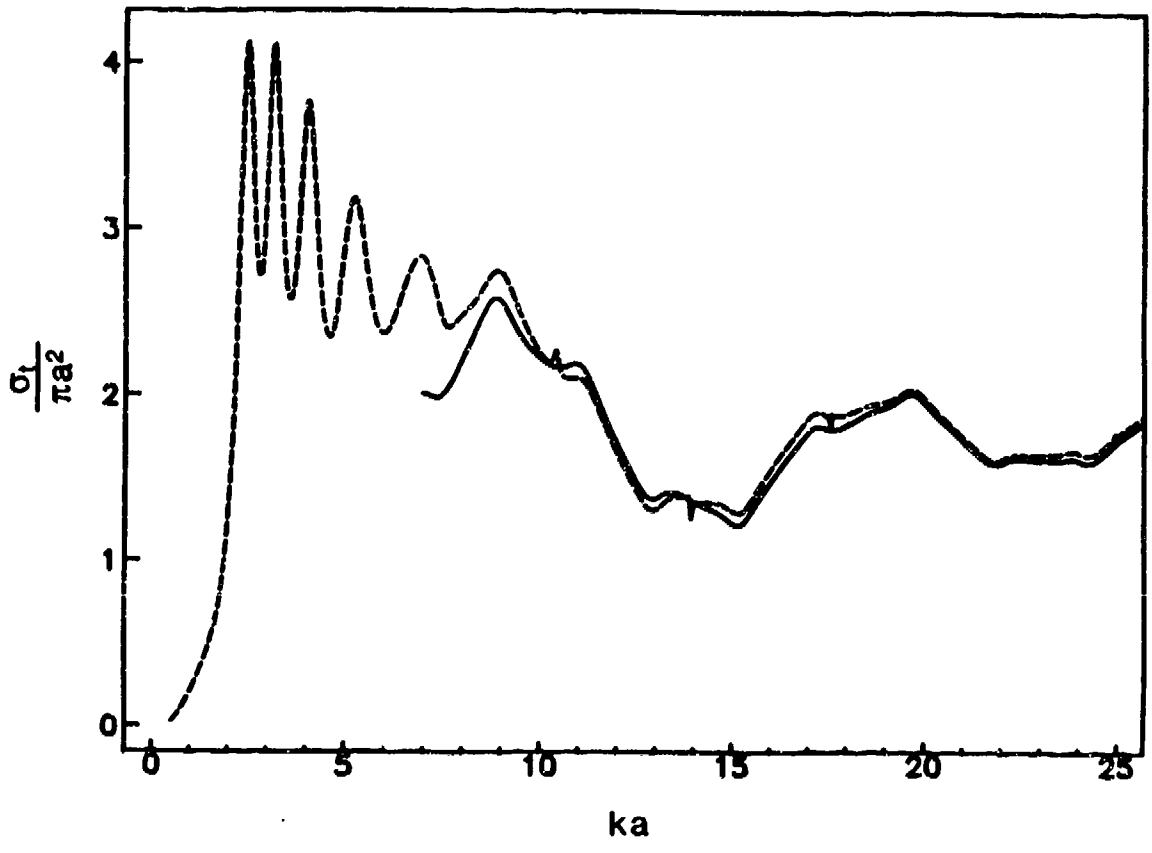

Fig. 3 A comparison of the exact partial wave series representation of the normalized total scattering cross section with the ray synthesis. The dashed curve is the partial wave series result, Eq. (5), and the solid line is the ray model. Only the σ_{FD} and σ_{a_0} contributions are include in the ray model.

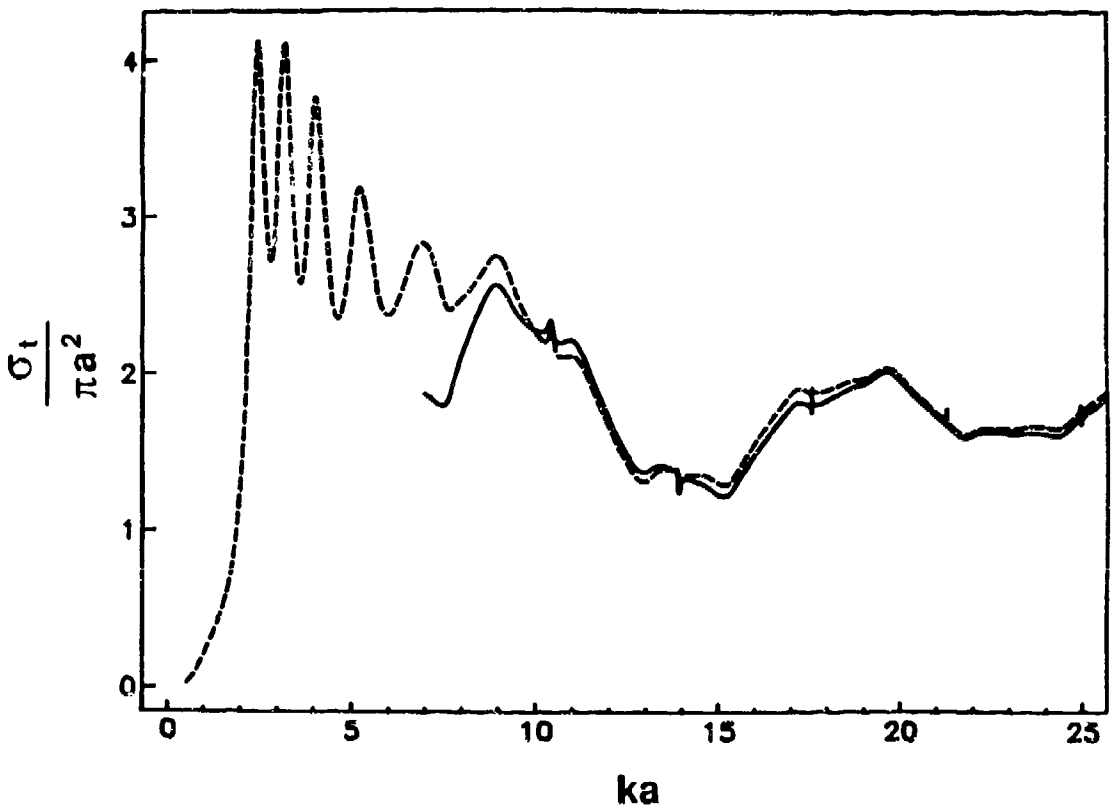

Fig. 4 A comparison of the same *ka* range as in Fig. 3, but the σ_{s_0} contribution has now been included in the ray synthesis. The broad and narrow structures appear to be correctly synthesized. The resolution of each plot was enhanced relative to the plots in Figs. 2 and 3 so as to more accurately describe the narrow s_0 lamb wave resonances.

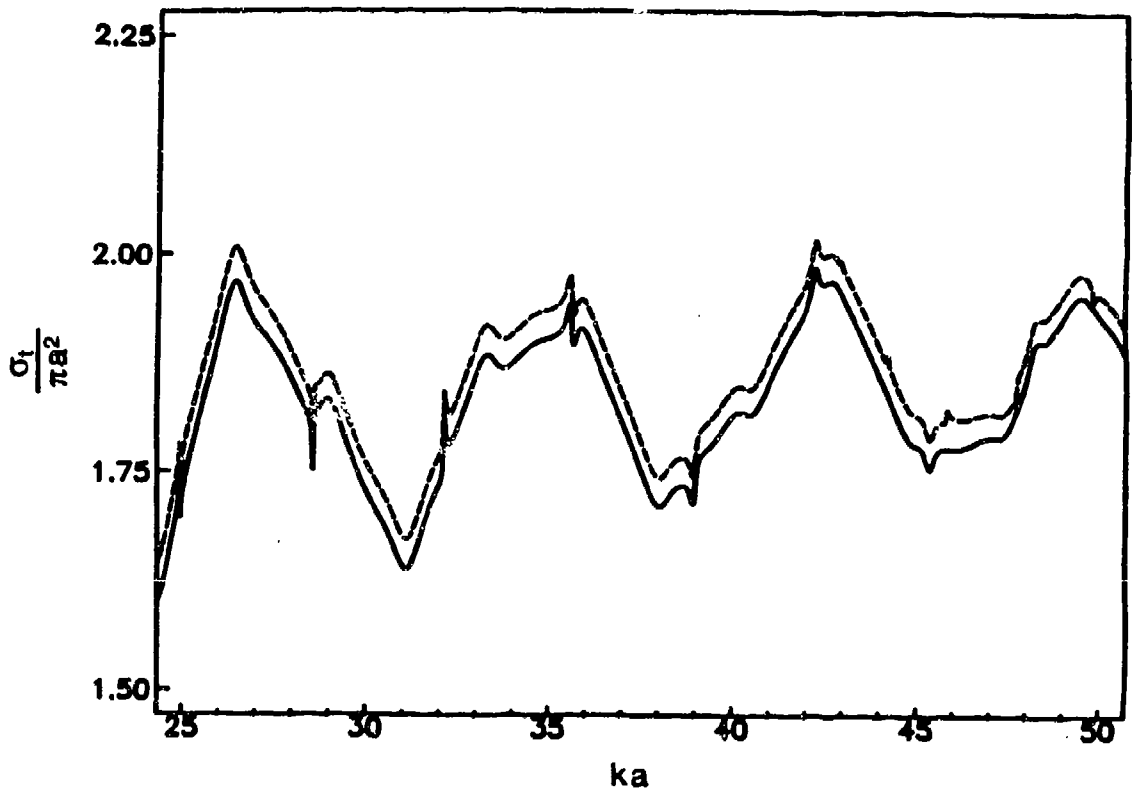

Fig. 5 The dashed curve is the partial wave series result for the normalized total scattering cross section. The ray synthesis (solid curve) contains the contributions σ_{FD}, σ_{a_0} and σ_{s_0}. The broad structure is associated with the a_0 Lamb wave; while the narrow peaks and dips are from the s_0 Lamb wave. This level of synthesis fails to reproduce features at $ka \approx 43$, 44, 46, 48, and 50.

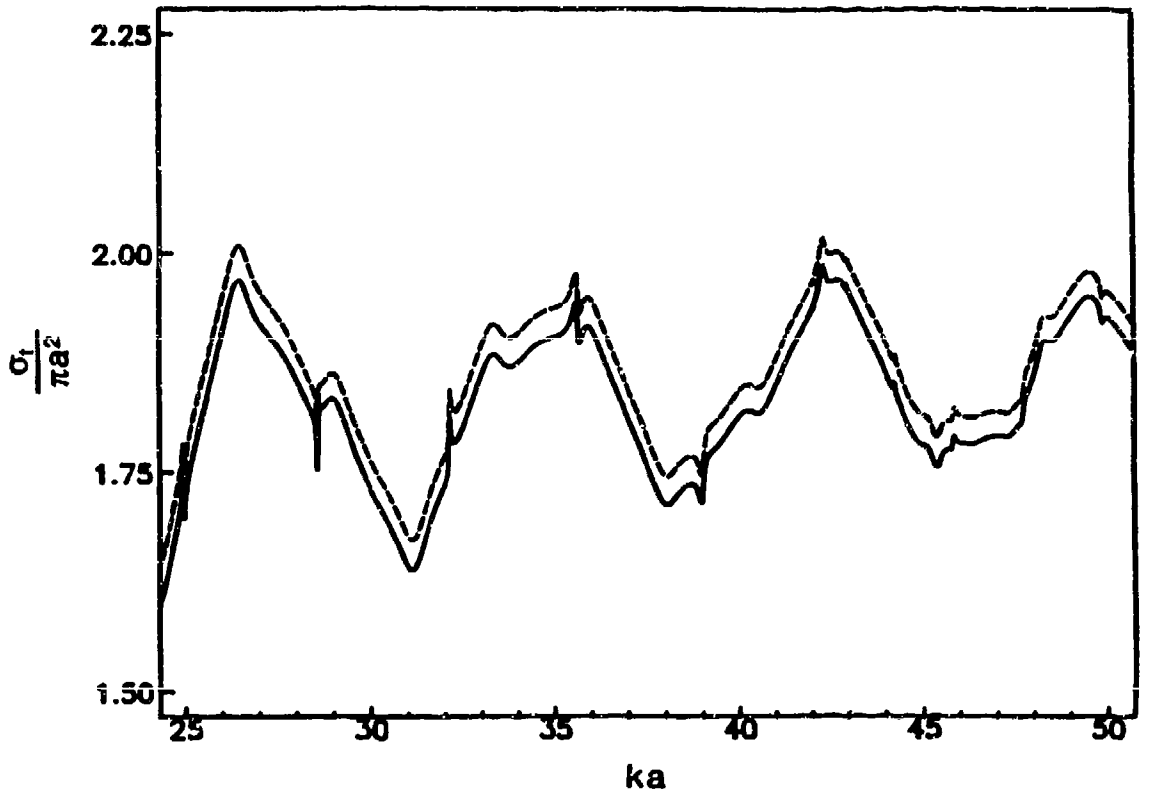

Fig. 6 Like Fig. 5 except the ray synthesis is improved by including σ_{a_1} in the region *ka* > 40.

The ray synthesis for $50 < x < 75$ is shown in Fig. 7. The exact PWS computation is the short dashed line. The solid line is a ray synthesis of the normalized σ_t; where the relevant contributions are: $(\sigma_{FD}/\pi a^2)$, a_0, s_0, and a_1. A comparison of the ray and PWS results demonstrates that these contributions are sufficient to describe both the broad and narrow resonances. In particular, the features in the normalized σ_t for $x < 71$ are entirely due to the a_0, s_0, and a_1 Lamb waves. For $x \geq 71$, the acoustic wavefield in water can couple into the s_1 Lamb wave. The significance of the s_1 Lamb wave to the ray synthesis is observed from the long dashed line in Fig. 7. By adding the s_1 Lamb wave, the ray model is found to give a better approximation of the PWS calculation for $50 < x < 75$.

The last figure, Fig. 8, corresponds to the range $75 < x < 100$. The ray model contains the $(\sigma_{FD}/\pi a^2)$, a_0, s_0, a_1, and s_1 contributions. An examination of the individual components in the synthesis allows one to identify the particular surface wave responsible for a specific structure. It is important to notice the synthesis is essentially the same as the PWS computation except for a small offset. That is, the ray synthesis accurately reproduces the resonance features in this region. Finally, the ray synthesis appears to be approaching the extinction-paradox value of 2.

The offset of the ray result from the PWS computation, evident in Figs. 5 - 8, does not appear to be related to the ray model of the Lamb wave contributions to σ_t since the shape of the modeled structure agrees with the PWS computation. The offset appears instead to be related to the use of a rigid sphere model of ordinary forward diffraction. Numerical tests show that the approximation for the total scattering cross section of a rigid sphere, Eq. (10), converges to the exact rigid PWS result, Eq. (9). For example, at $x = 75$, Eq. (10) yields a value of 1.8965 for $\sigma_{FD}/\pi a^2$, while the exact result from Eq. (9) is 1.8971. The difference of these two calculations is 0.0006; while the offset at $x = 75$ is 0.0344. Clearly, the use of Eq. (10), instead of Eq. (9), for the ordinary forward

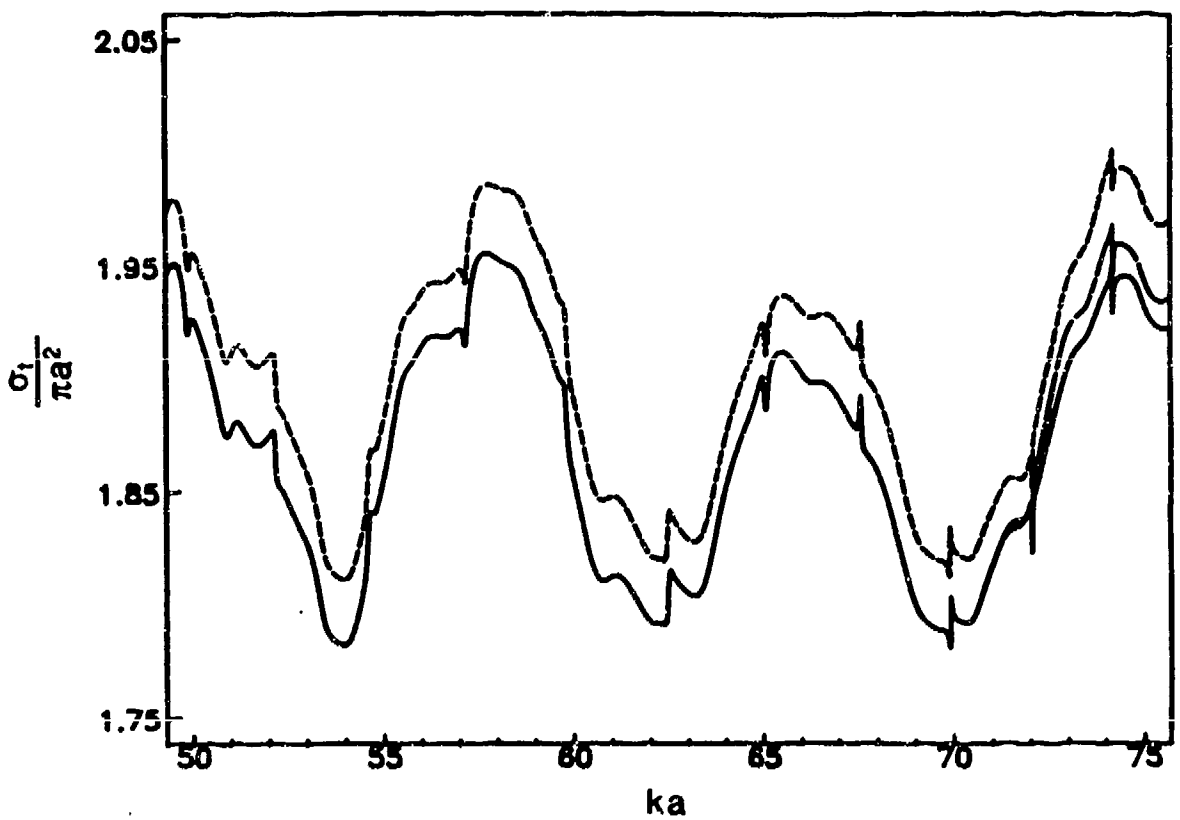

Fig. 7 Like Fig. 6 except for $ka > 70$ where the extra curve with long dashes is a synthesis which includes the s_1 Lamb wave contribution.

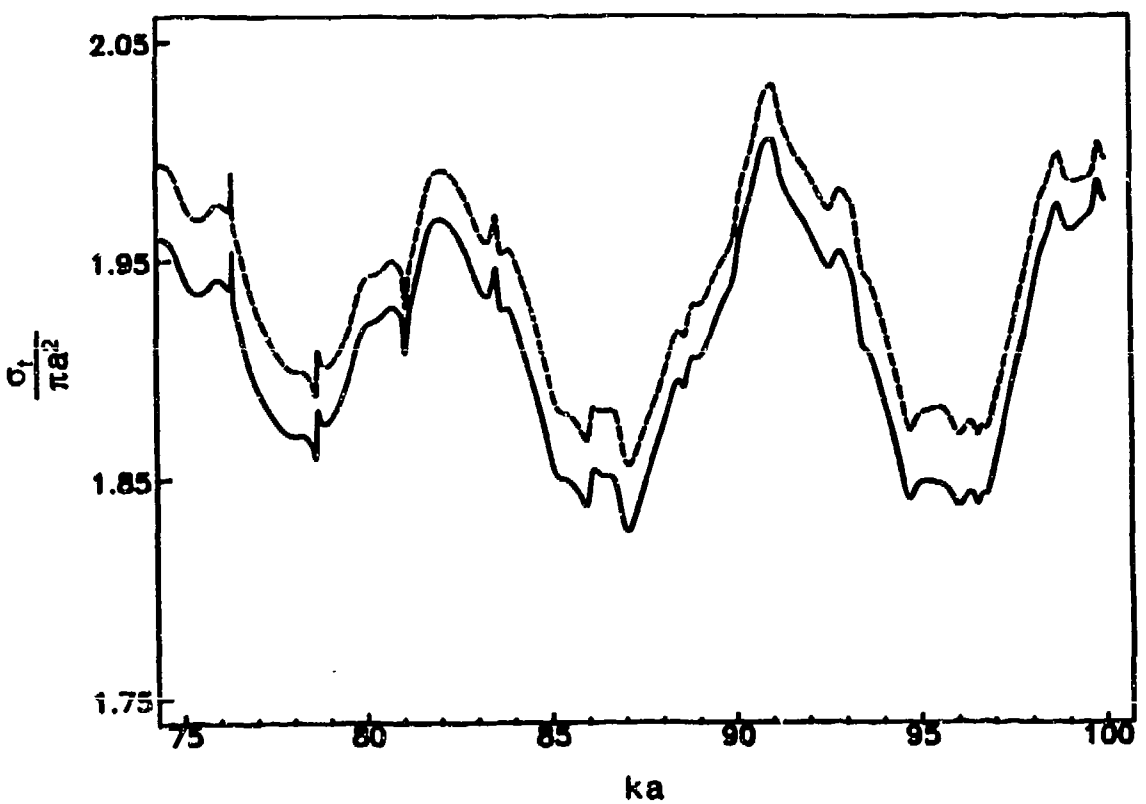

Fig. 8 The comparison of the exact calculation (dashed) and the ray synthesis from the contributions: σ_{FD}, σ_{a_0}, σ_{s_0}, σ_{a_1} and σ_{s_1}.

diffraction does not account for the offset. Furthermore, a comparison of a synthesis (not shown), employing Eq. (9), with the exact PWS, Eq. (5), shows a similar offset. Hence, the total scattering cross section for the rigid sphere is not entirely appropriate for the description of the ordinary forward diffraction contribution to σ_t of an elastic shell. The ordinary forward diffraction component is also not accurately modeled by the total scattering cross section of a soft sphere. That cross section for a soft sphere approaches 2 from above as $x \rightarrow \infty$ and diverges to $+\infty$ as $x \rightarrow 0$.[14,28] It appears that the correct model for σ_{FD} should lie between the values of the cross sections for rigid and soft spheres. This conjecture may also be supported by computations[6] indicating that for shells, poles in the complex *ka* plane "tentatively associated with the Franz wave are considerably removed from their counterparts for a rigid sphere, in the low-*ka* region."

It is noteworthy that the effect of including the s_1 Lamb wave near the right-hand side of Fig. 7 is to reduce an even greater offset between curves which is otherwise present. Inspection of Fig. A1 shows that in this region β_l for $l = s_1$ is relatively large which suggests that rays having large β_l can give rise to a smooth shift in σ_t.

The structure manifest in Fig. 4 in the region $x \lesssim 7$ merits discussion. It is apparently associated with relatively closely spaced resonances since near resonances,[25] the phase and magnitude of f in Eq. (3) can vary rapidly with x. Without attempting to model detailed resonance manifestations it is possible to comment on the nature of the relevant modes. It is shown in Eq. (A6) that the frequency of the lowest purely radial or "breathing" model occurs at $x \approx 6.3$. Calculations of contributions to $f(\theta = \pi)$ given by Sammelmann et al.,[6] based on a generalization of resonance scattering theory, indicate, however, that the breathing resonance contributes weakly to scattering unless the shell is much thinner than the one considered here. As evident from elementary considerations and

the discussion of Eqs. (A4) - (A7), the breathing mode is associated with the $i = s_0$ Lamb wave.

The structure in the region $x \lesssim 7$ is evidently associated with subsonic flexural ($l = a_0$) Lamb waves. Note that the peaks in the plot of $\sigma_t/\pi a^2$ are relatively similar in appearance for $x \lesssim 7$ so it may be anticipated that the underlying mechanism is similar for each peak. Furthermore it is physically plausible that each of these peaks should be associated in some way with resonance scattering, especially since we are viewing the total *scattering* in a region of x where $\sigma_{FD}/\pi a^2$ is relatively small. What may be surprising is that σ_t (and hence σ_e) has peaks of over four times the physical cross section, πa^2, of the sphere. The maximum having the lowest x occurs at $x \approx 2.5$. The elastic mode of a spherical shell having the lowest natural frequency is ordinarily associated with the $n = 2$ (or quadrupole) partial wave with $l = a_0$ (or flexural) motion of the shell. (See, e.g., Ref. 6, 32, and 33.) In conjunction with the aforementioned peak magnitude of $\sigma_e/\pi a^2$, the computations of Skelton and Waterhouse[33] of the acoustic energy streamlines in water near slightly absorbing steel shells are noteworthy. Those calculations, which were performed with an incident wave at the ω of the $n = 2$ resonance, suggest that the energy streamlines may be deflected toward the shell over a cross-sectional area much larger than that of the shell. (Computations of electromagnetic energy flow for light incident on particles[34] have similarly been useful for understanding large optical σ_e.) The other peaks in the region $x \lesssim 7$ are evidently associated with resonances with $n > 2$. Spherical shells typically have several flexural resonances with $n > 2$ at ω below the breathing resonance.[32]

2.6 Forward glory scattering, physical interpretation, and conclusions

The ray synthesis of the total scattering cross section σ_t for a 440c stainless steel shell demonstrates the usefulness and power of this method. The simple parameterization

of the ray model correctly gives the surface elastic wave resonance features of the Lamb wave contributions. Furthermore, this parameterization of σ_l reduces the problem to only the individual Lamb wave damping parameters, β_l, and the phase velocity ratios, c/c_l. Thus, a simple physical interpretation of the observed structure in Figs. 3 - 8 can be achieved.

These computations confirm the validity of the numerical methods used in obtaining β_l and c/c_l for the *lth* type Lamb wave. The above calculations give further support for Marston's approximation, Eq. (15), for the coupling coefficient.[9,29] Also, Figs. 3 - 8 demonstrate the correctness of the assumed phase φ_l of G_l. That is, if φ_l differs significantly from zero, then the contribution of the *lth* Lamb wave to σ_l would be altered by the optical theorem, Eq. (3). For example, we have confirmed that setting $\varphi_l = \pi$ inverts the resonance structure in the synthesis and destroys the agreement with the partial wave series result.

The ray shed in the forward direction from point B' in Fig. 2 appears to emanate from within the sphere. The location of the virtual source may be constructed by considering the crossing of the adjacent dashed ray which differs infinitesimally in direction. By generalization of a discussion given in the Appendix of Ref. 2 to the present case of forward scattering it may be shown that the virtual focus F_l where the dashed ray crosses the forward ray is located a distance equal to the outer radius a of the sphere behind the vertical line through C''. Since Fig. 2 may be rotated about the $C'C''$ axis, the virtual source is ring-like and the forward directed wavefront has locally the shape of a circular torus. Such outgoing toroidal wavefronts from spheres were previously investigated for acoustical backscattering[2,5,35] and give rise to what has been termed "glory scattering" because the enhancement of light scattering from cloud droplets (known as the optical glory) is attributable to toroidal outgoing optical wavefronts.[12]

From the discussion above it is evident that the structure in Figs. 3 - 8 attributable to Lamb wave contributions is also a manifestation of forward-directed glory scattering. The important point is that the rays associated with the Lamb waves couple on-to and off-of the sphere with nonzero impact parameters so the associated outgoing wavefront is toroidal and the contribution to the form function $f(\theta = 0)$ is enhanced by axial focusing. While the backward directed glory has long been of interest,[12] Nussenzveig and Wiscombe[36] relatively recently noted that the forward optical glory of dielectric spheres gives rise to an oscillation of the normalized optical extinction cross section which is quasi-periodic in the optical *ka*. (The mechanism for producing optical glory rays in solid dielectric spheres is somewhat different from that considered here for elastic shells.) The scattering pattern associated with a forward directed optical glory has been observed in polarized light scattered from bubbles in a viscous silicone oil.[37] Direct experimental evidence of forward glory scattering of sound from shells due to Lamb waves has been obtained for scattering of short tone bursts in experiments similar to those described in Ref. 5 but with the hydrophone placed on the forward axis.[38,39] What follows is a brief summary of an observation relevant to the present discussion.

Figure 9 shows a time record of the amplified signal from a hydrophone placed on the forward axis. The sphere is 440c stainless steel of radius $a = 19.05$ *mm* and $b/a = 0.838$. The incident burst was four cycles of a 653 *kHz* sine wave which corresponds to $ka \approx 53$. The experimental technique is similar to the one described in Ref. 5 for backscattering from the same shell. The large burst is attributable to rays in the water which graze the sphere. (That may be demonstrated by removing the sphere and observing the arrival time of a signal directly from the source.) The burst which arrives 11 μs prior to the large burst is attributable to forward glory scattering associated with Lamb waves on the sphere. It arrives prior to the large burst since the (slower) grazing ray has its entire path in

water. From inspection of Fig. 2, the burst which travels along path *ABB'A'* is advanced in time relative to a burst which just grazes the sphere at point *E* by an amount

$$\Delta t_l = (2a/c)\cos(\theta_l) - (a/c_{gl})(\pi - 2\theta_l)\,, \tag{17}$$

where the calculation of the group velocity c_{gl} for the *lth* Lamb wave is discussed in Ref. 5. This burst is associated with the $m = 0$ term in Eq. (12). It is noteworthy that for supersonic Lamb waves ($c_l > c$) where Fig. 2 is applicable, that $\Delta t_l > 0$ when (as is usually the case) $c_{gl} > c$. For the sphere under consideration, Eq. (17) predicts $\Delta t_l = 11$ μs for both $l = a_0$ and s_0 when $ka = 53$, in agreement with the observations. From the arrival time alone it is not possible to discriminate between $l = a_0$ and s_0 Lamb waves mechanisms at this *ka*. (At other *ka*, the calculated Δt_l for these *l* differ.) The late structure of the record shown in Fig. 9 is at least partially associated with Lamb waves which have traveled completely around the shell and radiate in the forward direction. A direct comparison of the amplitudes of the Lamb wave and edge diffracted bursts in Fig. 9 is not easily made with theory because of complications in calculating the edge diffracted ray amplitude for an observer not in the far field. Nevertheless, from the arrival time and appearance of the early burst in Fig. 9, *it can be concluded that forward directed Lamb wave contributions to scattering may be readily observed.* It was also observed[38,39] that the amplitude of the early Lamb wave burst decreases as the receiver is moved off the axis in the way characteristic of axially focused (or glory) scattering,[2,5,35]

Consider again the total cross section and form functions characteristic of steady state scattering. Inspection of Figs. 7 and 8 reveals the presence of a broad structure having a quasiperiod $\Delta x \approx 9$. This structure is primarily due to the variation in phase with *ka* of the f_l contribution with $l = a_0$ as shown by the analysis which follows. From inspection of Eqs. (3) and (14) it may be anticipated that σ_l contains a structure periodic in

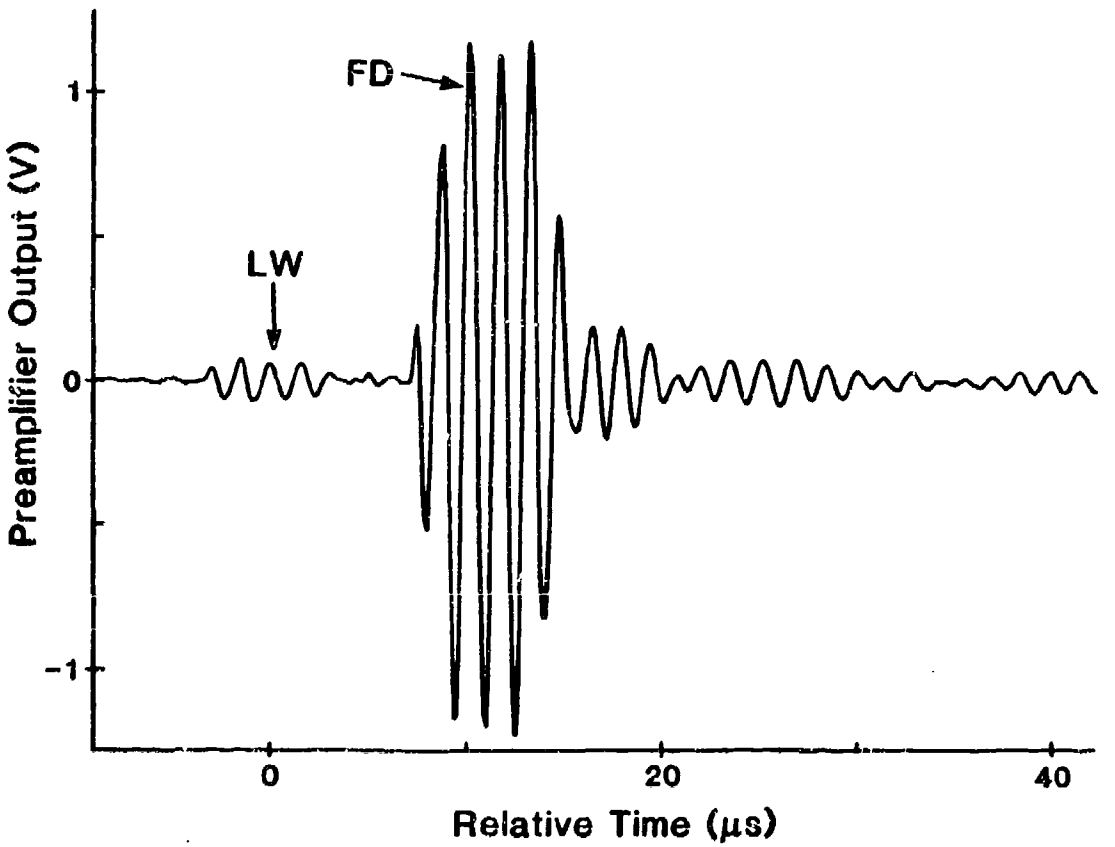

Fig. 9 Time record of on-axis forward scattering of a 653 *kHz* 4 cycle tone burst from a stainless steel shell. The contribution labeled FD is associated with ordinary forward diffraction. It is preceded by a contribution labeled LW attributed to Lamb waves because of its arrival time. The observation experimentally confirms the existence of a forward directed Lamb wave contribution. The structure following the FD burst is at least partially attributable to repeated circumnavigation of Lamb waves, though there may be some weak scattering from a three-pronged wire mount which supported the sphere.

changes of η_l by -2π. (It is noteworthy here that at resonance[3,9] $exp(i2\pi xc/c_l) = -1$ and the denominator in Eq. (14) has a specific phase.) From Eq. (13), the change in x associated with $\Delta\eta_l = -2\pi$ may be approximated as

$$\Delta x_l \approx 2\pi[2\cos(\theta_l) - (c/c_l)(\pi - 2\theta_l)]^{-1}, \qquad (18)$$

provided that c_l depends sufficiently weakly on x that dispersion may be neglected. Of particular interest is the result that for $l = a_0$, c_l/c increases only from 1.95 to 2.04 as x increases from 50 to 100. Taking $ka \approx 75$ gives $c_l/c = 2.028$ and Eq. (18) predicts $\Delta x_l \approx 9.0$ in agreement with the quasiperiod manifest in the calculations. The apparent relative importance of the $l = a_0$ contribution to the underlying structure may be attributable to the relatively large value of the associated $|G_l|$ evident in Fig. 13 of Ref. 5. (The $l = s_0$ contribution may also produce a superposed broad structure in σ_t; however, it is more difficult to estimate the associated quasiperiod because of dispersion.) *Note that the separation Δx_l is not directly caused by the separation of specific resonances though the finer structure in σ_t is attributable to resonances.* When the surface elastic waves are only weakly dispersive the spacing between resonances may be approximated as $\Delta x_l^{res} \approx c_{gl}/c$ (see, e.g., Ref. 7) and when dispersion is negligible this becomes[9] $\Delta x_l^{res} \approx c_l/c$. Hence for $l = a_0$ and the ka region considered above $\Delta x_l^{res} \approx 2$ which is much less than the quasiperiod of the broad structure.

Nussenzveig and Wiscombe[36] note that the structure in the optical σ_t of dielectric spheres (which is quasiperiodic in ka) arises from an "interference between the forward diffraction peak and forward glory contributions ...". Though the details of the glory contributions differ here, this interference condition also leads directly to Eq. (18) for weakly dispersive Lamb waves. [This may have been anticipated by comparing the form of Eq. (18) with the consequence of setting in Eq. (17), Δt_l to an integer multiple of the

wave period $2\pi/\omega$.] Another example of a broad modulation of a cross section is that of backscattering from a tungsten carbide sphere discussed by Williams and Marston.[3] For certain *ka* regions, resonance reduces the total amplitude, but at other regions, it causes an increase. In that case the relevant interference was between the specular contribution and the contribution due to Rayleigh waves on the sphere.

There has been increased interest in ray treatments of wave propagation on cylindrical shells.[8,9,40,41] It seems appropriate therefore to comment on the connection between ray methods for leaky surface elastic waves on cylinders (Sec. V of Ref. 9) with the present results for the forward glory of spheres. The connection is as outlined in Sec. VI of Ref. 9 where it is shown that ray results for cylinders may be adapted to construct the farfield amplitude due to surface elastic waves on spheres. The G_l used here in Eqs. (12) and (14) and elsewhere in Refs. 1, 3, 5, and 9 for spheres is descriptive of farfield amplitudes. The coupling coefficient G_l^{cy} for cylinders (Ref. 9, Sec. V) is at least approximately descriptive of near field as well as far field amplitudes. The cylinder analysis facilitates the approximation of the local amplitude of the outgoing toroidal wavefront near a sphere [Eqs. (54) and (57) of Ref. 9] and the approximation of the diffraction integral for glory scattering[35] relates those local amplitudes to the far-field form function f_l. [See Eq. (55) of Ref. 9.] It is the intent of one of us (P.L.M.) to give a more detailed description of the connection of results for spheres and cylinders in a subsequent publication.[42]

It is noteworthy that since the optical theorem in its most general form[11,12,19-21] relates σ_e to the forward scattering amplitude, it is applicable to objects having complicated shapes. In principle, at high frequencies ray methods could be developed to estimate forward acoustical amplitudes and give approximations for σ_e of complicated objects. Furthermore, ray methods could be used which include absorption by the object.

Acknowledgment

This research was supported by the Office of Naval Research. Partial results were presented at the 117*th* meeting of the Acoustical Society of America (Syracuse, New York, May 1989).

Appendix A. Lamb wave damping parameters, phase velocities, and the effect of the breathing mode

The Lamb waves considered in Ref. 5 are the lowest antisymmetric or flexural wave, a_0, and the lowest symmetric wave, s_0. The material and geometrical parameters for the particular shell studied in Ref. 5 are given here in Sec. 2.5 and the range considered was $20 < x < 75$. We extended, here, the range of $x = ka$ for both a_0 and s_0 to $7 < x < 100$. Furthermore, we find that the a_1 and s_1 waves can be excited on the elastic shell for x greater than 41 and 70, respectively. The contributions of the a_1 and s_1 waves to σ_t are discussed in Sec. 2.5.

The numerical method, implemented in the determination of β_l and c_l/c is given in Appendix A of Ref. 5. The equations to be solved are based on applying Watson transform methodology given for solid elastic spheres[1,3] to the case of a spherical shell.[5,9] The relevant results are as follows:

$$D_{\nu_l}(x) = 0 \,, \tag{A1}$$

$$\nu_l = \alpha_l + i\beta_l \,, \tag{A2}$$

$$(c_l/c) = x/(\alpha_l + 1/2) \,. \tag{A3}$$

Equation (A1) uses the determinant in the denominator of the PWS, Eq. (4), for the elastic shell; where the integer index, n, has been replaced everywhere by the complex index, ν_l.

The complex index, ν_l, is obtained by solving Eq. (A1) at fixed values of x. The damping parameter, $\beta_l = Im\{\nu_l\}$, is immediately obtained (as a function of x) for the *lth* type Lamb wave. Figure A1 is a plot of ν_l for four Lamb waves that can be excited on the shell considered. It should be noted that the radiation damping is not necessarily weak.[9] In solving Eq. (A1), Bessel functions of the first and second kind of complex order and real argument y must be calculated. A discussion of the algorithm employed for these functions is given in an appendix of Ref. 43. When the conditions $|\nu_l| \geq 3$ and $y/|\nu_l| \geq 10^{-6}$ hold, then the calculated values are asserted to have errors of less than 0.00001 + i0.00001. From inspection of Fig. A1, it is found that for the s_0 and a_1 Lamb waves the condition $|\nu_l| \geq 3$ is violated at small *ka*. However, the computations presented in Sec. 2.5 suggest that the accumulated error from these two contributions are not significant. We did not search for roots corresponding to a generalization[6] of rigid-sphere Franz waves to the shell since those would be expected to have large β_l and c_l near c.

The normalized phase velocity is determined by using Eq. (A3). The dispersion curves for the various Lamb waves are displayed in Fig. A2. There are three features that are important to note. First, the normalized velocities for the a_1 and s_1 Lamb waves appear to diverge as they approach their cut-off frequencies. (These cut-off frequencies are analogous to the cut-off frequencies for the propagation of particular modes in a waveguide. There is, however, additional structure near the cut-off of the s_1 mode, the detail of which is not shown in Figs. A1 and A2.) Second, the c_l for $l = s_0$ appears to diverge as ω approaches the natural frequency ω_B of the lowest purely radial or "breathing" mode of the shell. This divergence is plausible since radial motion of a shell can have the same phase at all surface points when $\omega = \omega_B$. For a thin spherical shell in a vacuum, ω_B is related to the lowest purely radial or "ring" frequency ω_R of an infinite cylindrical shell of the same material via the approximation

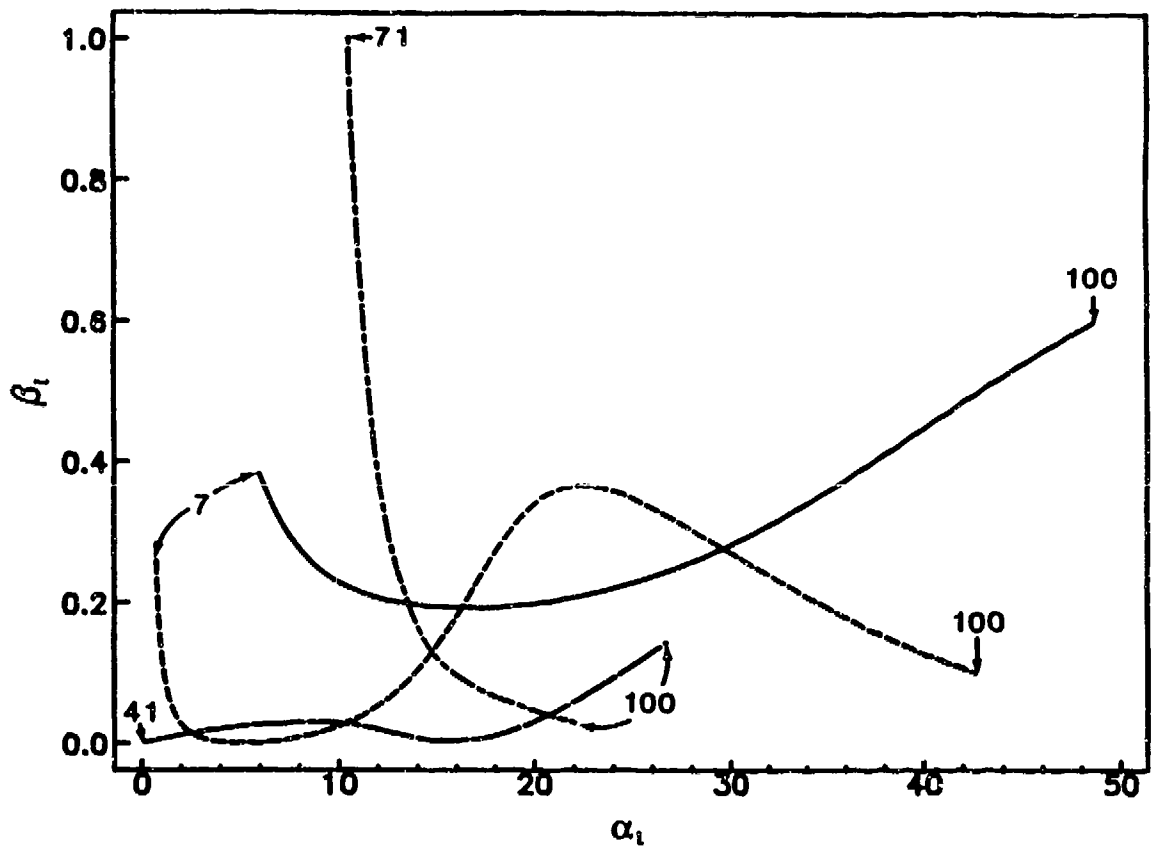

Fig. A1 The loci of roots, ν_l, from Eq. (A1) for the a_0, s_0, a_1, and s_1 Lamb waves on a fluid loaded stainless steel shell. These loci are respectively the solid, short-dashed, long-dashed, and short-long dashed curves. The arc length along each curve is monotonic in *ka* and the lower and upper values of *ka* are indicated.

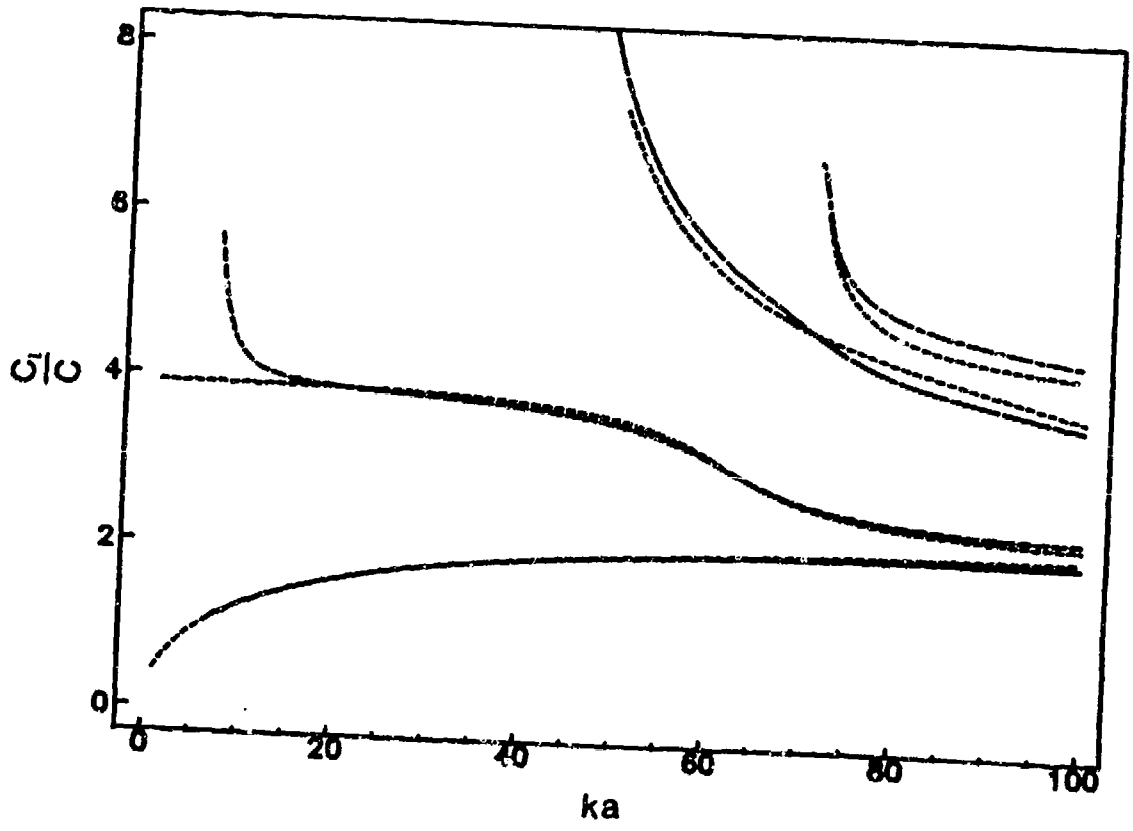

Fig. A2 Normalized phase velocities along the outer surface of the shell, for a_0, s_0, a_1, and s_1 Lamb waves. The legend is as in Fig. A1 except that adjacent to each curve is one with short dashes which was calculated from plate theory corrected approximately for curvature as described in Ref. 45 and Eq. (A8). Note that the true c_l, $l = s_0$, appears to diverge as the ka of the breathing mode is approached.

$$\omega_B \approx [2(1 + V)]^{1/2}\omega_R , \tag{A4}$$

where V denotes Poisson's ratio which for 440c stainless steel is 0.296. Equation (A4) follows from Eq. (7.114) of Ref. 32. For a thin shell[32]

$$\omega_R \approx c_{PL}/\bar{a} , \quad c_{PL} = [E/(1 - V^2)\rho_S]^{1/2} = 5.31 \text{ mm}/\mu\text{s}, \tag{A5}$$

where E denotes Young's modulus, c_{PL} is the low-frequency phase velocity of compressional waves in an elastic plate and $\bar{a} = (a + b)/2$ is the middle radius of the shell. (The combined result for ω_B also follows from Love.[44]) If the effects of fluid loading on resonance frequency are completely neglected, the estimated ka of the breathing resonance is

$$x_B = \frac{\omega_B a}{c} \approx [2(1 + V)]^{1/2}[1 - (h/2a)]^{-1}(c_{PL}/c) = 6.3 , \tag{A6}$$

where $h = a - b$ is the shell thickness. For a shell surrounded by water, fluid loading reduces x_B by a fraction of order

$$m_B/\rho_S h \approx (\rho/\rho_S)\,(a/h)\,x_B^{-2}, \tag{A7}$$

where $m_B \approx \rho a\, x_B^{-2}$ is the relevant "model accession to inertia" ratio.[32] Since $m_B/\rho_S h \approx 0.018 << 1$ for the sphere considered, fluid loading should cause x_B to be reduced only slightly from the estimate based on (A4). The third feature is a cut off frequency for the s_1 wave. It is somewhat analogous to the cutoff near the breathing mode since it lies close to the condition $ka \approx \pi c_L/c(1 - b/a) \approx 77$ of the lowest thickness resonance discussed in Sec. III of Ref. 5.

The shortest dashed curves in Fig. A2 are the results of introducing a curvature correction[45] into Lamb's equations (given in Ref. 5) for a flat plate in a vacuum. The thickness of the plate is the thickness $h = a(1 - b/a) \approx 3.1$ *mm* of the shell. The approximate curvature correction gives the phase velocity ratio as[45]

$$(c_l/c) = [(c_l)_p/c][1 - (h/2a)]^{-1}, \qquad \text{(A8)}$$

where $(c_l)_p$ is the phase velocity of the *lth* Lamb wave on the plate. The comparison in Fig. A2 shows that a useful initial estimate of the phase velocity ratio can still be obtained through Eq. (A8) and the plate equations. The deviation of the s_0 result from (A8) with the proper value from (A3) is a manifestation of the hoop stresses associated with the breathing mode discussed above. The difference between the curves for both the a_1 and s_1 Lamb waves may be due to the radiation loading. The curvature of the plot of c_l/c with $l = s_1$ at the mode onset may be associated with the relatively large value of β_l evident in Fig. A1.

Root computations not shown in Figs. A1 and A2 indicate that there is a mode for which the low-frequency cut off is at $x \approx 83$ for which c_l/c always exceeds 8 in the region between this cut off and $x = 100$. We have tentatively identified this mode as the s_2 mode. Computations indicate that it does not significantly affect σ_l in the region considered, evidently due to the smallness of the c/c_l factor in Eq. (15) and the magnitude of β_l.

References

1. K. L. Williams and P. L. Marston, "Backscattering from an elastic sphere: Sommerfeld-Watson transformation and experimental confirmation," J. Acoust. Soc. Am. 78, 1093-1102 (1985); 79, 2091 (1986).
2. K. L. Williams and P. L. Marston, "Axially focused (glory) scattering due to surface waves generated on spheres: Model and experimental confirmation using tungsten carbide spheres," J. Acoust. Soc. Am. 78, 722-728 (1985).
3. K. L. Williams and P. L. Marston, "Synthesis of backscattering from an elastic sphere using the Sommerfeld-Watson transformation and giving a Fabry-Perot analysis of resonances," J. Acoust. Soc. Am. 79, 1702-1708 (1986).
4. J. W. Dickey and H. Uberall, "Acoustic high-frequency scattering by elastic cylinders," J. Acoust. Soc. Am. 66, 275-283 (1979).
5. S. G. Kargl and P. L. Marston, "Observations and modeling of the backscattering of short tone bursts from a spherical shell: Lamb wave echoes, glory, and axial reverberations," J. Acoust. Soc. Am. 85, 1014-1028 (1989).
6. G. S. Sammelmann, D. H. Trivett and R. H. Hackman, "The acoustic scattering by a submerged, spherical shell. I: The bifurcation of the dispersion curve for the spherical antisymmetric Lamb wave," J. Acoust. Soc. Am. 85, 114-124 (1989).
7. G. C. Gaunaurd and M. F. Werby, "Lamb and creeping waves around submerged spherical shells resonantly excited by sound scattering," J. Acoust. Soc. Am. 82, 2021-2033 (1987).
8. V. A. Borovikov and N. D. Veksler, "Scattering of sound waves by smooth convex elastic cylindrical shells," Wave Motion 7, 143-152 (1985).

9. P. L. Marston, "GTD for backscattering from elastic spheres and cylinders in water and the coupling of surface elastic waves with the acoustic field," J. Acoust. Soc. Am. 83, 25-37 (1988).

10. G. Johnson and R. Truell, "Numerical computations of elastic scattering cross sections," J. Appl. Phys. 36, 3466-3474 (1965).

11. H. M. Nussenzveig, *Causality and Dispersion Relations* (Academic, New York, 1972) pp. 47-52.

12. H. C. van de Hulst, *Light Scattering by Small Particles* (Dover, New York, 1981) pp. 30-31, 107-108.

13. H. Levine and J. Schwinger, "On the theory of diffraction in an infinite plane screen. I," Phys. Rev. 74, 958-974 (1948). Although Eq. (2.29) from Levine and Schwinger is the transmission cross section for an aperture, it may be inferred from Babinet's principle that Eq. (2.29) is equivalent to the total scattering cross section for a complementary scatterer.

14. S. I. Rubinow and T. T. Wu, "First correction to the geometric-optics scattering cross section from cylinders and spheres," J. Appl. Phys. 27, 1032-1039 (1956).

15. T. T. Wu "High frequency scattering," Phys. Rev. 104, 1201-1212 (1956); I. G. Lisle *et al.*, "Numerical corrections of Wu's coefficients for scattering of high-frequency waves from spheres and cylinders," Phys. Rev. Lett. 55, 555-557 (1985).

16. V. C. Anderson, "Sound scattering from a fluid sphere," J. Acoust. Soc. Am. 22, 426-431 (1950).

17. R. W. Hart, "Sound scattering of a plane wave from a nonabsorbing sphere," J. Acoust. Soc. Am. 23, 323-329 (1951).

18. R. W. Hart and E. W. Montroll, "On the scattering of plane waves by soft obstacles. I. Spherical obstacles," J. Appl. Phys. 22, 376-386 (1951); E. W. Montroll and K. W. Hart, "Scattering of plane waves by soft obstacles. II. Scattering by cylinders, spheroids, and disks," J. Appl. Phys. 22, 1278 - 1289 (1951); E. W. Montroll and J. M. Greenberg, "Scattering of plane waves by soft obstacles. III. Scattering by obstacles with spherical and circular cylindrical symmetry," Phys. Rev. 86, 889-898 (1952).

19. R. G. Newton, "Optical theorem and beyond," Am. J. Phys. 44, 639-642 (1976).

20. H. C. van de Hulst, "On the attenuation of plane waves by obstacles of arbitrary size and form," Physica 15, 740-746 (1949).

21. D. S. Jones, "On the scattering cross section of an obstacle," Philos. Mag. 46, 957-962 (1955).

22. J. B. Keller, "Quantum mechanical cross sections for small wavelengths," Am. J. Phys. 40, 1035-1036 (1972).

23. J. B. Keller, "Geometrical theory of diffraction," J. Opt. Soc. Am. 52, 116-130 (1962).

24. A. D. Pierce, *Acoustics: An introduction to its physical principles and applications* (McGraw-Hill, New York 1981) p. 430.

25. L. Flax, G. C. Gaunaurd and H. Uberall, "Theory of resonance scattering," in *Physical Acoustics* edited by W. P. Mason and R. N. Thurston (Academic, New York 1981), vol. 15, pp. 191-294.

26. P. Beckmann and W. Franz, "Berechnung der streuquerschnitte von kugel und zylinder unter anwendneg einer modifizierten Watson-Transformation," Z. Naturforschg. 12a, 533-537 (1957).

27. A comparison of the appropriate series expressions in Refs. 15 and 26 shows that the third terms are different. Beckmann and Franz note the difference, but claim a direct comparison of the two methods of derivation to account for the discrepancy would have been difficult.

28. H. M. Nussenzveig, "Uniform approximation in scattering by spheres," J. Phys. A: Math. Gen. 21, 81-109 (1988).

29. P. L. Marston and K. L. Williams, "GTD for backscattering from elastic objects in water: Phase of the coupling coefficient and a simplified synthesis of the form function," J. Acoust. Soc. Am. Suppl. 83, 94 (1988).

30. S. G. Kargl and P. L. Marston, "GTD synthesis of resonance amplitudes in the backscattering from an elastic spherical shell," J. Acoust. Soc. Am. Suppl. 85, 150 (1989).

31. W. J. Wiscombe, "Improved Mie scattering algorithms," Appl. Opt. 19, 1505-1509 (1980).

32. M. C. Junger and D. Feit, *Sound Structures and Their Interaction*, second edition (MIT Press, Cambridge, 1986) Sec. 6.5, 7.15, 7.18, and 9.2.

33. E. A. Skelton and R. V. Waterhouse, "Energy streamlines for a spherical shell scattering plane waves," J. Acoust. Soc. Am. 80, 1473-1478 (1986).

34. C. F. Bohren, "How can a particle absorb more than the light incident on it?," Am. J. Phys. 51, 323-327 (1983).

35. P. L. Marston and D. S. Langley, "Glory- and rainbow-enhanced acoustic backscattering from fluid spheres: Models for diffracted axial focusing," J. Acoust. Soc. Am. 73, 1464-1475 (1983); 78, 1128 (1985).

36. H. M. Nussenzveig and W. J. Wiscombe, "Forward optical glory," Opt. Lett. 5, 455-457 (1980).

37. P. L. Marston and D. S. Langley, "Forward optical glory from bubbles (and clouds of bubbles) in liquids and other novel directional caustics," in *Multiple Scattering of Waves in Random Media and Random Rough Surfaces*, edited by V. V. Varadan and V. K. Varadan (Pennsylvania State University, University Park, PA, 1987) pp. 419-429.

38. P. L. Marston, *Annual Report for Contract N00014-85-C-0141*, 1986; available from the Defence Technical Information Center (Cameron Station, Alexandra, VA), Accession Number AD-A174401.

38. S. G. Kargl and P. L. Marston, "Forward-glory scattering from a spherical shell and backscattering from a convex hemispherical shell," J. Acoust. Soc. Am. Suppl. 84, 208 (1988).

40. A. D. Pierce, "Wave propagation on thin-walled elastic cylindrical shells," in *Elastic Wave Propagation*, edited by M. F. McCarthy and M. A. Hayes (Elsevier, New York, 1989), pp. 205-210.

41. L. B. Felsen and I. T. Lu, "Ray treatment of wave propagation on thin-walled curved elastic plates with truncations," J. Acoust. Soc. Am. 86, 360-374 (1989).

42. P. L. Marston, S. G. Kargl, and K. L. Williams, "Rayleigh, Lamb, and Whispering Gallery Wave Contributions to Backscattering from Smooth Elastic Objects in Water Described by a Generalization of GTD," in *Elastic Wave Propagation and Ultrasonic Nondestructive Evaluation*, edited by S. K. Datta, J. D. Achenbach, and Y. S. Rajapakse (Elsevier Science Publishers, Amsterdam, 1990) pp. 211 - 216.

43. K. L. Williams, Ph.D. thesis, Washington State University (1985); available from the Defence Technical Information Center (Cameron Station, Alexandra, VA), Accession Number AD-A158884.

44. A. E. H. Love, *A Treatise on the Mathematical Theory of Elasticity*, 4th edition (Dover, New York, 1944) article 335.

45. P. L. Marston, "Phase velocity of Lamb waves on a spherical shell: Approximate dependence on curvature from kinematics," J. Acoust. Soc. Am. 85, 2663-2665 (1989).

Chapter 3

Longitudinal resonances in the form function for backscattering from a spherical shell: Fluid shell case

Abstract

Reverberations of longitudinal waves in a hollow shell can strongly affect the backscattering amplitudes at frequencies associated with a thickness resonance. The phenomena is studied for the idealized case of vanishing shear stresses in the shell material by taking that material to be an inviscid fluid. The sound speed c_L for the fluid is taken to be that of longitudinal waves in elastic materials of interest; the surrounding fluid being water. An exact partial-wave series gives the form function f for backscattering and plots of $|f|$ as a function of ka display resonance features where a denotes the outer radius of the shell. These features are also recovered in a direct geometrical calculation of f which sums the amplitudes associated with rays multiply reflected within the curved shell. This geometric synthesis shows that the effects of curvature are essential to modeling f. In addition to numerical comparisons with the partial wave series, the geometrical calculation is tested by considering several limiting cases and results anticipated from elementary consideration are recovered.

3.1 Introduction

Various authors have considered how resonances affect the reflection of sound from flat elastic plates[1] and fluid layers.[2] Others have considered the significance of surface guided wave contributions to the backscattering of an incident plane wave from elastic spherical[3-6] and circular cylindrical shells.[6-8] The scattering amplitude can be represented in terms of contributions from surface guided waves which circumnavigate the shell, continually radiating energy into the surrounding water. This surface guided wave representation can give a simple quantitative description of resonances which has been studied in detail for solid spheres.[9,10] When exploring such a representation for elastic shells,[11] we have seen a justification for investigating the reverberation of bulk waves transmitted through curved shells which reflect from the inner surface. Associated with transmitted (bulk) longitudinal waves are thickness resonances.[3,12] To isolate the contribution of reverberation of transmitted longitudinal waves from other contributions, we restrict our attention to backscattering from an evacuated, idealized spherical fluid shell in water. This simplification allows a quantitative ray representation of the scattering amplitude to be developed and tested without considering contributions associated with transverse waves. The testing of ray models for fluid objects can be justified because of insight gained into the behavior of more complicated situations.[13]

The usual condition for the existence of a longitudinal resonance is that the thickness of an empty shell should be an integral number of $\lambda_L/2$ where λ_L is the longitudinal wavelength within the fluid. This condition is applicable when the impedance $\rho_e c_L$ of the shell material exceeds ρc of the surrounding fluid. For an incident acoustic plane wave with angular frequency ω, the resonance condition can be written as

$$k_L h = n\pi, \qquad (n = 1, 2, \ldots), \qquad (1)$$

where $k_L = \omega/c_L$ is the wavenumber and c_L is the speed of sound in the fluid.[3] As will be shown below, the manifestation of thickness resonances is contained within the specular reflection form function f_{sp} and is intimately related to the curvatures of the inner and outer surfaces of the shell. Examination of $|f_{sp}|$ shows that the effects of curvature are largest for those $k_L h$ satisfying Eq. (1).

The organization of this paper is as follows. A derivation of a ray acoustical representation of the form function is summarized in Sec. 3.2. This geometrical synthesis of f_{sp} decomposes into a contribution for the reflection from a vacuum-backed flat plate and a curvature dependent component, f_{cc}. In Sec. 3.2, the synthesis is compared with exact computations employing the *partial-wave series* (PWS) representation of the form function for backscatter. Section 3.3 examine the significance of the curvature correction f_{cc}. Within Sec. 3.3, the most significant contributions to f_{cc} are observed to occur at the resonance condition Eq. (1). To further support the claim that the form obtained for f_{cc} is correct, Sec. 3.4 considers several limiting cases of the fluid shell parameters. Each limiting case produces the expected result and thus supports the geometrically derived form of the curvature correction. Section 3.5 contains concluding remarks and notes the importance of f_{cc} to the scattering of an acoustic plane wave from an elastic spherical shell.

The article contains three appendices. Appendix A contains the essential details of the matrix method employed in determining the geometrical spreading factor and amplitude coefficient introduced in Sec. 3.2. As noted in Appendix A, the matrix method is similar to the paraxial matrix methods of geometric optics. Appendix B is included for completeness and contains information pertinent to the PWS representation of f for backscattering from a fluid shell. Finally, Appendix C describes a technique which rapidly sums the infinite series in f_{cc}.[14] An example of the rapid summation technique is compared to the exact summation of the series where the convergence of the series is explicitly tested.

3.2 The specular reflection for a fluid shell from geometric ray methods.

Consider an empty spherical shell of inviscid fluid embedded in a fluid (water). The outer radius of the shell is denoted by a and the inner radius is given by b. The interior of the fluid shell is taken to be a vacuum. That is, the inner surface at b is a pressure release surface. The relevant parameters for the water are the sound speed, c, and the density, ρ. The sound speed and density of the fluid are c_L and ρ_e, respectively. The scattered pressure in the farfield is

$$p_{sc} = p_0 \frac{af}{2} \frac{e^{ikr}}{r}, \tag{2}$$

where the harmonic time dependence $exp(-i\omega t)$ has been suppressed.[6,9] The wavenumber of the incident plane wave in water is $k = \omega/c = 2\pi/\lambda$ where ω is the angular frequency and λ is the wavelength. The pressure amplitude of the incident plane wave is p_0 and the distance from the center of the sphere to an observation point is r. The scattering amplitude or form function, f, can be approximately partitioned as $f \approx f_{sp} + f_{sw}$ where f_{sp} is a contribution from a specular reflection and f_{sw} is a term associated with the possible excitation of surface guided waves. As stated above, Sec. 3.2 is concerned with a geometric synthesis of f_{sp}.

Figure 1 is a simplified ray diagram for the backscattering of an acoustic plane wave from an ideal fluid spherical shell.. The plane wave is assumed to be traveling in the positive z-direction and the origin of the coordinate system is located at the center of the shell at point O. The z-axis coincides with the line SO. The specular reflection appears to come from the point S. This point may be referred to as the specular point.[15] A ray, perpendicular to the wavefront, with impact parameter s propagates from point A to point B

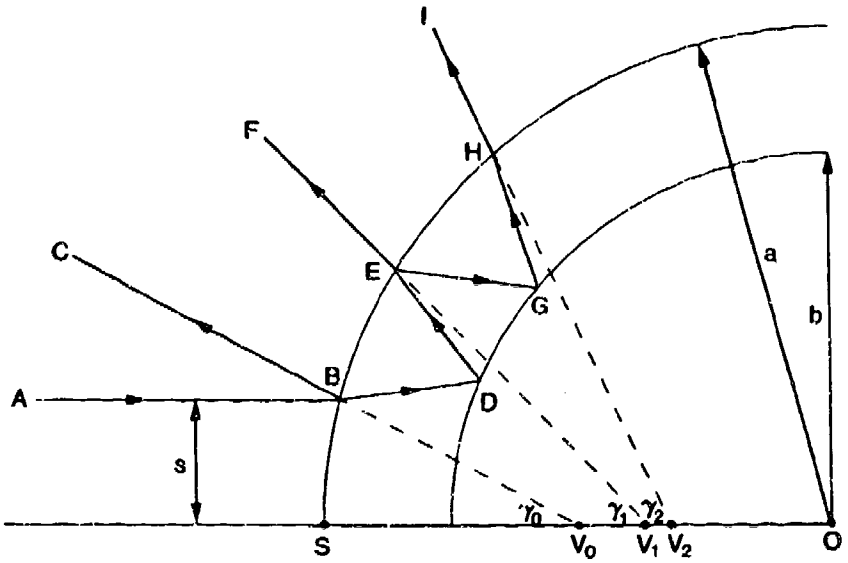

Fig. 1 The ray diagram for the geometric synthesis of the specular reflection form function from a vacuum-filled fluid shell. The point *S* is the vertex of the refracting surface and *O* is the origin of a coordinate axis located at the center of the shell. The inner and outer radii are denoted by *b* and *a*, respectively. A ray, infinitesimally close to the *z*-axis, *SO*, is incident on the fluid shell with impact parameter *s*. The ray *ABC* is the *normal* specular ray; while rays *ABDEF* and *ABDEGHI* are the first two internal reflection contributions. At the points *B*, *E* and *H* partial reflection and/or transmission of a given ray occurs. The internal rays are totally reflected at all points on the inner surface $r = b$. Intersections of the projection (dashed lines) of the outgoing rays (*BC*, *FE* and *HI*) and the *z*-axis define locations of virtual point sources which determine local curvature of the outgoing wavefront associated with a given ray. The virtual point sources are denoted V_n ($n = 0, 1, ...$) and the local backscattering angles are γ_n. Superposition of the acoustic wavefields from the virtual sources in the limit $\gamma_n \rightarrow 0$ gives an expression for the specular reflection contribution to the form function for backscatter as described in Sec. 3.2 and Appendix A.

on the surface of the shell. Rotation of the ray diagram about the line *SO* generates all rays having an infinitesimal impact parameter *s*. At *B* the ray is partially reflected back into the water and partially transmitted into the fluid shell. The intersection of the reflected ray *BC* (dashed line) and the *z*-axis at V_0 defines the location of a virtual source. For backwards and near backwards directions, spherical aberration may be neglected and this virtual source may be modeled as a point source. With the appropriate amplitude and phase shift, this virtual point source describes the propagation of the local outgoing wavefront associated with ray *BC*. The transmitted ray at *B* is refracted and propagates along the path *BD*. After total internal reflection at *D*, the ray propagates to *E* and is, again, partially reflected and transmitted. The transmitted ray *EF*, after refraction, can be projected back to a second virtual source located at V_1. The partial reflection and/or transmission and refraction of subsequent rays at the outer surface generates an infinite set of virtual point sources located at points V_n. Hence, each virtual point source describes the local outgoing wavefront associated with a specific ray.

For each point V_n, define the local backscattering angle, γ_n, as the angle between the outgoing ray and the *z*-axis (see Fig. 1). As the impact parameter approaches zero, the local backscattering angle γ_n also goes to zero. Hence, as $s \rightarrow 0$, the contribution of the specular reflection to the backscattered farfield pressure can be expressed as a superposition of the acoustic fields from the virtual point sources. In particular, the farfield specular pressure is

$$p_{sp} = p_0 \frac{e^{ikr}}{r} \left(H_0 r + \sum_{n=1}^{\infty} H_n C_n e^{i2nk_L h} \right) e^{-i2x}, \qquad (3)$$

where $h = (a - b)$ is the thickness of the shell and $x = ka$ is a dimensionless size parameter. The $2x$ phase shift in Eq. (3) accounts for the path length difference between a ray

propagating in water from point S in Fig. 1 to O and back to S and a ray which is reflected in the backward direction at S. The quantity H_n is a geometric spreading factor associated with the *nth* virtual source. An expression for H_n is derived in Appendix A using a geometric method analogous to the matrix methods of geometric optics. The factor C_n accounts for the partial reflection and/or transmission of the ray at each surface (see Appendix A). The exponential factor within the summation is the additional phase delay of a wave which reverberates n times within the shell before being transmitted in the backscattered direction. The longitudinal wavenumber is $k_L = \omega/c_L = 2\pi/\lambda_L$ where λ_L is the wavelength of the acoustic field in the fluid. Finally, r is the reflection coefficient for an acoustic plane wave at normal incidence on a flat liquid-liquid interface. The reflection coefficient is

$$r = \frac{\rho_e c_L - \rho c}{\rho_e c_L + \rho c}, \tag{4}$$

for the above material parameters.

Using Eqs. (A7) and (A8) for H_n and C_n, the contribution of the specular reflection to the backscattered farfield pressure is

$$p_{sp} = p_0 \frac{ae^{ikr}}{2r}\left(r - \frac{(1 - r^2)}{r} \sum_{n=1}^{\infty} \frac{r^n e^{in\alpha}}{1 + nB} \right) e^{-i2x}, \tag{5}$$

where $\alpha = 2k_L h = 2x(c/c_L)(1 - b/a)$. Equation (A6) defines B which depends only on the relative index of refraction $M_L = c/c_L$ and the ratio of radii b/a. Comparison of Eq. (5) with Eq. (2) reveals that the specular reflection contribution to the backscattered form function is

$$f_{sp} = \left(r - \frac{(1 - r^2)}{r} \sum_{n=1}^{\infty} \frac{r^n e^{in\alpha}}{1 + nB} \right) e^{-i2x}. \tag{6}$$

Although Eq. (6) is a geometrical synthesis of the specular reflection form function, it can be expressed in a manner more easily understood.[16] Simple algebraic manipulations allow one to rewrite Eq. (6). First, the factor $[1+ nB]^{-1}$ is expressed as $1 - nB[1+ nB]^{-1}$. With this substitution, the infinite series in Eq. (6) splits into two series. The summand of the first of the resulting series is $(re^{i\alpha})^n$ where $| re^{i\alpha} | < 1$. Comparing this series with the geometric series demonstrates that the first series is summable and is equivalent to $re^{i\alpha}[1- r e^{i\alpha}]^{-1}$. Substitution into Eq. (6) leads to

$$f_{sp} = \mathcal{R}e^{-i2x} + f_{cc} \tag{7}$$

where

$$\mathcal{R} = r - \frac{(1 - r^2)e^{i\alpha}}{1 - re^{i\alpha}}, \qquad f_{cc} = \left(\frac{(1 - r^2)}{r} \sum_{n=1}^{\infty} \frac{nBr^n e^{in\alpha}}{1 + nB} \right) e^{-i2x}, \tag{8a,b}$$

Equation (7) is the desired expression for the contribution of the specular reflection to the backscattered form function. Define $f_p = \mathcal{R}exp(-i2x)$; the coefficient $\mathcal{R}$ is the complex reflection coefficient for a vacuum-backed flat plate of thickness h at normal incidence.[7] The phase shift $exp(-i2x)$ is due to the phase reference at the shell's center used in Eq. (2). Hence f_p describes the reflection from a spherical shell where the complex reflectivity is modeled as that for a flat plate. Consequently, Eq. (8b) accounts for the correction to f_{sp} due to the curvature of the shell within the geometric approximation. At present, an analytical expression for f_{cc} is not available, however, a rapid summation technique can be employed to perform the indicated summation (see Appendix C).

Figures 2 and 3 are comparisons of the exact PWS calculation of $|f|$ with the geometrical synthesis as given by Eqs. (7) and (8). Appendix *B* contains the PWS representation for f and some relevant remarks concerning its computation. These

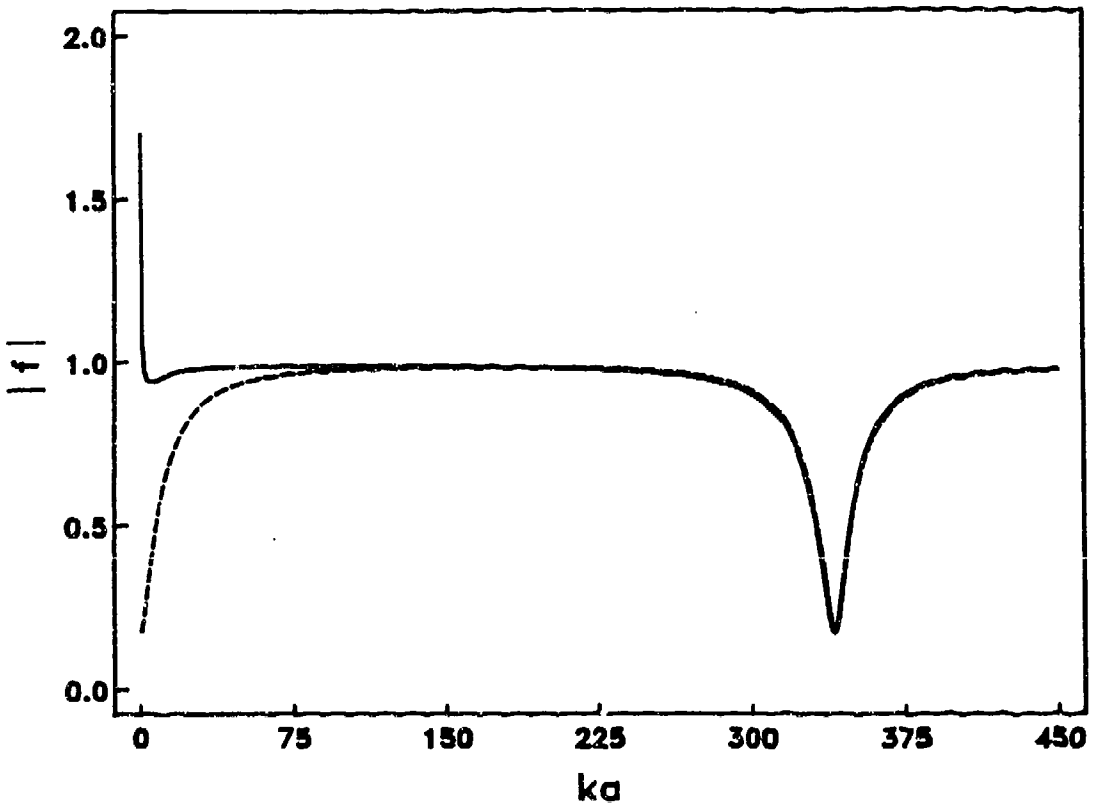

Fig. 2 The solid curve is the exact PWS computation of the form function for backscattering for a 4% thick *aluminum* fluid shell with the parameters listed in Table I. The geometric synthesis of the specular reflection contribution is the dashed line and is calculated via Eqs. (7) and (8). The broad minimum at $x \approx 340$ is the lowest longitudinal resonance. Without the curvature correction (as discussed in Sec. 3.3), the synthesis would not model the longitudinal resonance since the synthesis simplifies to $|f_{sp}| = 1$.

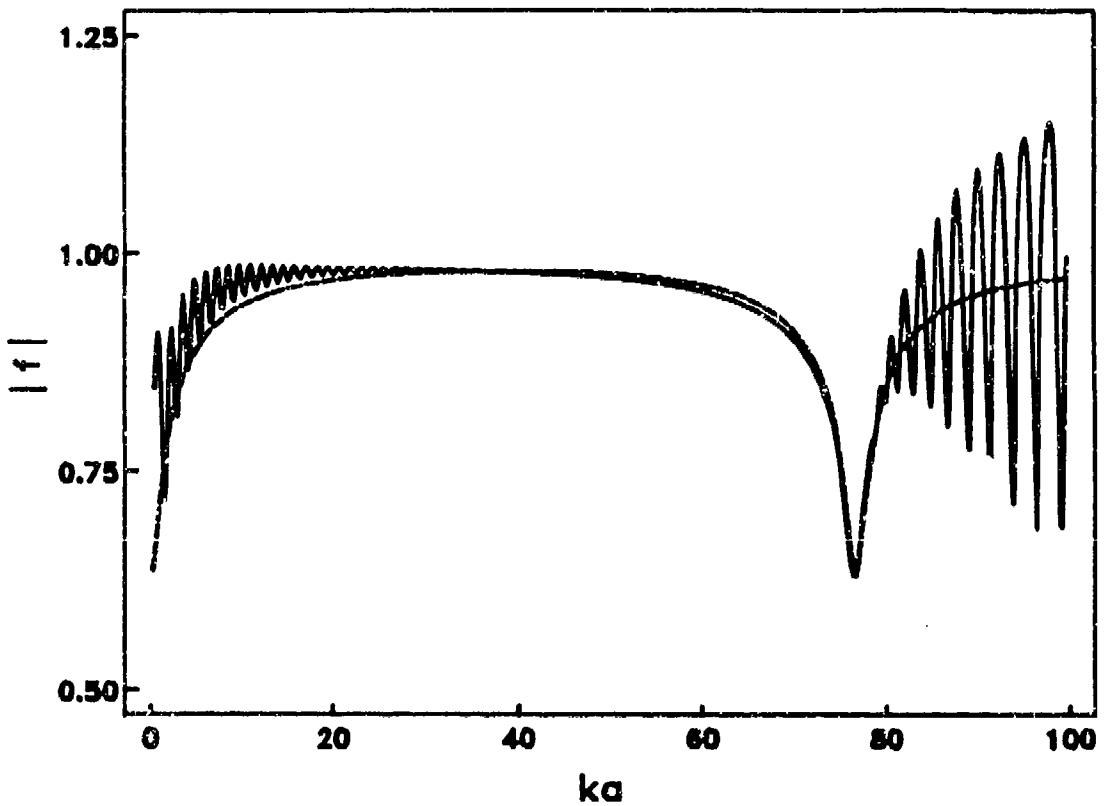

Fig. 3 The exact PWS and geometric synthesis are the solid and dashed lines, respectively. These computations are for a 16.2% thick *440c stainless steel* fluid shell (see Table I). The broad dip at $x \approx 76.8$ corresponds to the first longitudinal resonance. The oscillatory behavior in the ranges $0 < x < 40$ and $77 < x < 100$ is presumably attributable to waves in the fluid shell shedding energy into the water while circumnavigating the shell, as such contributions were not included in the synthesis.

computations are intended to give insight into the more complicated problem of resonances in backscattering from elastic shells, so the choice of the fluid parameters corresponds to elastic material parameters instead of parameters for actual liquids. The parameters for the fluid shells and surrounding water, used in the various calculations, are listed in Table I. Figure 2 corresponds to an *aluminum* fluid shell with $b/a = 0.96$ where the solid line is the PWS result and the dashed line is the geometrical synthesis. The resonance condition, Eq. (1), predicts the first thickness resonance occurs at $x \approx 340$. Clearly, the broad minimum in Fig. 2 corresponds to this longitudinal resonance. The synthesis of $|f_{sp}|$ and $|f|$ via the PWS are in excellent agreement for $x >> 0$.

A *440c stainless steel* fluid shell with $b/a = 0.838$ has its first longitudinal resonance at $x \approx 76.8$ (see Fig. 3). The material parameters of 440c stainless steel and this particular value of the radii ratio correspond to the properties of a spherical shell studied extensively in experiments with tone bursts.[3] As in Fig. 2, the solid and dashed lines are for the PWS and geometrical synthesis, respectively. Again, the broad dip at $x \approx 76.8$ in Fig. 3 is a manifestation of the longitudinal resonance and the synthesis is in good agreement with the PWS calculation. The oscillatory behavior observed in Fig. 3 is attributable to the symmetric (or s_1) surface guided wave which contributes significantly to the backscattering for $x > 76.8$. That is, the contribution of f_{sw} to $|f|$ is no longer negligible for the 440c stainless steel fluid shell. The shell acts like a curved fluid waveguide which leaks energy back into the surrounding water.[17]

For fluid shells where $\rho_e c_L < \rho c$, the resonance condition in Eq. (1) does not apply. The proper expression for predicting a thickness resonance is $k_L h = (n + 1/2)\pi$, (n = 0, 1, ...). Since internal rays reflected at $r = a$ do not sustain a π phase shift, then the resonance requirement of the internal rays adding in phase leads to the additional $\pi/2$. Although the resonance condition is different for $\rho_e c_L < \rho c$, Eqs. (7) and (8) still describe

TABLE I. Material parameters used in the calculations.

Fluid/Water	ρ_e (g/cm^3)	c_L (km/s)	c (km/s)	ρ (g/cm^3)
aluminum/water	2.70	6.42	1.4825	1.00
440c stainless steel/water	7.84	5.854	1.479	1.00

the specular reflection contribution to the form function for backscattering. Figure 4 is a comparison of the PWS result and the synthesis using Eqs. (7) and (8). The fluid shell and water parameters are the same as the 440c stainless steel parameters with $b/a = 0.838$ except $\rho_e = 0.1\ g/cm^3$. The modified condition predicts the first thickness resonance at $x \approx 38.4$, i.e. half the resonance value for the high impedance case of 76.8. Inspection of Fig. 4 demonstrates that the geometrical model agrees with the exact PWS result.

3.3 The importance of curvature to $|f_{sp}|$

An examination of the curvature correction f_{cc} is merited. The significance of the shell's curvature to the manifestation of thickness resonances can be elucidated by examining its dependence on $k_L h$. First, it is noted that the flat plate contribution f_p, alone, does not reproduce the longitudinal resonance structure observed in $|f|$ since $|f_p| = 1$. The approximation $|f| \approx |f_p|$ does not exhibit structure at values of x which satisfy Eq. (1). To obtain the minima, the curvature correction f_{cc} needs to be included such that $|f| \approx |f_p + f_{cc}|$. The resonance condition indicates that $|f_{cc}|$ should have its first maximum at $k_L h = \pi$ when $\rho_e c_L > \rho c$. For a specific fluid, the curvature correction depends on the two parameters x and b/a. For the discussion below, the material parameters are those of 440c stainless steel.

In Fig. 5, $|f_{cc}|$ is plotted as a function of $k_L h = xM_L(1 - b/a)$; where $x = 20$ or 60 is held fixed while $0 < b/a < 1$. For fixed x, $b/a = 1$ corresponds to $k_L h = 0$ and as $b/a \rightarrow 0$, $k_L h \rightarrow xM_L$. The peaks in Fig. 5 are at the expected value $k_L h = \pi$ and these peaks tend to be narrow resonances in the variable $k_L h$. The interpretation is, that for fixed x, shells with h in the vicinity of $\lambda_L/2$ can support the first thickness resonance. Computations for larger values of $k_L h$ exhibit similar sharp peaks at the higher order longitudinal resonances.

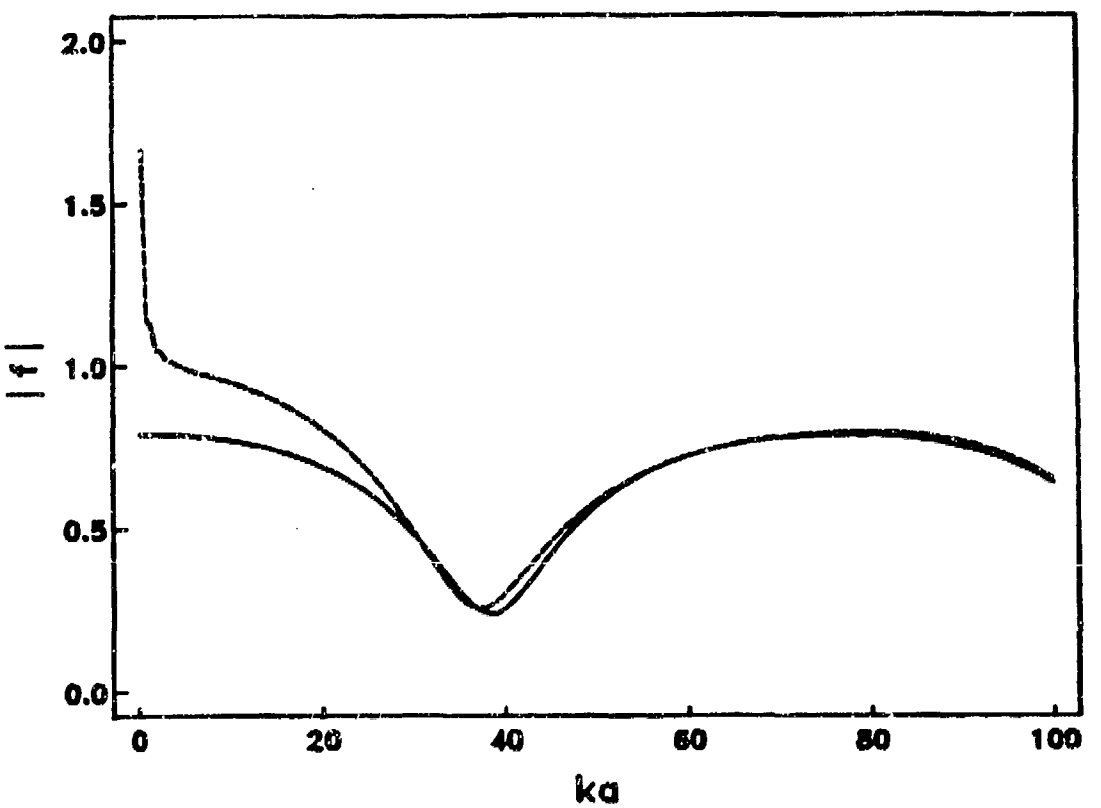

Fig.4 The parameters here are like Fig. 3 except that $\rho_e = 0.1\ g/cm^3$. The condition in Eq. (1) no longer applies for this case since $\rho_e c_L < \rho c$. The correct resonance condition becomes $k_L h = (n + 1/2)\pi$, $(n = 0,1,...)$ and predicts a longitudinal resonance at $x \approx 38.4$. Comparison of the PWS (dashed) and the synthesis (solid) shows a minimum at $x \approx 38.4$. The material parameters for these computations are given in Sec. 3.2.

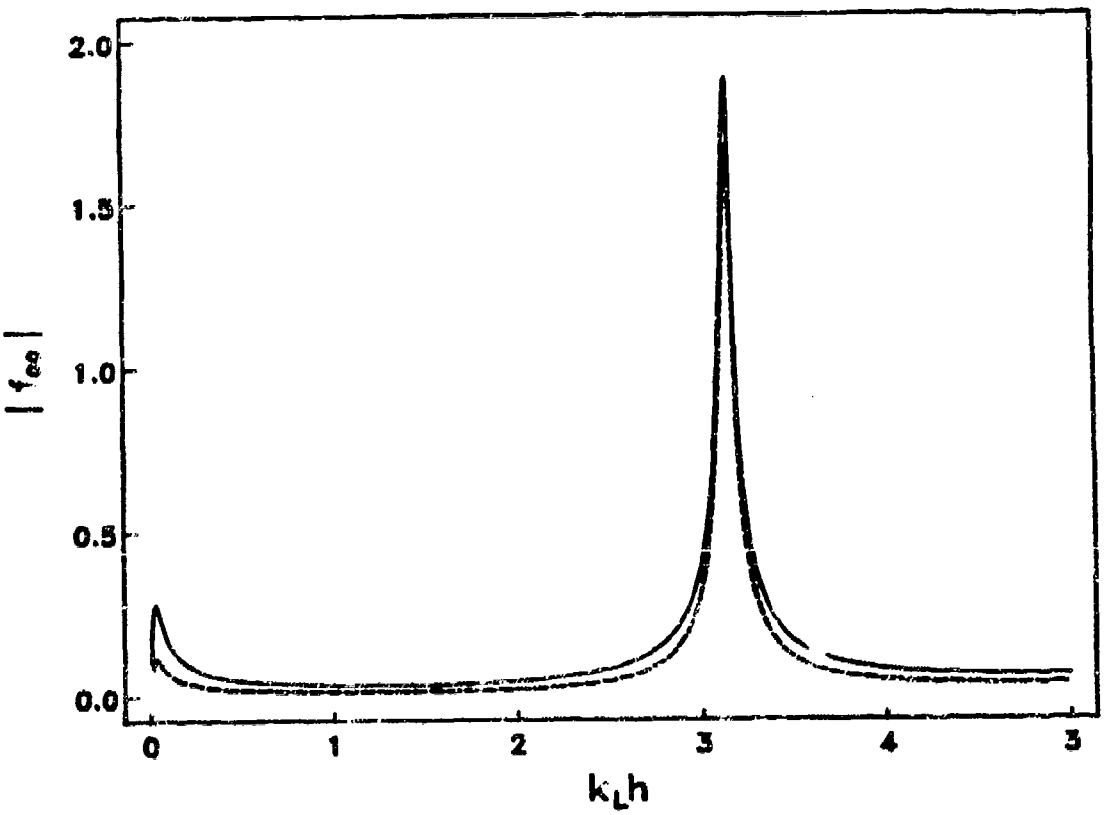

Fig. 5 The magnitude of the curvature correction $f_{cc}(k_L h)$ for fixed values of x and variable b/a. The solid curve is for $x = 20$ and the dashed line is for $x = 60$. The sharp peaks occur at the expected value $k_L h = \pi$ where the first longitudinal resonance is supported within the fluid shell. The material properties of the shell correspond to 440c stainless steel.

Thus, a thickness resonance can be excited within a fluid shell at fixed x provided h is in the vicinity of an integral number of $\lambda_L/2$.

The resonance condition still holds if b/a is now held constant and the frequency of the incident plane wave is varied. Figure 6 displays $|f_{cc}|$ where $b/a = 0.838$ (solid line) or 0.920 (dashed line) and $x = ka = \omega a/c$ is varied. The linear relationship between x and $k_L h$ implies that as x increases $k_L h$ increases. Although, the sharp peaks in Fig. 6 occur at $k_L h = \pi$, the interpretation of the physical nature of the peaks is more subtle. Inspection of Fig. 6 reveals that the width of the peaks are comparable; however, the x values at which the two peaks occur are different. These x are approximately 76.8 and 155 for $b/a = 0.838$ and 0.920, respectively. From the resonance condition, it is inferred that the range of x, for which a longitudinal resonance is excited, is wider for a thin shell than a thick shell of the same fluid. Furthermore, comparison of Figs. 2 and 3 illustrates the width in x is strongly affected by the parameter $M_L(1 - b/a)$.

3.4 Limiting cases for scattering of an acoustic plane wave from an ideal, fluid shell

A. Scattering from a perfectly soft bubble

For the limiting case $b \rightarrow a$, the fluid shell becomes a perfectly soft bubble and Eq. (7) should describe the linear backscattering of an acoustic plane wave from a bubble of radius a within the geometric limit. For $b \rightarrow a$, inspection of Eq. (A6) reveals the constant $B \rightarrow 0$ which leads to the result that the curvature correction component in Eq. (7) also vanishes. In this limit, it is straightforward to show $f_{sp} = f_p = -exp(-i2x)$. In Sec. 3.2, $\mathcal{R}$ was found to be the complex reflection coefficient for a vacuum-backed flat plate. Since the thickness of the plate is approaching zero, then the plate becomes a water-vacuum interface. The reflection coefficient for a normal incidence plane wave in water on a

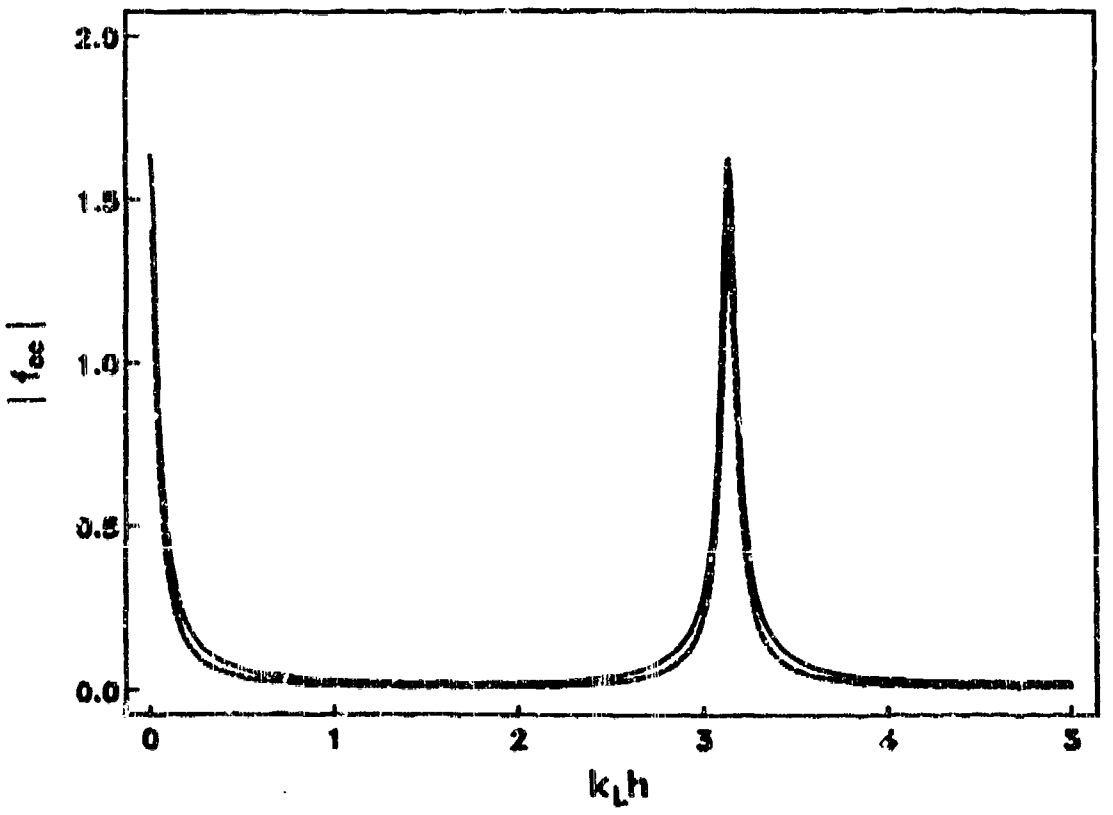

Fig. 6 The magnitude of $f_{cc}(k_L h)$ for fixed values of b/a and variable x. The solid curve is for $b/a = 0.838$ and the dashed line is for $b/a = 0.920$. As in Fig. 5, the narrow peaks occur where the first longitudinal resonance is supported within the fluid shell and the material parameters are for 440c stainless steel.

pressure release surface is -1. Hence, Eq. (8a) reduces to the expected value and the backscattered farfield pressure due to the specular reflection becomes

$$p_{sp} = -p_0 \frac{a}{2r} e^{-i2x} e^{ikr}. \tag{9}$$

The upper two curves in Fig. 7 are $|f|$ and $|f_{sp}|$ where the dashed line is the PWS result within the limit $b \to a$ and the horizontal line is the magnitude of the form function obtained from the acoustic ray method.[18] Both $|f|$ and $|f_{sp}|$ are scaled by $b/a = 0.838$ in Fig 7. The reason for this scaling will be discussed in Sec. 3.4B. For $x > 20$, these curves become indistinguishable; while for values of $x < 20$, the PWS deviates substantially from the synthesis. This result may be anticipated since geometrical acoustics is implicitly a high-frequency approximation.

B. Scattering from an impedance-matched fluid spherical shell

For the scattering from an impedance-matched fluid, the reflection coefficient defined in Eq. (4) is identically zero. That is, $\rho_e c_L = \rho c$ for an impedance-matched fluid and $r = 0$. Equation (7) reduces to

$$f_{sp} = -\frac{e^{i\alpha}}{1+B} e^{-i2x}, \tag{10}$$

where B is defined by Eq. (A6). Figure 7 contains computations of $|f|$ and $|f_{sp}|$ for a fluid with the sound speed of 440c stainless steel and ρ_e was determined from $\rho_e = \rho M_L$. The lower two curves in Fig. 7 are for this limiting case. The dashed line is the exact PWS result and the horizontal line corresponds to Eq. (10). Although, the two curves are vastly different for $x < 40$, for $x \approx 50$ the difference between the ray tracing synthesis and the PWS is less than 7.2%. It is anticipated that the agreement will improve as x becomes large.

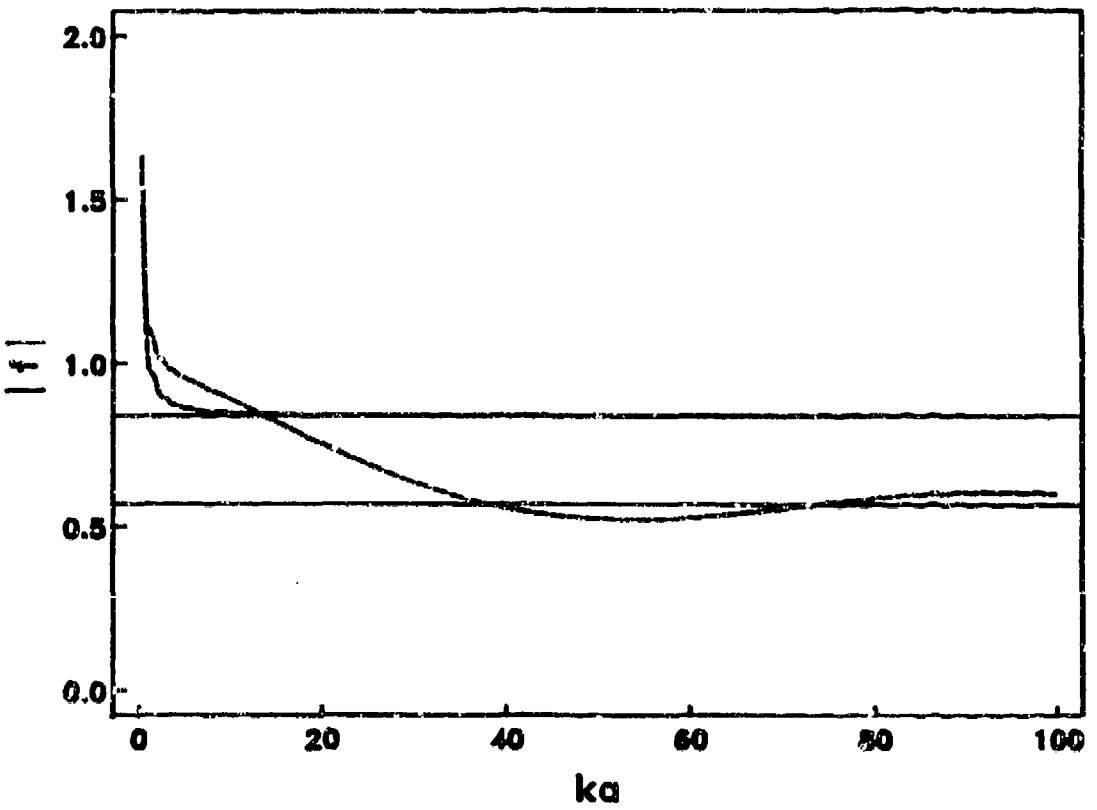

Fig. 7 The upper two curves are for the limiting case of the scattering from a perfectly soft bubble. The horizontal line is $|f_{sp}|$ and the dashed line is $|f|$ calculated via the PWS result. Both curves have been scaled by 0.838 (see Sec. 3.4B). The lower set of curves is the limiting case of an impedance-matched fluid (i.e., $\rho_e c_L = \rho c$). Again, the horizontal line is $|f_{sp}|$ and the dashed line is the PWS for $|f|$. The two sets of curves demonstrate that the synthesis of f_{sp} correctly approximates the high-frequency scattering for these limiting cases.

Within the impedance-matched fluid case, there is the special case $\rho_e = \rho$ and $c_L = c$. That is, the fluid shell is essentially a perfectly soft bubble of radius b. The denominator of Eq. (10) becomes $(1 + B) = a/b$ and the phase shift $\alpha = 2kh$. Equation (10) in this special case reduces to $f_{sp} = -(b/a)e^{-ikb}$ which gives

$$p_{sp} = -p_0 \frac{b}{2r} e^{-i2kb} e^{ikr}, \tag{11}$$

for the contribution of the specular reflection to the backscattered, farfield pressure. Comparison of Eqs. (9) and (11) gives the motivation of the scaling of the upper two curves in Fig. 7 by b/a. That is, Eq. (11) is the expected backscattered pressure from a bubble of radius b in the geometric limit.

C. Scattering from a fluid sphere

The final limiting case is the backscattering from an ideal fluid sphere.[13,18-20] For a fluid sphere the inner surface has vanished ($b \rightarrow 0$) and the derivation of the spreading factor H_n in Appendix A is no longer applicable. That is, the rays are reflected from the opposite side of the sphere and hence from a surface with a radius of curvature of $-a$. To properly determine the limiting form of the specular reflection form function, the refractive powers given in Eq. (A3) need to be redefined by allowing $b \rightarrow -a$. Alternately, the appropriate form function can be obtained by taking the limit $b \rightarrow -a$ in Eq. (7). The result is

$$f_{sp} = \left(r - \frac{(1 - r^2)}{r} \sum_{n=1}^{\infty} \frac{M_L}{M_L - 2n} r^{2n} e^{in\alpha} \right) e^{-i2x}, \tag{12}$$

where $\alpha = 2k_L h = 4k_L a$. The magnitude of the contribution of the nth internal ray to f_{sp} is $|(1 - r^2)r^{2n-1}M_L / (2n - M_L)|$. Comparison of Eq. (34) of Ref. 13 with the magnitude of the nth internal ray here shows that for the fluid sphere limit Eq. (7) reduces to the

appropriate form. It is noted that the rays here are enumerated consecutive while the numbering scheme in Ref. 13 is based on the number of internal chords associated with each ray. Finally, it can be shown that the results here for $n = 1$ are equivalent to those given in Appendix C of Ref. 13 for the first axial ray.

3.5 Conclusion

When the incident wave is at a frequency of a resonance, the terms of the series in Eq. (5) are mutually in-phase: there is constructive interference between all of the internally reflected backward directed rays. At resonance, the externally reflected ray (which reflects from S in Fig. 1) interferes either destructively or constructively with the summed contributions of the internally reflected rays, depending on the sign of r. For the usual case where $r > 0$, Eq. (1) gives the resonance condition. Unlike the series for sequential surface wave contributions, which may be expressed in a Fabry-Perot form,[6,7,10] the series in Eq. (5) does not generally take on the form of a geometric series. If the radius of curvature of the shell is truly negligible in comparison to the thickness, $B = c_L h/cb \rightarrow 0$, and the series becomes a geometric series. That series, when summed, gives the first term of Eq. (7) since the curvature correction f_{cc} must vanish in that limit. The general form of the series in Eq. (5) is not that of a geometric series since the spreading factor H_n and the virtual source location V_n depend on n.

The curvature of the shell is essential to the manifestation of longitudinal resonances in the modulus of the backscattering form function of fluid spherical shells. The specular reflection form function decomposes into a contribution attributable to the reflection from a flat vacuum-backed fluid plate and a curvature correction component: $f_{sp} \approx f_p + f_{cc}$. The dependence of f_{cc} on $k_L h$ manifests the resonance condition given in Eq. (1). Finally,

without the inclusion of f_{cc} in the synthesis of f_{sp}, the approximation $f \approx f_{sp}$ does not exhibit the longitudinal resonances in $|f|$.

The verification of the geometrical synthesis of f_{sp} follows from comparison of $|f_{sp}|$ with the exact calculation of the PWS representation of $|f|$. The excellent agreement between $|f|$ and $|f_{sp}|$ demonstrates the correctness of f_{sp} especially for $x >> 0$. Furthermore, the limiting cases of a perfectly soft bubble, fluid sphere, and impedance-matched fluid shell supports the claim that Eqs. (7) and (8) correctly describe the high-frequency specular scattering of sound from an ideal, fluid shell.

A synthesis of the backscattering of an elastic stainless steel spherical shell, summarized in Ref. 11, neglected the curvature correction f_{cc} since the expression for f_{cc} was unavailable at the time of that work. The synthesis used the method described in Ref. 6 for the contributions from leaky Lamb waves. It has been subsequently demonstrated that inclusion of f_{cc} improves the synthesis and it is our intent to discuss that in a subsequent publication since the synthesis of the Lamb wave contributions is beyond the scope of the present paper.

Though the present analysis has been restricted to backscattering, the ray diagram, Fig. 1, gives insight into how such rays contribute to the angular scattering pattern for near backwards directions. The virtual sources V_0, V_1, V_2, ... lie along the backward axis. Consider first the case of only two such sources. The interference pattern near the axis is the well known ring or bull's-eye pattern exhibited in an optical Michelson interferometer or Newton's ring experiment.[21,22] The center of the ring pattern is the backwards direction. This pattern was previously exhibited in a ray synthesis of backscattering from fluid spheres in cases where only axial ray contributions were included.[13] (See the curves labeled $|f_0 + f_2|$ in Fig. 5 - 7 of Ref. 13.) The central scattering amplitude is maximized when the outgoing wavefronts (which are locally spherical but of different radii) have a

tangential point of contact on the backward axis. It may be anticipated that the situation depicted in Fig. 1 yields ring patterns, but with a richer structure due to the additional virtual sources V_2, V_3, ... The method of analysis of the present paper and these comments on the scattering pattern should also be applicable to understanding the consequences of multiple reflections in spherical domes which enclose sonar transducers.

While the analysis given here has been limited to spherical shells, Fig. 1 also applies to a right circular cylindrical shell. Extension of the analysis to that case should give the curvature correction to the specular contribution previously modeled by Borovikov and Veksler.[7]

This research was supported by the Office of Naval Research.

Appendix A. Determination of H_n and C_n from geometrical ray methods

The factor H_n is derived by applying the matrix method of geometric optics to the acoustic ray representation of the wavefield in water and fluid shell. Each factor is associated with a virtual point source as discussed in Sec. 3.2, (see Fig.1). In particular, the ray associated with the local outgoing wavefront produced by the point source V_n will be called the *nth* ray. The local backscattering angle γ_n is the angle between the *nth* ray and the z-axis. The square of the spreading factor in terms of the impact parameter s and γ_n is[23]

$$H_n^2 = \left[\frac{d\sigma}{d\Omega}\right]_n = \frac{s}{\gamma_n}\left|\frac{ds}{d\gamma_n}\right|, \qquad \text{as } \gamma_n \to 0, \tag{A1}$$

where $[d\sigma / d\Omega]_n$ is the spreading factor part of a differential scattering cross section for the *nth* ray. This is a specialization to $\gamma \to 0$ of the more general result $(d\sigma/d\Omega) = s(\sin\gamma)^{-1}|ds/d\gamma|$ derivable from flux conservation.[24] The purpose of this appendix is to outline the

method used to relate the impact parameter to the local backscattering angle and, ultimately, to obtain a simple analytic expression for H_n.

The matrix methods of geometric optics are employed to related s and γ_n.[21,22] Since the concern here is backscattering, then the paraxial form of the matrix representation can be used. The conventions as outlined in Refs. 21 and 22 and summarized below are adopted for the following discussion. The relevant matrices are:

$$\mathbf{X} = \begin{pmatrix} 0 \\ s \end{pmatrix}, \quad \mathbf{X}_n = \begin{pmatrix} \gamma_n \\ x_n \end{pmatrix}, \quad \mathbf{R}_i = \begin{pmatrix} 1 & -\mathcal{P}_i \\ 0 & 1 \end{pmatrix}, \quad \mathbf{T}_{21} = \begin{pmatrix} 1 & 0 \\ \tilde{h} & 1 \end{pmatrix}, \tag{A2}$$

where $\mathbf{X}$ is the matrix defining the initial angle of inclination and displacement from the z-axis of the incident ray at point B in Fig. 1. The final angle of inclination γ_n and displacement x_n of the nth ray are represented by $\mathbf{X}_n$. In the paraxial approximation, x_n is the ray displacement from the z-axis in the vertical plane through vertex S. The matrix $\mathbf{X}_n$ applies to the point where the ray exits the shell. The refraction and translation matrices are $\mathbf{R}_i$ and $\mathbf{T}_{21}$. The subscript $i = 1, 2$ corresponds to the surface $r = a, b$. For paraxial rays $\mathbf{T}_{21} = \mathbf{T}_{12}$ and $\tilde{h} = a(1 - b/a)/M_L$ where $M_L = c/c_L$ is the relative index of refraction. Noting that a prime on $\mathbf{R}_i$ indicates a reflection at the surface i, the relevant constants are:

$$\mathcal{P}_1 = \frac{1 - M_L}{a}, \quad \mathcal{P}_2' = \frac{-2M_L}{b}, \quad \mathcal{P}_1' = \frac{-\mathcal{P}_2' b}{a}, \quad \mathcal{P}_0 = \frac{-2}{a}, \tag{A3}$$

where $\mathcal{P}_0$ represents the special case of the zeroth ray. The $\mathcal{P}_i$ are referred to as the refractive powers of the ith surface. The trajectory of the nth ray is described by the matrix equations,

$$\begin{aligned} \mathbf{X}_0 &= \mathbf{R}_0\mathbf{X}, && (n = 0), \\ \mathbf{X}_n &= [\,\mathbf{JM}\,]^{n-1}\mathbf{JX}, && (n > 0), \end{aligned} \tag{A4}$$

where $\mathbf{J} = \mathbf{R}_1\mathbf{T}_{12}\mathbf{R}_2'\mathbf{T}_{21}\mathbf{R}_1$ and $\mathbf{M} = \mathbf{R}_1^{-1}\mathbf{R}_1'\mathbf{R}_1^{-1}$. The exponent in Eq. (A4) implies a repeated product, i.e., **JMJM** for $n = 3$. Performing the matrix multiplications leads to the result,

$$\mathbf{X}_n = \begin{pmatrix} \gamma_n \\ x_n \end{pmatrix} = \begin{pmatrix} (2/a)(1 + nB)s \\ (1 + 2nB)s \end{pmatrix}, \qquad (n > 0), \qquad \text{(A5)}$$

where

$$B = \frac{1 - b/a}{M_L(b/a)} = \frac{h}{M_L b}. \qquad \text{(A6)}$$

Equation (A5) contains the desired relationship between s and γ_n. The analytic form of the spreading factor, determined by using Eqs. (A1) and (A5), gives

$$H_n = \frac{(a/2)}{1 + nB}, \qquad (n = 0, 1, \ldots). \qquad \text{(A7)}$$

From inspection of Fig. 1, in the paraxial approximation the distance of the virtual source V_n from O is $a - (x_n/\gamma_n)$. From Eqs. (A5) and (A7), we find that $a - (x_n/\gamma_n) = H_n$. Hence, $V_n \rightarrow O$ as $n \rightarrow \infty$.

The amplitude factor C_n in Eq. (3) is found by considering the partial reflection and/or transmission of a ray at each interface. From Fig. 1, it is observed that the zeroth ray is partially reflected at $r = a$ without further interaction with an interface. The appropriate constant is $C_0 = r$, where r is the reflection coefficient defined in Eq. (4). The ray *ABDEF* has the amplitude factor $C_1 = tr_2t'$. The transmission coefficients t and t' are for rays which propagate from water into the fluid and from the fluid into water, respectively. The transmission coefficients are related to the reflection coefficient in Eq. (4) by $t = 1 - r$ and $t' = 1 + r$. The reflection coefficient at the inner surface at $r = b$ is $r_2 = -1$. Using these relationships gives $C_1 = -(1 - r^2)$. The amplitude constant for the ray

ABDEGHI is $C_2 = tr_2\, r' r_2 t'$ where $r' = -r$ is the reflection coefficient for the ray incident in the fluid on the fluid-water interface. The constant C_2 in terms of r is $C_2 = -r(1 - r^2)$. In general, the amplitude constant for the *nth* ray is

$$C_n = -r^{n-1}(1 - r^2) \tag{A8}$$

Appendix B. The partial wave series representation of f

The PWS representation of the backscattered form function is included for completeness. This PWS is for the backscattering of an acoustic plane wave from an ideal fluid spherical shell. The interior of the shell is assumed to be a vacuum. The analysis is similar to those in Refs. 3 and 19 and gives f as

$$f = \frac{2}{ix} \sum_{n=0}^{\infty} (-1)^n (2n + 1) \frac{B_n(x)}{D_n(x)}, \tag{B1}$$

where B_n and D_n are 3×3 determinants obtained from the boundary conditions at $r = a$ and b. In Appendix B, n denotes the partial-wave index. The elements of the determinants are:

$$b_{11} = \tilde{\rho}\,(c/c_L)\, j_n(x), \qquad d_{11} = -\tilde{\rho}\,(c/c_L)\, h_n^{(1)}(x),$$
$$b_{21} = j_n'(x), \qquad d_{21} = -h_n^{(1)'}(x),$$
$$b_{31} = d_{31} = 0, \qquad b_{12} = d_{12} = j_n(x_L),$$
$$b_{13} = d_{13} = n_n(x_L), \qquad b_{22} = d_{22} = j_n'(x_L),$$
$$b_{23} = d_{23} = n_n'(x_L), \qquad b_{32} = d_{32} = j_n(y_L),$$
$$b_{33} = d_{33} = n_n(y_L),$$

where the parameters are defined as follows: $\tilde{\rho} = \rho/\rho_e$, $x = ka$, $x_L = xc/c_L$ and $y_L = x_L b/a$. The spherical Bessel and Neumann functions and Hankel function of the first kind of

integer order are denoted by j_n, n_n, and h_n, respectively. The prime on a function indicates differentiation with respect to the argument.

The numerical implementation of the PWS requires that the infinite series must be truncated. A discussion of a choice of the maximum partial-wave index for the truncated series is given in Ref. 25. The result is

$$\begin{aligned} n_{max} &= 2 + [\, x + 4.0x^{1/3} \,], && x < 8, \\ n_{max} &= 3 + [\, x + 4.05x^{1/3} \,], && x \geq 8, \end{aligned} \tag{B2}$$

where [ ] implies truncation to the nearest integer. The criterion of Eq. (B2) was used for the PWS computations shown in Figs. 2 - 4. The number of terms exceeds x and the PWS converges slowly until $n > x$.

Appendix C. Rapid summation technique for f_{cc}

Since an analytic expression is unavailable at this time for f_{cc}, then the infinite series in Eq. (8b) must be evaluated. For the material parameters given in Table I, the infinite series converges fairly fast, but for other values the series may not converge rapidly. Here, we investigate a method that may increase the convergence of $f_{cc} = \mathcal{R}_c e^{-i2x}$ where

$$\mathcal{R}_c = \frac{(1 - r^2)}{r} \sum_{n=1}^{\infty} \frac{nBr^n e^{in\alpha}}{1 + nB}, \tag{C1}$$

or at least give a good approximation for the infinite sum. First, it is noted that there exists an integer $n = N$ such that $NB > 1$ for any B. Now, the summation in Eq. (C1) is split into two summations,

$$S = G(N) + \sum_{n=N+1}^{\infty} \frac{nBr^n e^{in\alpha}}{1 + nB}, \tag{C2}$$

where S denotes the sum in Eq. (C1) and $G(N)$ is the finite sum of the first N terms. Shifting the summation index in the second term of Eq. (C2) and dividing the numerator and denominator by $(n + N)B$, this sum is rewritten as

$$\sum_{n=N+1}^{\infty} \frac{nB r^n e^{in\alpha}}{1 + nB} = r^N e^{iN\alpha} \sum_{n=1}^{\infty} \frac{r^n e^{in\alpha}}{1 + [(n + N)B]^{-1}} . \tag{C3}$$

Since $[(n + N)B]^{-1} < 1$, then the denominator may be expanded by the binomial expansion. Neglecting terms of order $[(n + N)B]^{-2}$, the summation on the right hand side of Eq. (C3) is approximated by two infinite series. The first is a geometric series and can be summed analytically; while the second is the first correction to the rapid summation technique. Equation (C2) becomes

$$S = G(N) + \frac{r^{N+1} e^{i(N+1)\alpha}}{1 - r e^{i\alpha}} - r^N e^{iN\alpha} \sum_{n=1}^{\infty} \frac{r^n e^{in\alpha}}{(n + N)B} . \tag{C4}$$

Finally, the rapid summation technique consists of approximating S by the first two terms in Eq. (C4). An estimate of the error in implementing the rapid summation technique can be ascertained by summing the last term in Eq. (C4).

Numerical tests of the above technique indicate that suitable converges occurs for the choice of $N = \{B^{-1}\} + 10$ where $\{\}$ implies the integer part of B^{-1}. (If $B^{-1} - \{B^{-1}\} > 0.5$, then $\{\}$ is increased by one.) For example, for a fluid shell with the parameters of 440c stainless steel and $b/a = 0.838$, the constant $B = 0.765$ which gives $\{B^{-1}\} = 1$. Hence, the rapid summation technique involves the calculation of 12 terms; while directly summing S requires between 215 to 220 terms for convergence to six decimal places of precision. Figure C1 is a comparison of the results of the rapid summation technique and the truncated infinite series. Agreement between the two curves is good and it is anticipated that a small increase in N will give even better agreement.

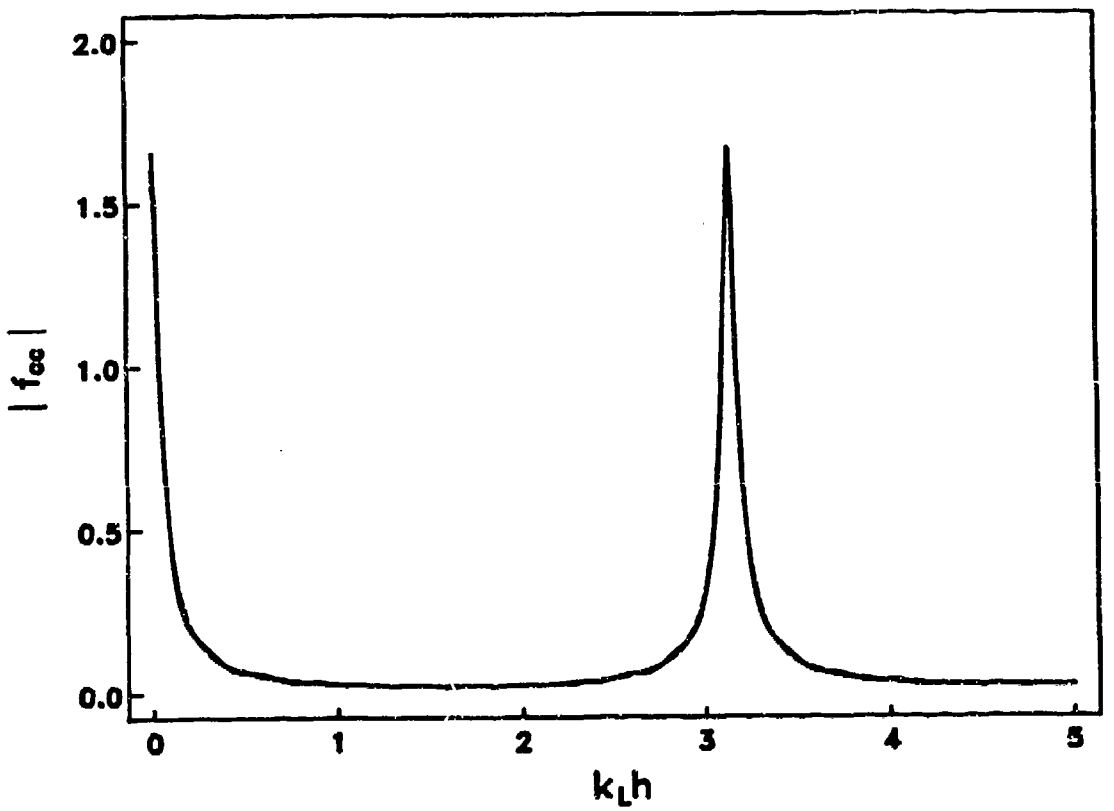

Fig. C1 Calculation of $|f_{cc}|$ employing a rapid summation technique. The rapid summation of $|f_{cc}|$ is the solid line. The dashed curve is $|f_{cc}|$ where the infinite series in Eq. (C1) is truncated after sufficient convergence.

References

1. R. Fiorito, W. Madigosky and H. Uberall, "Resonance theory of acoustic waves interacting with an elastic plate," J. Acoust. Soc. Am. 66, 1857 - 1866 (1979).
2. R. Fiorito and H. Uberall, "Resonance theory of acoustic reflection and transmission through a fluid layer," J. Acoust. Soc. Am. 65, 9 - 14 (1979).
3. S.G. Kargl and P.L. Marston, "Observations and modeling of the backscattering of short tone bursts from a spherical shell: Lamb wave echoes, glory, and axial reverberations," J. Acoust. Soc. Am. 85, 1014 - 1028 (1989). Section III contains a short discussion of the thickness resonance condition for such a shell; b/a = 0.838 corresponds to that of the shell studied and computationally modeled in Ref. 11.
4. G.S. Sammelmann, D.H. Trivett and R.H. Hackman, "The acoustic scattering by a submerged, spherical shell. I: The bifurcation of the dispersion curve for the spherical antisymmetric Lamb wave," J. Acoust. Soc. Am. 85, 114 - 124 (1989).
5. G.C. Gaunaurd and M.F. Werby, "Lamb and creeping waves around submerged spherical shells resonantly excited by sound scattering," J. Acoust. Soc. Am. 82, 2021 - 2033 (1987).
6. P.L. Marston, "GTD for backscattering from elastic spheres and cylinders in water and the coupling of surface elastic waves with the acoustic field," J. Acoust. Soc. Am. 83, 25 - 37 (1988).
7. V.A. Borovikov and N.D. Veksler, "Scattering of sound waves by smooth convex elastic cylindrical shells," Wave Motion 7, 143 - 152 (1985).
8. L.B. Felsen, J.M. Ho and I.T. Lu, "Three-dimensional Green's function for fluid-loaded thin elastic cylindrical shell: Formulation and solution," J. Acoust. Soc. Am.87, 543 - 553 (1990); L.B. Felsen, J.M. Ho and I.T. Lu,"Three-dimensional Green's function for fluid-loaded thin elastic cylindrical shell: Alternate

representations and ray acoustic forms," J.Acoust. Soc. Am. 87, 554 - 569 (1990).

9. K.L. Williams and P.L. Marston, "Backscattering from an elastic sphere: Sommerfeld-Watson transformation and experimental confirmation," J. Acoust. Soc. Am. 78, 1093 - 1102 (1985).

10. K.L. Williams and P.L. Marston, "Synthesis of backscattering from an elastic sphere using the Sommerfeld-Watson transformation and giving a Fabry-Perot analysis of resonances," J. Acoust. Soc. Am. 79, 1702 - 1708 (1986).

11. P.L. Marston and S.G. Kargl, "Elastic surface wave contributions to backscattering from smooth objects described by a generalization of GTD," Oceans '89 Conference record (IEEE publication number 89CH2780-5, New York, 1989) pp. 1194-1198.

12. T. Pialucha, C.C.H. Guyott and P. Cawley, "Amplitude spectrum method for the measurement of phase velocity," Ultrasonics 27, 270 - 279 (1989).

13. P.L. Marston and D.S. Langley, "Glory- and rainbow-enhanced acoustic backscattering from fluid spheres: Models for diffracted axial focusing," J. Acoust. Soc. Am. 73, 1464 - 1474 (1983).

14. The technique has similarities with that described in I.T. Lu and L.B. Felsen, "Ray, mode, and hybrid options for source excited propagation in an elastic plate," J. Acoust. Soc. Am. 78, 701 - 714 (1985). The hybrid method employed by Lu and Felsen consists of splitting a field vector **V** into a finite summation, **V**(N - 1), and a remainder $\mathbf{R}_N$ which is an integral. Suitable deformation of the contour of integration results in a rapid convergence of the remainder. In an analogous manner, the infinite series in f_{cc} is split into a finite summation and a remainder which can be adequately approximated (see Appendix C).

15. W.V.T. Rusch and O. Sorenson, "On determining if a specular point exists," IEEE Trans. Antennas Propag. AP-27, 99 - 101 (1979).

16. The quantity within the parenthesis in Eq. (6) is, in general, a complex reflection coefficient for an evacuated spherical shell. This reflection coefficient contains both geometrical as well as reflectivity information. The early work of Keller and co-workers demonstrated that the reflection coefficient is composed of a reflectivity, a geometrical and a phase factor. Although the formalism and results in these papers are not easily compared to the present result in Eq. (6), the following papers are nevertheless noteworthy. H. Primakoff and J.B. Keller, "Reflection and transmission of sound by thin curved shells," J. Acoust. Soc. Am. 19, 820 - 832 (1947). J.B. Keller and H.B. Keller, "Reflection and transmission of sound by a spherical shell," J. Acoust. Soc. Am. 20, 310 - 313 (1948).

17. For a vacuum, for a flat fluid layer of thickness $h = a - b$ the s_1 mode can be shown to cut off at the frequency corresponding to $x = 76.8$. This explains why the oscillations are not present at smaller x.

18. J.J. Bowman, T.B.A. Senior and P.L.E. Uslenghi, *Electromagnetic and Acoustic Scattering by Simple Shapes*, (Hemisphere Pub. Corp., New York 1987) p. 356ff. It is noted that the PWS representation in Appendix B correctly goes over to the acoustically soft sphere. In particular, comparison of Fig. 10.4 on p. 360 is observed to be similar to the PWS result in Fig. 6 here.

19. V.C. Anderson, "Sound scattering from a fluid sphere," J. Acoust. Soc. Am. 22, 426 - 431 (1950).

20. H.G. Frey and R.R. Goodman, "Acoustic scattering from fluid spheres," J. Acoust.Soc. Am. 40, 417 - 420 (1966).

21. A. Nussbaum and R.A. Phillips, *Contemporary Optics for Scientists and Engineers*, (Prentice-Hall, Englewood Cliff, NJ, 1976).

22. M.V. Klein and T.E. Furtak, *Optics*, (Wiley, New York, 1986) 2nd. ed.

23. W.P. Arnott and P.L. Marston, "Optical glory of small freely rising gas bubbles in water: Observed and computed cross-polarized backscattering patterns," J. Opt. Soc. Am. A5, 496 - 506 (1988).

24. H. Goldstein, *Classical Mechanics*, (Addison-Wesley, Reading, MA 1980) 2nd. ed. pp. 105-107.

25. S.G. Kargl and P.L. Marston, "Ray synthesis of Lamb wave contributions to the total scattering cross section for an elastic spherical shell," accepted for publication, J. Acoust. Soc. Am.)

Chapter 4

Ray synthesis of the form function for backscattering from an elastic spherical shell: Leaky Lamb waves and longitudinal resonances.

Abstract

An acoustic ray analysis is employed in synthesizing the form function for backscattering, $f(\theta = \pi, ka)$, from a fluid-loaded evacuated elastic spherical shell where k is the wavenumber of the incident plane wave and a is the outer radius of the shell. The synthesis contains a component associated with a specular reflection, f_{sp}, and contributions from leaky Lamb waves. The contribution f_l of the *lth* leaky Lamb wave is expressible in a Fabry-Perot resonator form [P. L. Marston, J. Acoust. Soc. Am. 83, 25 - 37, (1988)]. The present synthesis differs from previous results by including the effects of longitudinal resonances on f_{sp}. A novel ray synthesis of f_{sp} indicates a significant resonance effect near the condition $k_L h = n\pi$ ($n = 1, 2, ...$). The thickness of the shell is h and $k_L = \omega/c_L$ is the longitudinal wavenumber where c_L is the longitudinal speed of sound in the elastic material. The ray synthesis demonstrates that the curvature of the shell is essential to the modeling of longitudinal resonances. A comparison of the ray synthesis for $f(ka)$ with the exact partial-wave series representation for a 440c stainless steel shell displays the usefulness of the ray synthesis. Although acoustic ray modeling is generally a high-frequency technique, the ray synthesis of $f(ka)$ for a 440c stainless steel shell appears to be applicable for ka as small as 7. Certain anomalies in the synthesis are investigated to better understand the limitations of the present ray model.

4.1 Introduction

The application of novel ray techniques to canonical scattering problems allows one to test the integrity and efficiency of ray representations.[1-4] Since ray representations of the interaction of sound with a scatterer give a simple picture of the scattering process, they merit investigation. Ray representations have the potential to be generalized to non-canonical problems not easily treated by other methods. Furthermore, the need for generalized ray theories has been recognized in structural acoustics.[5] In developing such ray techniques, comparison of an available exact solution and a ray model for a canonical problem gives physical insight into regions where the techniques are applicable. This article investigates a novel ray synthesis of the canonical problem of high-frequency backscattering from a fluid-loaded evacuated elastic spherical shell. It is anticipated that the ray synthesis developed here may be generalized to scattering from other smooth convex elastic objects. Hence, both the success and failure of the present level of ray synthesis may be instructive for more advanced ray models.

The ray synthesis is based on the application of the principles of the generalized geometric theory of diffraction.[1,6-8] It has been proposed and demonstrated that for sufficiently high frequencies, the steady-state form function f for backscattering from elastic spheres can be partitioned into three distinct components. These contributions are an ordinary specular reflection, transmitted bulk waves, and surface guided elastic waves. In the development of a ray synthesis of f for an elastic shell, the ordinary specular reflection and transmitted bulk wave contributions are grouped to form a generalized specular reflection component denoted by f_{sp}. The present ray synthesis of f_{sp} differs from a previous ray model[9-11] by introducing a curvature correction, f_{cc}. Inclusion of f_{cc} in the synthesis shows that f_{sp} can be significantly affected near longitudinal resonances within the shell. The conditions for excitation of longitudinal resonances are

$$k_L h = n\pi, \qquad (n = 1, 2, ...), \tag{1a}$$

$$k_L h = (n + 1/2)\pi, \qquad (n = 0, 1, ...), \tag{1b}$$

where $h = (a - b)$ is the thickness of the shell. Equation (1a) corresponds to the usual case (the one considered here) where the acoustic impedance of the elastic material $\rho_e c_L$ is greater than the impedance of the surrounding water ρc. When $\rho_e c_L$ is less than ρc then Eq. (1b) is the appropriate condition. These resonance conditions are obtained from the requirement of constructive interference of consecutive internally reflected rays upon transmission back into the water. Finally, for high-frequency scattering from the elastic shell considered here, the relevant surface guided elastic waves are leaky Lamb waves.

The steady-state scattered pressure in the farfield from an evacuated elastic spherical shell has the form[12]

$$p_s = p_0 \frac{af}{2r} e^{ikr}, \tag{2}$$

where p_0 is the pressure amplitude of the incident acoustic plane wave. The wavenumber k of the incident plane wave is defined by $k = \omega/c$ where ω is the angular frequency and c is the speed of sound in water. The harmonic time dependence $exp(-i\omega t)$ has been suppressed. The outer radius of the spherical shell is a and r is the distance from the center of the shell to some distant observation point. The complex scattering amplitude or form function in the backscattered direction has the exact partial-wave series representation[12]

$$f = \frac{2}{ix} \sum_{n=0}^{\infty} (-1)^n (2n + 1) \frac{B_n(x)}{D_n(x)}, \tag{3}$$

where $x = ka = 2\pi a/\lambda$ and λ is the wavelength of the incident plane wave. The functions $B_n(x)$ and $D_n(x)$ are 5×5 determinants obtained by satisfying the appropriate boundary conditions.[12] The elements of these determinants, which are complicated expressions of spherical Bessel functions and spherical Hankel functions of the first kind, are listed in

Ref. 12. The material parameters for the elastic shell are the longitudinal sound speed c_L, the shear or transverse sound speed c_s and the density ρ_e while the density of water is denoted by ρ.

The organization of this article is as follows. In Sec. 4.2.A, the ray synthesis of an individual leaky Lamb wave contribution, f_l, to the form function for backscattering is developed. The expression for f_l is cast in a form analogous to a Fabry-Perot resonator. Section 4.2.B summarizes a ray synthesis of f_{sp} and demonstrates that f_{sp} can be separated into a term associated with reflection from a vacuum-backed flat elastic plate and a curvature dependent correction. Using parameters corresponding to a 440c stainless steel shell studied in Ref. 12, the results of the ray synthesis and exact partial-wave series are compared in Secs. 4.3 and 4.4. Since a longitudinal resonance does not significantly affect the ranges $0 < x < 60$ and $80 < x < 100$, the computations in Sec. 4.3 consider these regions. The presence of a longitudinal resonance in the range $60 < x < 80$ complicates the analysis and this region is investigated in more detail in Sec.4.4. A general discussion and concluding remarks are contained in section 4.5. Appendix A contains a discussion of the radiation damping parameter and normalized phase velocity for each leaky Lamb wave contribution. These leaky Lamb wave parameters are essential to the ray synthesis calculations and are included for completeness. The first antisymmetric and symmetric leaky Lamb wave contributions are isolated in Appendix B. The Fabry-Perot form of f_l is investigated and a discussion of off-resonance contributions from a Lamb wave to the form function for backscattering is presented. Finally, Appendix C studies a peak near $x = 71$ in the ray synthesis of f which is not contained in the exact partial-wave series result. The discussion in Appendix C is based in part on a localization principle analysis of individual partial waves similar to that used by van de Hulst for light scattering.[13]

4.2. Ray synthesis of the form function for backscattering

A. Leaky Lamb wave contributions

The methodology of the generalized geometrical theory of diffraction[1,7] is applied to the backscattering of a plane wave from a hollow elastic spherical shell. For the canonical problem of high-frequency scattering from elastic shells, leaky Lamb waves are the relevant surface guided elastic waves which produce the resonance structure observed in the form function for backscattering. (In Sec. 4.3 below, it is demonstrated that the ray synthesis works well down to $x \approx 7$ for the particular shell considered. For smaller x the contributions of *subsonic*[14] Lamb and Franz-type waves may be significant.) The ray diagram in Fig. 1 provides a fundamental illustration of the ray synthesis of f_l. This diagram is similar to those discussed in Refs. 1, 6, 12, and 15. The diagram represents an elastic spherical shell of outer radius a and inner radius b situated such that the shell's center C coincides with the origin of the coordinate axis. A plane wave propagates in the positive z-direction along the ray AB in Fig. 1. At point B the acoustic wavefield in water couples to the shell and launches a leaky Lamb wave. The Lamb wave is guided by the shell along the arc BB' continuously re-radiating energy into the water. At B', the radiated energy is backscattered along the ray $B'A'$. (Physically, B and B' actually locate surface regions where the interaction takes place. The width of the regions correspond to the size of *Fresnel zones*.[16]) The leaky Lamb wave repeatedly circumnavigates the shell radiating energy in the backscattering direction with each circumnavigation. The points B and B' are obtained from the phase velocity trace-matching condition,[1,12]

$$\theta_l = \arcsin(c/c_l), \qquad c_l \geq c, \tag{4}$$

where θ_l is the local angle of incidence and c_l is the phase velocity of the leaky Lamb wave. The phase velocity is taken to be the phase velocity of the leaky Lamb wave along the outer surface of the shell[17] and is assumed to be supersonic.

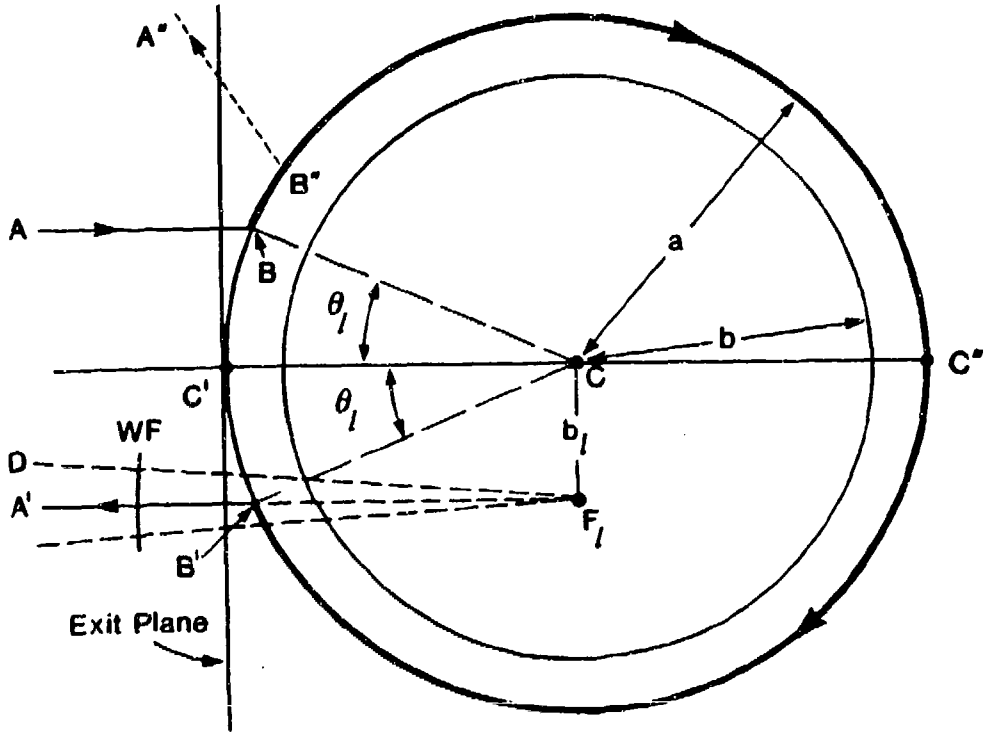

Fig. 1 A ray diagram for a contribution from a leaky Lamb wave to the form function for backscattering from an elastic spherical shell of outer radius a and inner radius b. A plane wave represented by the ray AB couples to shell at B launching a leaky Lamb wave. The Lamb wave is guided by the shell through a polar caustic at C'' to B'. At B' the radiated energy is shed in the backscattered direction along the ray $B'A'$. The points B and B' are determined from Eq. (4) where θ_l is the local angle of incidence. The Lamb wave continues to circumnavigate the shell shedding some energy at B' with each passage. The point C' is the specular point and the location of a second polar caustic. For backwards and near backwards scattering the rays $B'A'$ and DF_l appear to diverge from a virtual source located at point F_l. When the diagram is rotated about $C'C$, the point F_l traces out a virtual ring-like source. The vertical line through C' represents an exit plane for an outgoing toroidal wavefront associated with the ring-like source.

The form of an individual leaky wave contribution to the backscattering amplitude is obtained by summing the backscattering amplitudes for each circumnavigation,[1,7]

$$f_l = -G_l e^{i\eta_l} e^{-2(\pi - \theta_l)\beta_l} \sum_{m=0}^{\infty} e^{im\pi} e^{-2\pi m\beta_l} e^{i2\pi mxc/c_l}. \qquad (5)$$

The geometrical phase shift $\eta_l = [2x(c/c_l)(\pi - \theta_l) - 2xcos(\theta_l) - \pi/2]$ accounts for the phase difference between a Lamb wave propagating along the arc BB' and a wave in water propagating from C' to C and back to C' as if the shell were not present. The $\pi/2$ term in η_l is associated with the propagation of the leaky Lamb wave through the polar caustic at C''. The additional phase shift, $2\pi xc/c_l$, is attributable to repeated circumnavigation of the leaky Lamb wave about the shell. The π phase shift results from the polar caustics at C' and C''. The radiation damping of the leaky Lamb wave is characterized by the radiation damping parameter β_l with units of *Np/rad*. The factor $exp[-2(\pi - \theta_l)\beta_l]$ is the radiation damping of the partial circumnavigation of the Lamb wave along BB'; while $exp(-2\pi\beta_l)$ accounts for the additional radiation damping due to repeated circumnavigation. The efficiency of the coupling between the wavefield in water and the leaky Lamb wave at the points B and B' is characterized by a complex coupling coefficient G_l. Inspection of the summation in Eq. (5) shows that it is a geometric series and Eq. (5) reduces to

$$f_l = [\, -G_l e^{i\eta_l} e^{-2(\pi - \theta_l)\beta_l} \,] / [\, 1 + e^{-2\pi\beta_l} e^{i2\pi xc/c_l} \,]. \qquad (6)$$

The form of the denominator in Eq. (6) is that of a Fabry-Perot resonator.[1,7] Appendix B contains a discussion of $|f_l|$ for the lowest antisymmetric and symmetric leaky Lamb waves. Finally, Eq. (6) is the ray synthesis of the contribution of an individual leaky Lamb wave to the form function for backscattering.

Williams and Marston[6] applied the Sommerfeld-Watson transformation to the partial-wave series representation of f for backscattering from a solid elastic sphere. From

their analysis a complicated expression for the complex coupling coefficient G_l was obtained (see Eq. (28) of Ref. 6). Subsequently, Marston[1] developed an approximation for G_l which gives explicit dependence of $|G_l|$ on the leaky Lamb wave parameters β_l and c_l/c. The approximation can be expressed as

$$G_l = 8\pi\beta_l (c/c_l) e^{i\phi_l}, \tag{7}$$

where ϕ_l denotes the phase of G_l and it may be argued that $\phi_l \approx 0$ for elastic spheres or shells.[11,18] For the computations of the ray synthesis of $|f|$ in Secs. 4.3 and 4.4, ϕ_l for the *lth* leaky Lamb wave is taken to be identically equal to zero. Equation (7) was employed in the modeling of backwards and near backwards scattering of short tone bursts from a 440c stainless steel shell in experiments discussed in Ref. 12. Further confirmation of the applicability of Eq. (7) to the backscattering from elastic spherical shells is demonstrated below in Secs. 4.3 and 4.4. An alternative derivation of Eq. (7) with $\phi_l = 0$ has been given for a thin fluid-loaded spherical shell.[2]

Consider again the ray diagram in Fig. 1. For an observation point on the negative z-axis a finite distance from C, the ray that reaches the observation point is DF_l not ray $B'A'$. It can be argued that the appropriate modifications to the ray synthesis of f_l are negligible provided the observation point is sufficiently distant.[1] The intersection of rays $B'A'$ and DF_l at the point F_l locates a virtual source. The point F_l is situated in the vertical plane perpendicular to the z-axis through the point C.[19] From the symmetry of the shell, it is apparent that the virtual source is ring-like and has a radius $b_l = a\ sin(\theta_l)$. Hence, the backwards and near backwards contribution of a leaky Lamb wave may be modeled by a virtual ring-like source. The local outgoing wavefront in the vertical plane through point C' from a ring-like source has a toroidal shape. A toroidal wavefront is associated with the phenomena of axial focusing or glory scattering.[15,19-22] Axial focusing of the

backscattering from solid elastic spheres[19,20] and elastic spherical shells[12] has been observed.

B. Specular reflection contribution

The specular reflection contribution f_{sp} in the form function for backscattering from an evacuated elastic spherical shell can be approximated by ray methods. Figure 2 shows a simplified ray diagram which facilitates the ray synthesis. The diagram is similar to the one discussed in Ref. 23. The orientation of the shell with respect to the incident plane wave is the same as in Fig. 1 where the points S and O in Fig. 2 correspond to C' and C in Fig. 1, respectively. The specular reflection appears to originate at S and is often referred to as the specular point.[24] The incident rays which significantly affect f_{sp} lie close to the z-axis. Consider the incident ray AB in Fig. 2 with infinitesimal impact parameter s. Rotation of the figure about the line SO generates all the incident rays with impact parameter s. At point B the ray is partially reflected back into the water and partially transmitted into the elastic shell. The intersection of the reflected ray BC with the axis SO at V_0 defines the location of a virtual source. For backwards and near backwards scattering, spherical aberration may be neglected and the virtual source can be described as a point source. Since the impact parameter s is assumed small, then the angle between the incident ray and the outward unit normal at point B is infinitesimal. Hence,the ray AB is approximately at normal incidence with the shell and the energy transmitted into the shell will produce a (bulk) longitudinal wave. To simplify the ray synthesis, the weak mode conversion between a longitudinal wave and a transverse (shear) wave upon reflection at a surface is *neglected* since the angle of incidence is infinitesimal. The transmitted ray at B is refracted and propagates along BD. At D (again neglecting mode conversion), total internal reflection occurs and the longitudinal wave propagates along DE. The ray is again partially reflected and transmitted at E. Projection of the transmitted ray after refraction at E back to

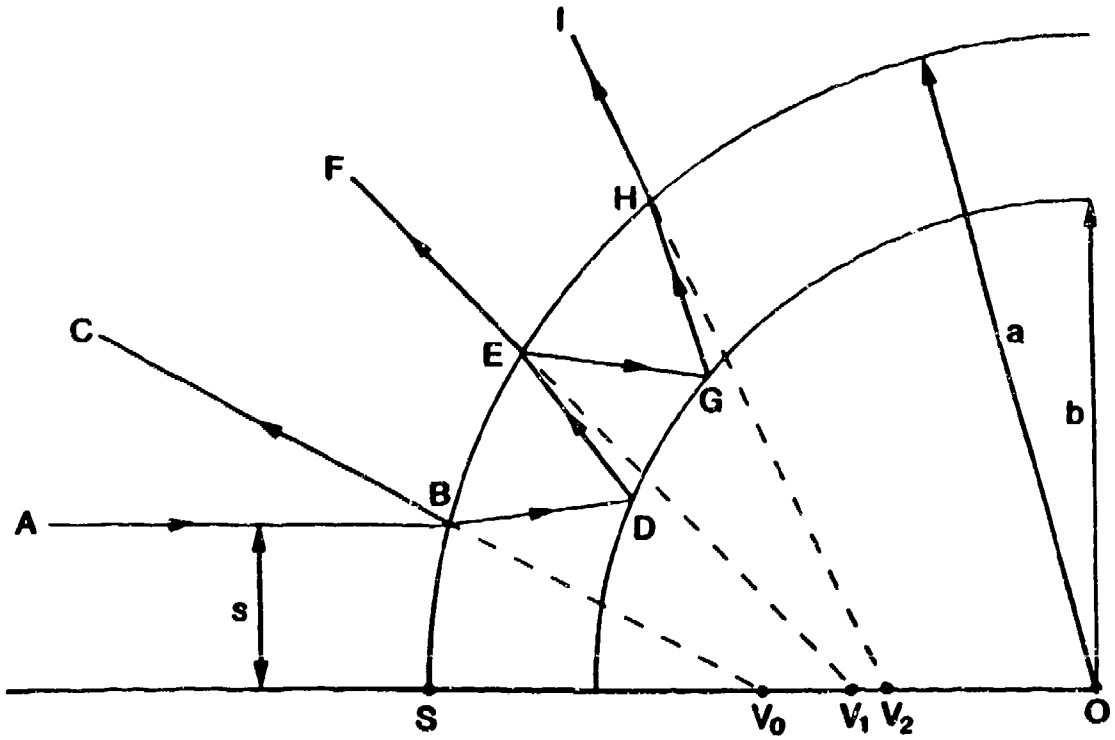

Fig. 2 The ray diagram for the specular reflection from an evacuated elastic spherical shell of outer radius a and inner radius b. The point S is the vertex of the refracting surface and O is the origin of a coordinate axis located at the center of the shell. The ray AB infinitesimally close to the z-axis is incident on the shell with impact parameter s. The ray ABC is the ordinary specular ray; while $ABDEF$ and $ABDEGHI$ are the first two internal specular reflection contributions. At $r = b$, the rays are totally reflected and the rays are partially reflected and/or transmitted at the water-shell interface. Intersection of the projection (dashed lines) of the outgoing rays and the z-axis define locations of virtual point sources, V_n, which describe local curvature of the wavefront associated with each ray. The specular reflection contribution to the form function for backscattering is determined from a superposition of the wavefields from the virtual sources.

the z-axis gives the location of a second virtual point source V_1. By continuing to trace the ray trajectories of the higher internal reflections an infinite set of virtual point source locations V_n on the z-axis can be generated.

Each virtual point source V_n describes the propagation of a local outgoing wavefront associated with the *nth* ray. In the limit $s \rightarrow 0$, the specular reflection contribution to the farfield pressure is a superposition of the acoustic wavefields from the virtual point sources,

$$p_{sp} = p_0 \frac{e^{ikr}}{r}\left(e^{-i2x} \sum_{n=0}^{\infty} H_n C_n e^{i2nk_L h} \right), \tag{8}$$

where $k_L = \omega/c_L$. The $2x$ phase shift accounts for the path length difference between a ray propagating in water from S to O and back to S and a ray which is backscattered at S. The additional phase delay within the summation comes from a longitudinal wave which reverberates n times within the shell before being transmitted in the backscattered direction. The amplitude of the *nth* virtual point source is H_nC_n where H_n represents a geometric divergence factor and C_n accounts for the cumulative effects of partial reflection and/or transmission. By applying an acoustic ray analysis of longitudinal resonances within a fluid shell the following expressions for H_n and C_n were obtained[23]

$$H_n = \frac{(a/2)}{1 + nB}, \tag{9}$$

and

$$\begin{aligned} C_0 &= r, \\ C_n &= -r^{n-1}(1 - r^2), \quad (n > 0), \end{aligned} \tag{10}$$

where $B = (c_L h/cb)$ and $r = [\rho_e c_L - \rho c]/[\rho_e c_L + \rho c]$. The constant B depends on only the normalized longitudinal sound speed of the elastic material and the radii of curvature of the

inner and outer surfaces. The reflection coefficient for the scattering of an acoustic plane wave at normal incidence from an interface between water and an elastic half-space is r.

After substitution of Eqs. (9) and (10) into Eq. (8), comparison with Eq. (2) gives an expression for f_{sp} which depends on the geometric and material parameters of the shell,

$$f_{sp} = \left(r - \frac{(1 - r^2)}{r} \sum_{n=1}^{\infty} \frac{r^n e^{i2nk_L h}}{1 + nB} \right) e^{-i2x}. \tag{11}$$

Although Eq. (11) is a ray synthesis of the contribution of the specular reflection to the form function for backscattering, it can be manipulated such that each resulting term has a simple physical interpretation. With the replacement of $[1+nB]^{-1}$ by $1 - nB[1+nB]^{-1}$, the summation in Eq. (11) can be split into two summations. The first summation, via a geometric series, has the analytic form $rexp(i2k_Lh)[1-rexp(i2k_Lh)]^{-1}$. Hence, f_{sp} becomes

$$f_{sp} = \mathcal{R} e^{-i2x} + f_{cc}, \tag{12}$$

where

$$\mathcal{R} = r - \frac{(1 - r^2) e^{i2k_L h}}{1 - r e^{i2k_L h}}, \tag{13}$$

and

$$f_{cc} = \left(\frac{(1 - r^2)}{r} \sum_{n=1}^{\infty} \frac{nB r^n e^{i2nk_L h}}{1 + nB} \right) e^{-i2x}. \tag{14}$$

Define $f_p = \mathcal{R} exp(-i2x)$ where $\mathcal{R}$ is the complex reflection coefficient associated with the scattering of a normal incidence plane wave from a vacuum-backed flat elastic plate of thickness h.[25,26] Hence, f_p describes the reflection from an elastic spherical shell where the complex reflectivity is modeled as that for a flat elastic plate. Consequently, the

influence of the curvature of the shell on f_{sp} within the paraxial approximation must be contained in Eq. (14). At present a simple analytic expression for f_{cc} is unavailable, but a rapid summation technique has been described and implemented in Appendix C of Ref. 23.

Figure 3 demonstrates the importance of f_{cc} to the ray synthesis of $|f_{sp}|$. The material and geometric parameters used in the computation correspond to the parameters of a 440c stainless steel shell studied in Ref. 12. The values of these parameters are as follow: $c_L = 5.854$ *km/s*, $c_s = 3.150$ *km/s*, $\rho_e = 7.84$ *g/cm*^{3} and $b/a = 0.838$ for the elastic shell; $c = 1.479$ *km/s* and $\rho = 1.00$ *g/cm*^{3} for water. The resonance condition given in Eq. (1a) predicts that the a longitudinal resonance should occur at $x_{LR} \approx 76.8$. Clearly, the minimum observed in Fig. 3 at $x \approx 77$ is a manifestation of this longitudinal resonance. It is noted that the approximation $f_{sp} \approx f_p$ is not sufficient to produce the observed minimum. It is relatively simple to demonstrate that $|f_p| = 1$ for all x. The importance of f_{cc} in the synthesis of $|f|$ for a 440c stainless steel shell will be examined in more detailed below in Sec. 4.4. Hence, the curvature of the shell appears to be intimately related to the presence of a longitudinal resonance in the specular contribution to the form function for backscattering.

4.3. Comparison of the ray synthesis and exact calculation of $|f|$ for x outside the region of a longitudinal resonance

To facilitate a discussion of a comparison between the ray synthesis and the exact partial-wave series computation of $|f|$, the range $0 < x < 100$ is split into five intervals. By displaying these smaller regions, the finer details of the high Q resonance structure caused by some of the leaky Lamb wave contributions are more easily resolved. The range $60 < x < 80$ is examined in more detail in Sec. 4.4 because the presence of a longitudinal

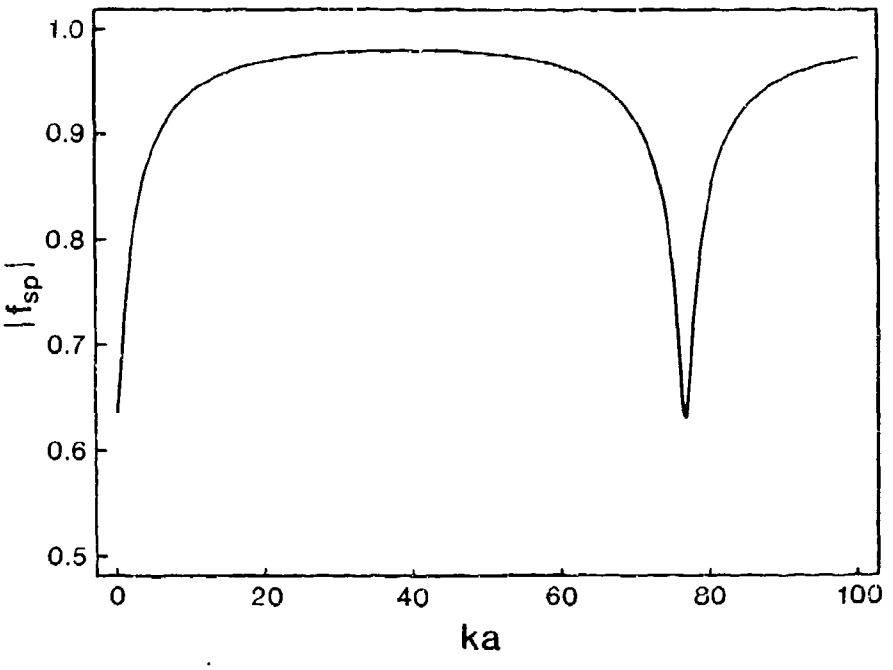

Fig. 3 The modulus of specular reflection f_{sp} from an elastic spherical shell as defined by Eqs. (12) - (14). The broad minimum at $x \simeq 77$ is a manifestation of a longitudinal resonance. The resonance condition in Eq. (1a) predicts a longitudinal resonance occurs at $x_{LR} = 76.8$. As discussed in 4.2.B, if the curvature correction component f_{cc} were omitted in Eq. (12), then $| f_{sp} | \simeq | f_p | = 1$ for all x.

resonance obfuscates the cause of certain resonance features. In the calculations below, unless otherwise stated, the ray synthesis is

$$f_{ray} \approx f_{sp} + \sum_l f_l = f_p + f_{cc} + \sum_l f_l, \tag{15}$$

where the summation in Eq. (15) is over the possible leaky Lamb wave contributions. The material of the elastic shell is 440c stainless steel with the parameters listed above in Sec. 4.2.B.

The computation of the partial-wave series for the form function for backscattering requires the truncation of the infinite summation in Eq. (3). The minimum number of terms (or maximum partial-wave index) n_{max} retained for sufficient convergence of f_{PWS} exceeds x. The following criterion was tested and determined to ensure adequate convergence of the series for the shell considered:

$$\begin{aligned} n_{max} &= 2 + [\, x + 4.0x^{1/3} \,], \qquad x < 8, \\ n_{max} &= 3 + [\, x + 4.05x^{1/3} \,], \qquad x \geq 8, \end{aligned} \tag{16}$$

where the square brackets imply truncation to the nearest integer. For very thin shells caution in the use of Eq. (16) for determining n_{max} may be required since subsonic guided wave contributions can be significant. From the localization principle subsonic guided waves are associated with partial waves having $n > x$. Discussions concerning the choice of Eq. (16) are contained in Refs. 15 and 23. Secondly, to ensure adequate resolution of the high Q resonance structure, the increment Δx needs to be small. For the computations of $|f_{PWS}|$ shown below $\Delta x = 0.01$ except in the vicinity of the very narrow resonance structure caused by the s_0 leaky Lamb wave (see Appendix B). Near these resonances, it was necessary to take steps in Δx as small as 0.00001. Hence, it is evident from Eq. (16) and the small size of Δx that the partial-wave representation of f in high-frequency backscattering calculations can be numerically intensive.

The relevant leaky Lamb waves are analogous to Lamb waves that can be excited on a flat elastic plate of thickness h in vacuum.[27,28] Using the terminology associated with the flat plate results, the leaky Lamb waves excited on the shell for $0 < x < 100$ are designated a_0 and a_1 for antisymmetric or flexural Lamb waves and s_0, s_1, and s_2 for symmetric or dilatational Lamb waves. As the frequency increases, higher Lamb wave resonances can couple with the acoustic wavefield in water and these higher modes can easily be included in the synthesis. The computation of Eq. (15) requires the parameters $\beta_l(x)$ and $c_l(x)/c$ for the *lth* leaky Lamb wave. These parameters can be determined by extending certain results of the Sommerfeld-Watson transformation analysis of the backscattering from a solid elastic sphere.[6,7] The pertinent results from this analysis are summarized in Appendix A and $\beta_l(x)$ and $c_l(x)/c$ for the *lth* leaky Lamb wave are examined. The values of $\beta_l(x)$ and $c_l(x)/c$ depicted in Figs. A1 and A2 are employed in the present calculations. Finally, Eqs. (6) and (12) - (14) are the expressions necessary for the calculation of $|f_{ray}|$.

Figure 4 displays the comparison of $|f_{PWS}|$ and $|f_{ray}|$ where the dashed curve corresponds to the exact partial-wave representation and the solid line is the ray synthesis result. In the interval $0 < x < 20$, Fig. 4a, the shell can support both the a_0 and s_0 leaky Lamb waves. The ray synthesis, Eq. (15), is truncated at $x = 7$ since the phase velocity for the a_0 leaky Lamb wave becomes subsonic. From inspection of Eq. (4), the present ray synthesis is implicitly a supersonic theory. Comparing Figs. 4a, B1, and B2 demonstrates that the broad resonance structure is attributable to the a_0 mode; while the s_0 Lamb wave is responsible for the sharp (high Q) resonance features at $x \approx 10$, 14, and 18. *It is noteworthy that the high-frequency ray synthesis gives fairly good agreement even though x is not very large.* To accurately model the exact $|f_{PWS}|$ for $x < 7$, both the subsonic portion of the a_0 Lamb wave and Franz-type (creeping) waves would need to be considered. Figure 4b shows the range $20 < x < 40$ where the relevant leaky Lamb wave

contributions are a_0 and s_0. Again, the broad resonance structure is due to a_0 and the sharp features are associated with the s_0 Lamb wave. The agreement between the synthesis and exact solution is excellent. Finally, Fig. 4c compares $|f_{PWS}|$ and $|f_{ray}|$ where the next possible leaky Lamb wave can contribute to the backscattering. This new contribution is the a_1 leaky Lamb wave which appears to have a cutoff frequency near $x = 41$. Inclusion of the a_0, s_0, and a_1 leaky Lamb waves not only reproduces all the resonance features, but the agreement between the ray synthesis and the exact partial-wave series representation is excellent.

The range $80 < x < 100$ is shown in Fig.5. The relevant contributions to the ray synthesis contained in Fig. 5a are a_0, a_1, s_0, and s_1 as well as the specular reflection. Although the ray synthesis seems to reproduce the resonance features in $|f_{PWS}|$, some differences are evident. For $x > 83$ the ray synthesis can be improved by including the s_2 leaky Lamb wave which appears to have a cutoff frequency near $x = 83$. By including the s_2 leaky Lamb wave contribution in the synthesis of Fig. 5b, the exact result is modeled more accurately by $|f_{ray}|$ particularly for $x > 88$. The difference between $|f_{ray}|$ and $|f_{PWS}|$ for $x < 85$ might be associated with a longitudinal resonance discussed in Sec. 4.4. The broad minimum in the specular reflection contribution shown in Fig. 3 caused by a longitudinal resonance at $x_{LR} \approx 76.8$ may significantly affect the form function for $x < 85$. Inspection of Fig. 5 demonstrates, however, that the geometric ray synthesis contains the resonance structure caused by various leaky Lamb wave contributions.

4.4. Form function in the vicinity of a longitudinal resonance.

The resonance structure in $|f_{PWS}|$ for the interval $60 < x < 80$ is perhaps the most difficult region to interpret physically. Within this range, a longitudinal resonance can be

Fig. 4a

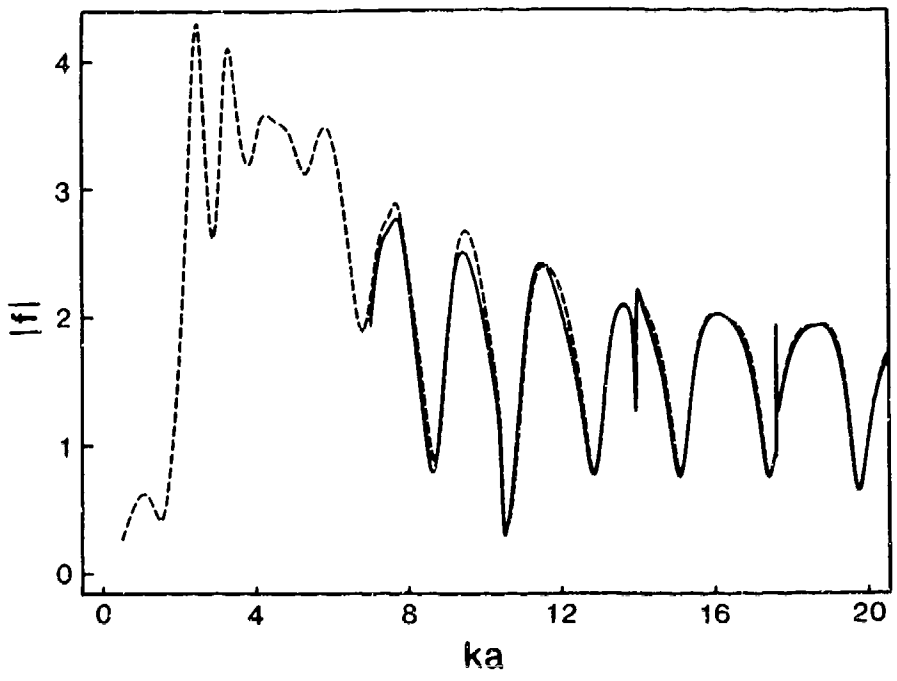

Fig. 4b

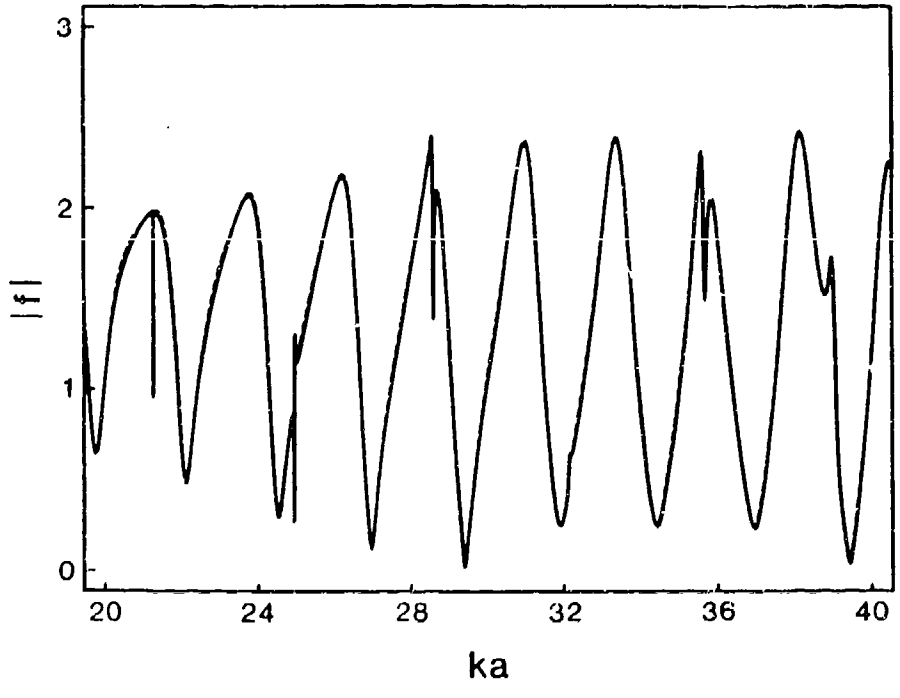

Fig. 4c

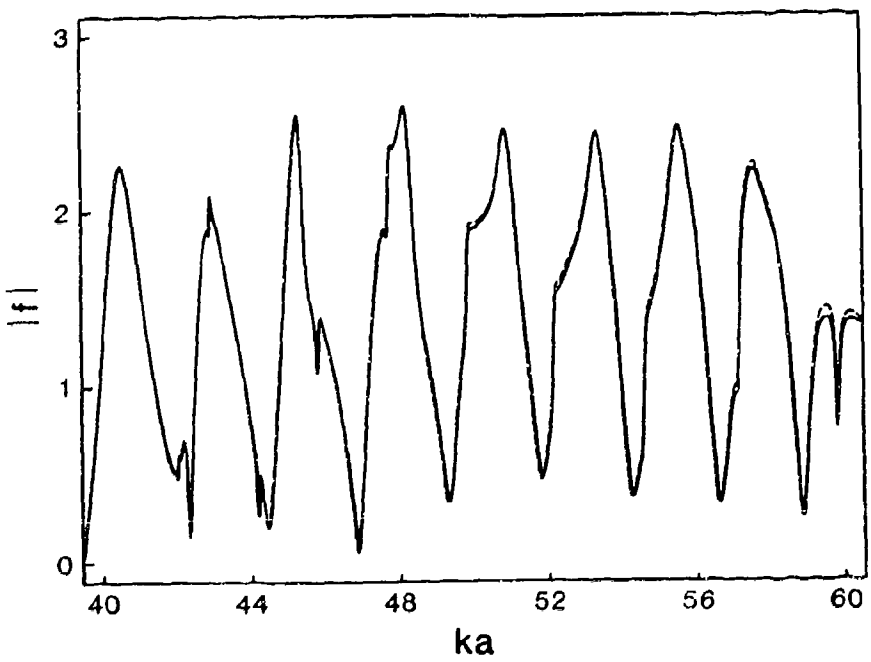

Fig. 4 The dashed line is the exact partial-wave representation, $|f_{PWS}|$, and the solid line is the ray synthesis, $|f_{ray}|$ for the stainless steel shell considered with $b/a = 0.838$. The pertinent leaky Lamb waves included in each synthesis are: (a) a_0 and s_0; (b) a_0 and s_0; (c) a_0, s_0, and a_1. In (a) the ray synthesis is truncated below $x = 7$ since a_0 becomes subsonic and the ray synthesis is implicitly a supersonic theory. The agreement between the high-frequency ray synthesis and the exact results indicate that the ray synthesis may be useful for non-canonical scattering problems.

Fig. 5a

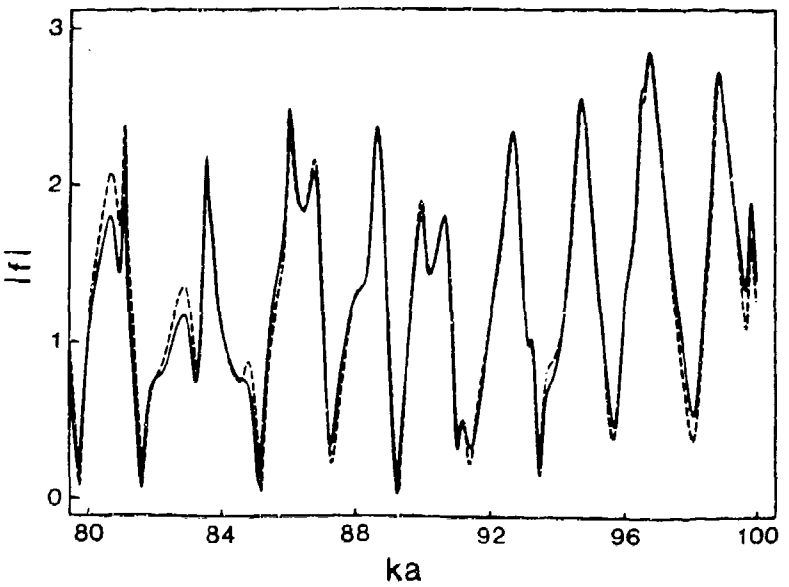

Fig. 5b

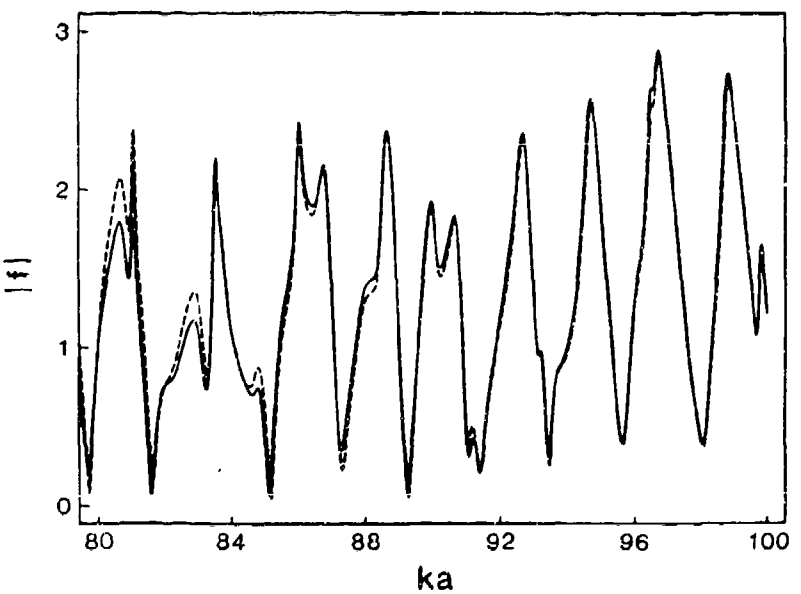

Fig. 5 The exact $|f_{PWS}|$ and $|f_{ray}|$ are the dashed and solid curves, respectively. In (a) the relevant leaky Lamb wave contributions are: a_0, a_1, s_0, and s_1; while in (b) the leaky Lamb waves are: a_0, a_1, s_0, s_1, and s_2. The specular reflection employed in $|f_{ray}|$ is given by Eqs. (12) - (14). The importance of these figures is that the ray synthesis accurately models the resonance structure in the exact result and the inclusion of the s_2 leaky Lamb wave in (b) improves the synthesis.

supported by the elastic shell. From Eq. (1a), the longitudinal resonance is predicted to occur at $x_{LR} \approx 76.8$. It is observed in Fig. 3 that the longitudinal resonance can affect a relatively broad range of x in the vicinity of x_{LR}. Also, within this region of x the 440c stainless steel shell can support the a_0, a_1, s_0, and s_1 leaky Lamb waves. Of these Lamb waves, the physical nature of the s_1 Lamb wave contribution to $|f_{ray}|$ becomes difficult to understand. The s_1 Lamb wave on a 440c stainless steel flat plate of thickness h in vacuum has a cutoff frequency corresponding to[29] $x \approx 76.8$, but the dispersion curve in Fig. A2 for s_1 does not demonstrate an abrupt cutoff. (The dispersion curve near a cutoff should be particularly sensitive to the fluid loading.) Furthermore, the group velocity for the s_1 leaky Lamb wave becomes negative for $x < 71$ (see Appendix A). As discussed below, the presence of a longitudinal resonance and the behavior of the s_1 leaky Lamb wave for $x < 71$ obfuscates a physical interpretation of the scattering process.

Figure 6a compares $|f_{PWS}|$ and $|f_{ray}|$ where the curvature correction f_{cc} is omitted in Eq. (15). The ray synthesis works well for $x < 70$, but for $x > 70$ the synthesis fails to model the exact result. In particular, in the vicinity of $x = 76.8$ the ray synthesis gives a completely erroneous representation of the form function for backscattering. However, it is evident from Fig. 6a that the positions of the sharp resonance features caused by the presence of leaky Lamb waves seem to be correctly predicted. Figure 6b compares $|f_{ray}|$ and $|f_{PWS}|$, but f_{cc} is now included in the synthesis. It is immediately evident that the inclusion of the curvature correction improves the synthesis. Although $|f_{ray}|$ does not fully replicate $|f_{PWS}|$, Fig. 6b indicates that the contribution from a longitudinal resonance (as presently modeled) is an important contribution in the exact result. Furthermore, the ray method employed in determining an expression for f_{sp} necessarily includes the influence of the shell's curvature explicitly in f_{cc}.

An examination of the absolute error may give some insight into the cause of the

Fig .6a

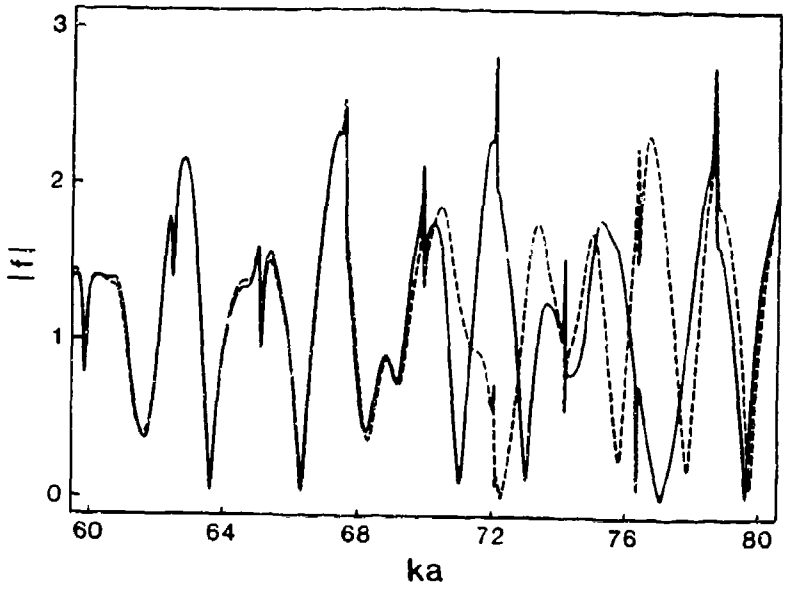

Fig. 6b

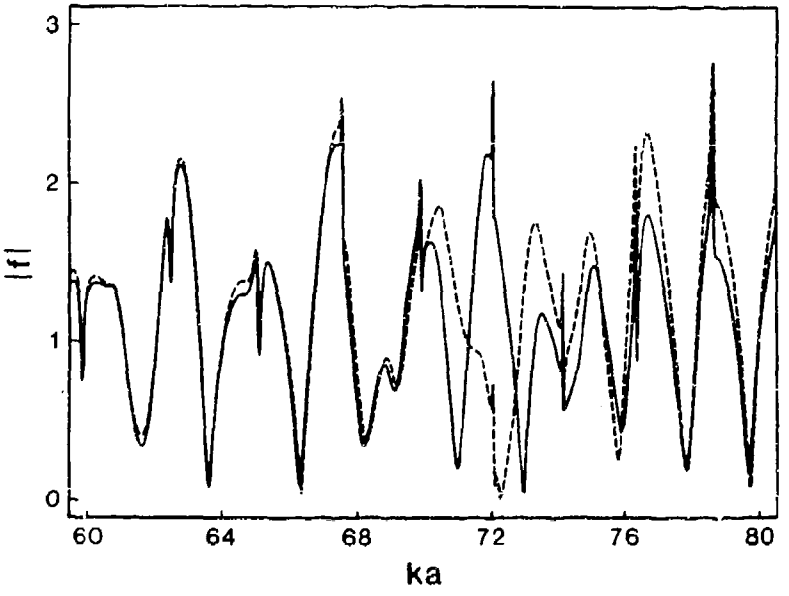

Fig. 6 The relevant leaky Lamb wave contributions are a_0, a_1, s_0, and s_1. In (a) the curvature correction f_{cc} is omitted in Eq. (15). The agreement between $|f_{ray}|$ (solid line) and $|f_{PWS}|$ (dashed line) is good for $x < 70$, but $|f_{ray}|$ fails to model $|f_{PWS}|$ for $x > 70$. Inclusion of f_{cc} in $|f_{ray}|$ in (b) replicates $|f_{PWS}|$ for $x < 70$ and $x > 74$, but the agreement above $x = 74$ is marginal. At present, the cause of the anomaly in $|f_{ray}|$ near $x = 71$ is not fully understood (see Secs. 4.4 and 4.5 and Appendix C).

discrepancy between $|f_{PWS}|$ and $|f_{ray}|$ near $x = 71$. A measure of the absolute error in the ray synthesis is given by $E_j = |f_{PWS} - f_{ray}|$, j = 1, 2. Figure 7 contains three curves. The solid line is E_1 where the curvature correction in Eq. (15) has been omitted. The short-dashed line is E_2 when f_{cc} is included in f_{ray}. The long-dashed line corresponds to $|f_{cc}|$ where Eq. (14) is employed. The reduction in E_j when f_{cc} is included is given roughly by $|f_{cc}|$. The cause of the peak near $x = 76.8$ in E_1 is due to the omission of f_{cc} in f_{ray} and the peak near $x = 71$ must not be related exclusively to a longitudinal resonance.

The identification of specific resonance features associated with the *lth* leaky Lamb wave can be achieved by comparing $|f_l|$ in Figs. B1 and B2 with $|f_{PWS}|$ in Fig. 6a. The narrow resonance structure (at $x \approx 62.5$, 65.0, 67.5, 69.8, 72.0, 74.2, 76.3, and 78.7) is a result of the a_1 leaky Lamb wave contribution. The broad structure is a combination of the a_0 and s_0 leaky Lamb waves. Since the widths of the a_0 and s_0 resonances are fairly broad, it is difficult to unambiguously identify a feature in $|f_{PWS}|$ with either Lamb wave. However, it is apparent from the magnitude of each contribution that neither the a_0 nor the s_0 leaky Lamb wave is responsible for the significant difference between $|f_{ray}|$ and $|f_{PWS}|$ near $x = 71$. The final contribution to the ray synthesis is the s_1 leaky Lamb wave. The Fabry-Perot representation as developed in Sec. 4.2.A accounts for the partial circumnavigation and all subsequent circumnavigations of a Lamb wave about the shell. Furthermore, inspection of Eq. (6) and Fig. A1 demonstrates that the large radiation damping of the s_1 Lamb wave effectively makes its contribution to $|f_{ray}|$ negligible for $x <$ 72. It is noteworthy that our ray model[15] of the structure in the forward scattering amplitude (and the total scattering cross via the optical theorem) for the same shell has no anomalies near either $x \approx 71$ or 76.8. Hence, the deficiency in the present model does not affect the forward scattering.

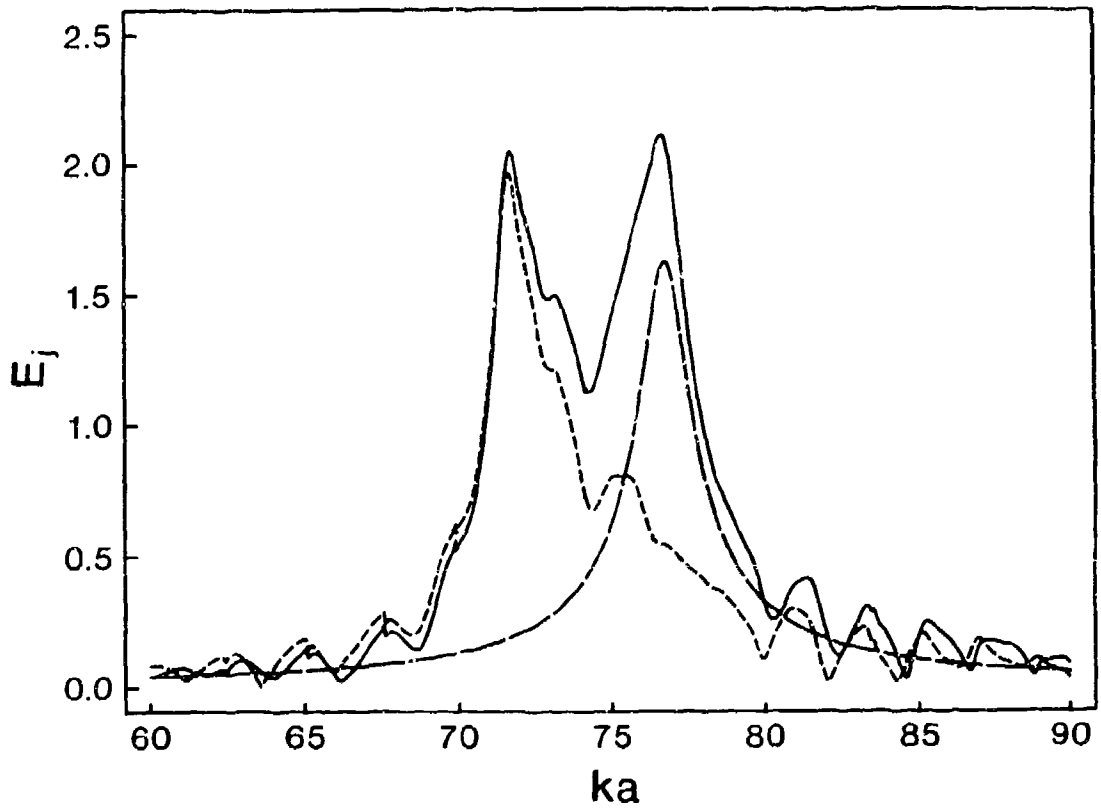

Fig. 7 The absolute error between the ray synthesis and the exact partial-wave series is given by $E_j = |f_{PWS} - f_{ray}|, j = 1, 2$. The solid line is E_1 where f_{cc} in Eq. (15) has been omitted. The short-dashed line, E_2, includes the effects of f_{cc} on f_{ray}. For comparison, the long-dashed line is $|f_{cc}|$. The inclusion of the curvature correction in f_{ray} accounts for the presence of a longitudinal resonance at $x_{LR} \approx 76.8$. Furthermore, the longitudinal resonance is not responsible for the anomaly near $x = 71$.

Inspection of Figs. 1 and A2 suggests a possible cause of the anomalous behavior near $x = 71$. As x is decreased to $x_{LR} = 76.8$ and below, c_l/c becomes large for the s_1 Lamb wave. As noted above, the frequency for which $x = x_{LR}$ corresponds to the cutoff frequency of the s_1 mode for the corresponding flat plate in vacuum of the same thickness $h = a - b$. Hence, the trace velocity-matching angle θ_l becomes small and the s_1 wave may radiate nearly backwards directly. This corresponds to the radiation along ray $B''A''$ (with B and B' shifted closer to C' than illustrated in Fig. 1). Such radiation was not included in Eq. (15) or elsewhere in the present analysis. It is plausible that such rays can contribute to backscattering even without being backward directed if the rays intercept the *Fresnel volume*[16] of a backwards directed ray. The essential concept is that rays in effect occupy a region of space (the Fresnel volume) and that sound radiated primarily in some direction (say along $B''A''$) can contribute to the scattering in other directions (e.g., the backwards axis). Further support for this mechanism is evident from inspection of Fig. A1 which shows that β_l for $l = s_1$ is very large for x in the region of interest. The large β_l indicates the s_1 leaky Lamb wave is strongly coupled to the acoustic field near the shell, thus enhancing the radiation in the general direction of the ray reflected with a local angle of incidence $\approx \theta_l$.

While the aforementioned mechanism for the anomaly near $x \approx 71$ has not been quantitatively modeled, additional support can be seen by inspection of the group velocity plotted in Fig. A3 for the $l = s_1$ mode of this shell. This mode is seen to have a negative group velocity for $x < 71$ when computed by the Watson transform methodology. This suggests that energy can be radiated back towards the source without circumnavigating the shell. It can be argued by inspection of Eqs. (39) and (40) of Ref. 1 that the final approximation for G_l, Eq. (7), may break down if c_{gl} is negative. The group velocity anomaly is further discussed in Appendix A.

The influence of a longitudinal resonance on the form function has also been seen for a set of material parameters for an aluminum shell. Figure 8 shows $|f_{PWS}|$ and $|f_{sp}|$ where the parameters are: $c_L = 6.42$ *km/s*, $c_s = 3.04$ *km/s*, $\rho_e = 2.70$ *g/cm*^{3}, c = 1.4825 *km/s*, and $\rho = 1.00$ *g/cm*^{3}. The thickness of the shell is $(h/a) = (1 - b/a) = 0.04$. The solid line in Fig. 8 is $|f_{PWS}|$ and the dashed line is $|f_{sp}|$. From Eq. (1a), a longitudinal resonance is predicted to occur at $x_{LR} \approx 340$. Clearly, the dip near $x = 340$ corresponds to the presence of the longitudinal resonance. Although, a detailed analysis of the surface guided elastic wave contributions for the aluminum shell has not been carried out, presumably the calculated resonance structure is a result of leaky Lamb waves. The large peak near $x = 300$ may be a manifestation of prompt radiation along path $B''A''$ as noted above.

4.5 Discussion and conclusion

The canonical problem of the backscattering of an acoustic plane wave from an elastic spherical shell has been re-examined by novel ray techniques. A form function for backscattering including leaky Lamb waves and a specular reflection has been developed and tested. The Fabry-Perot expression in Eq. (6) for a leaky Lamb wave contribution had previously been established[9-12] and the subsequent approximation of G_l by Eq. (7) had been verified for backscattering from spheres and shells.[18] The calculations presented here give further verification of the applicability of Eqs. (6) and (7) in describing leaky Lamb wave contributions to backscattering. The ray synthesis of the specular reflection is composed of a component associated with reflection from a flat elastic plate of a normal incidence plane wave and a novel curvature correction contribution f_{cc}. A comparison of the partial-wave representation and ray synthesis of the form function in Sec. 4.3 demonstrated regions of x where the exact result and synthesis were in excellent agreement.

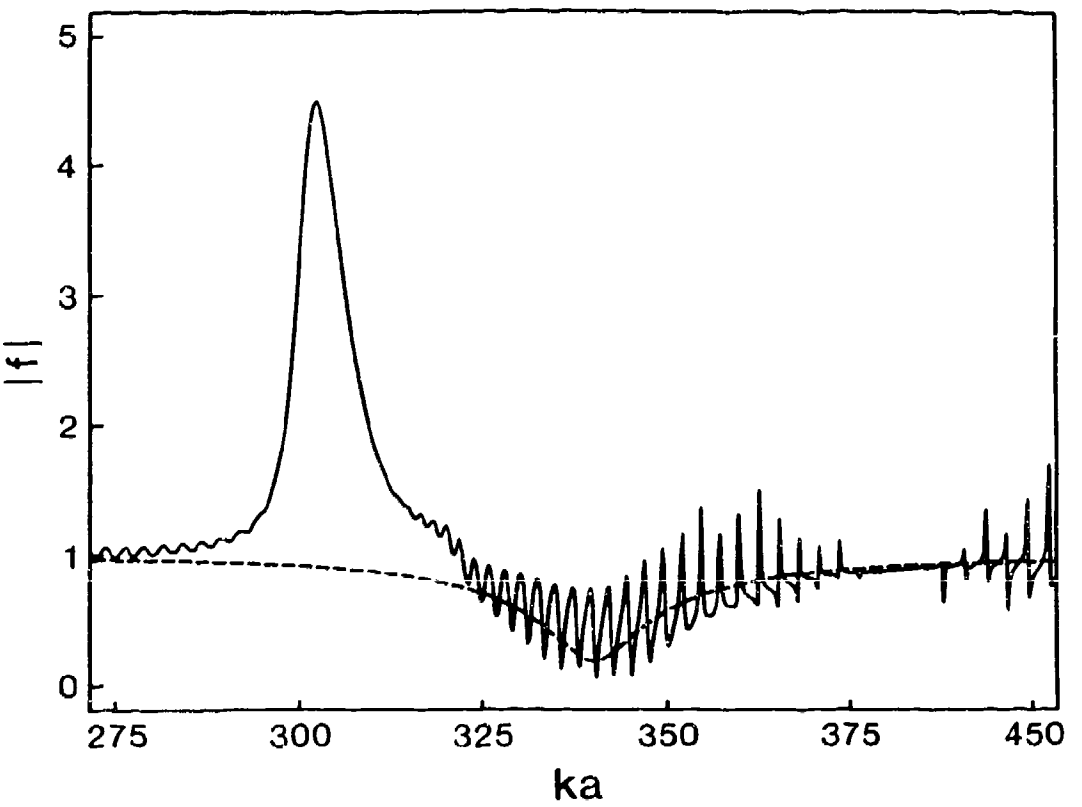

Fig. 8 For an aluminum shell with $b/a = 0.96$ and $c_L = 6.42$ *km/s*, Eq. (1a) predicts a longitudinal resonance at $x_{LR} \approx 340$. The solid line is the exact $|f_{PWS}|$ and $|f_{sp}|$ is the dashed line. The minimum in both $|f_{PWS}|$ and $|f_{sp}|$ at x_{LR} is a manifestation of this longitudinal resonance.

It is shown in Sec. 4.4 that inclusion of f_{cc} in f_{ray} accounted for the resonance structure in the form function caused by a longitudinal resonance. In Sec. 4.4, a comparison of the exact and synthesized results illustrated that the present ray model breaks down in a range of x where the s_1 leaky Lamb wave was found to have a negative group velocity. Finally, although a ray model is a high-frequency approximation, the synthesis displayed here for a 440c stainless steel shell was applicable down to $x \approx 7$.

While the inclusion of f_{cc} in Eq. (15) (and Fig. 5b) improves the synthesis in the vicinity of $x = x_{LR}$, it is noteworthy that the use of f_{cc} in Eq. (15) tends to increase the discrepancy between $|f_{PWS}|$ and $|f_{ray}|$ for $x < 12$. Figure 9 compares $|f_{PWS}|$ and $|f_{ray}|$ where $f_{cc} = 0$ in Eq. (15). That is, the specular reflection contribution to f is modeled as the specular reflection from a vacuum-backed flat elastic plate at normal incidence. Inspection of Figs. 4a and 9 suggests that for $x < 12$, f_{ray} with $f_{cc} = 0$ gives a more accurate representation of the exact $|f_{PWS}|$. This may be anticipated since the assumptions used in the modeling of f_{sp} as $f_p + f_{cc}$ breakdown for sufficiently low frequencies.

Three improvements to the current ray synthesis which should extend the range of applicability are as follows. *First*, extension of the ray synthesis to smaller values of x requires the inclusion of contributions from the subsonic portion of the a_0 leaky Lamb wave and Franz-type waves. These were not included in the present model since for subsonic waves Eq. (4) predicts $sin(\theta_l) > 1$. (During the course of this research, a method for including such contributions for thin shells has been proposed.[2]) Presumably, these types of surface guided elastic waves contribute to the structure in $|f|$ for $x < 7$. *Second*, improvements in the approximation for the specular contribution f_{sp} when x is not large may be needed. *Third*, a thorough investigation of the s_1 leaky Lamb wave behavior in the vicinity of the anomaly discussed in Sec. 4.4 should be conducted. As suggested in Sec. 4.4, a modified ray picture may be needed in this region. The consequence of a

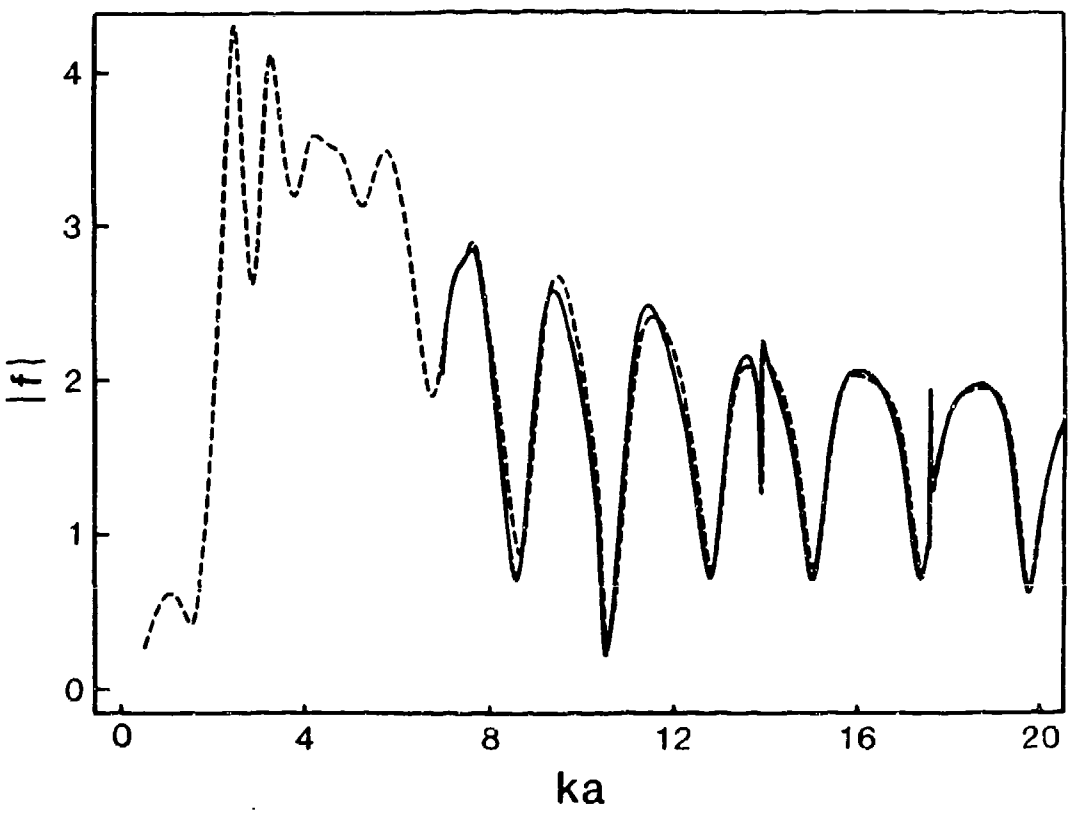

Fig. 9 The dashed line is $|f_{PWS}|$ and the solid line is $|f_{ray}|$ for the stainless steel shell. The leaky Lamb waves included in f_{ray} are a_0 and s_0. The present figure differs from Fig. 4a by setting $f_{cc} = 0$ in Eq. (15) so that the curvature correction to the reflected wave amplitude is neglected. The improved agreement over part of this x region between $|f_{PWS}|$ and $|f_{ray}|$ is discussed in Sec. 4.5.

negative group velocity on the s_1 contribution needs to be more fully explored as well as any connection between the first longitudinal resonance and the cutoff of the s_1 Lamb wave for curved fluid loaded shells.

Comments on the significance of the fractional thickness h/a are appropriate. For the present numerical investigation for the stainless steel shell, we took $h/a = 0.162$ to correspond to the shell studied in the scattering experiments in Ref. 12 and subsequent theoretical studies.[15,17,23] Some of the changes which may be anticipated for smaller h/a will now be noted. For flat plates in a vacuum, the cutoff frequencies increase with decreasing h. While the dispersion relations near cutoffs may be strongly affected by fluid loading, as a general rule it may be anticipated that for a given frequency, fewer leaky Lamb modes will be required as h is decreased. The frequency for which c_l of the lowest flexural (or antisymmetric) Lamb mode equals c of the surrounding fluid is commonly referred to as the "coincidence frequency." (See also comments in Appendix A on the bifurcation of the a_0 dispersion curve.) While for the shell considered, coincidence occurs for $x \approx 7$; smaller values of h/a would raise the coincidence frequency. Even away from cutoff and coincidence frequencies, as h/a is decreased, the effect of the fluid loading on the phase velocity curves, Fig. A2, will be more pronounced. It may be anticipated that c_l/c (as given by the Watson methodology) will be shifted below the plate in-a-vacuum curvature-corrected values. Finally, the longitudinal resonance condition, Eq. (1a), may be expressed as $x_{LR} = n\pi(c_l/c)[h/a]^{-1}$. Consequently, for a given n, x_{LR} increases with decreasing h/a.

While the emphasis of the present research has been on scattering in the exact backwards direction, the generalization of leaky Lamb wave contributions to near backwards (but off-axis) directions follows from the discussions of axial focusing given in Refs. 1, 12, and 19. Insight into the high-frequency near-backwards scattering patterns for

shells which are only slightly spheroidal may be obtained by adapting the analysis given in Ref. 22.

Acknowledgements

This work was supported by the Office of Naval Research. Partial results were presented at the 119th Meeting of the Acoustical Society of America (State College, PA, May 1990) and at the 117th Meeting of the Acoustical Society of America as noted in Ref. 9.

Appendix A. Leaky Lamb wave parameters β_l and c_l/c

A Sommerfeld-Watson transformation has not been directly applied to the exact partial-wave series for the backscattering from a evacuated elastic spherical shell. However, some results from a Sommerfeld-Watson transformation of the form function for backscattering from an solid elastic sphere can be extended to the case of a shell. It can be argued from the geometric similarity of the two scatterers that certain results of a Sommerfeld-Watson transformation of f for the shell will produce analogous results. In Sec. 4.2.A, a geometric interpretation of the backscattering of surface guided elastic waves from a solid elastic sphere was employed in modeling the backscattering from a shell. In this Appendix, the methodology for the determination of $\beta_l(x)$and $c_l(x)/c$ is briefly reviewed.

From Williams and Marston's analysis,[7] the radiation damping parameter and surface guided elastic wave phase velocity are obtained by solving the following equations:

$$D_{\nu_l}(x) = 0, \tag{A1}$$

$$\nu_l = \alpha_l + i\beta_l, \tag{A2}$$

$$(c_l/c) = x/(\alpha_l + 1/2). \tag{A3}$$

Equation (A1) is the determinant of the denominator in Eq. (3) where the integer index n has been replaced everywhere by a complex index ν_l. The complex index ν_l for fixed x is obtained by numerical techniques described in Ref. 12. These numerical techniques involve the evaluation of residues of certain integrals. Once ν_l is determined, then both β_l and (c_l/c) via Eq. (A3) are known. The radiation damping parameters $\beta_l(x)$ for the various leaky Lamb waves are shown in Fig. A1. An important feature in Fig. A1 is that β_l for the a_0, s_0, a_1, and s_2 leaky Lamb waves are relatively small throughout the range of x investigated; while β_l for the s_1 leaky Lamb wave appears to diverge. The truncation of the vertical axis at 0.8 *Np/rad* resolves the detail of some the Lamb wave damping parameters, but it obscures the fact that the s_1 damping parameter becomes large for $x < 72$ ($\beta_l \approx 3.5$ at $x = 70$ and $\beta_l \approx 7.5$ at $x = 65$). The derivation[1] leading to Eq. (7) made the assumption $2\pi\beta_l << 1$. It may be argued, however, that Eq. (7) is a good approximation for G_l even when $2\pi\beta_l$ violates this assumption.[1] Inspection of Figs. 4 - 6 supports the claim that Eq. (7) with $\phi_l = 0$ is a valid approximation for G_l even if $2\pi\beta_l$ is not $<< 1$.

The normalized dispersion curves for the leaky Lamb waves are shown in Fig. A2. Mode identification was confirmed by comparison with curvature corrected results for a flat plate in vacuum following the method of Ref. 17. Several characteristics should be noted. First, the a_0 leaky Lamb wave (solid line) becomes subsonic for $x < 7$. Sammelmann et al.[30] have reported a bifurcation of the a_0 leaky Lamb wave dispersion curve for the fluid-loaded spherical shell near a value of x associated with the transition from a supersonic to subsonic phase velocity for the dispersion curve of the a_0 Lamb wave on a spherical shell in vacuum. Since the relevant contributions to the present ray synthesis are implicitly supersonic, the subsonic branch was not included in Fig. A2. The dispersion curves for a_1 (long-dashed line) and s_2 (dot-dashed line) are analogous to the flat-plate Lamb wave dispersion curves. Both the a_1 and s_2 modes appear to approach well defined

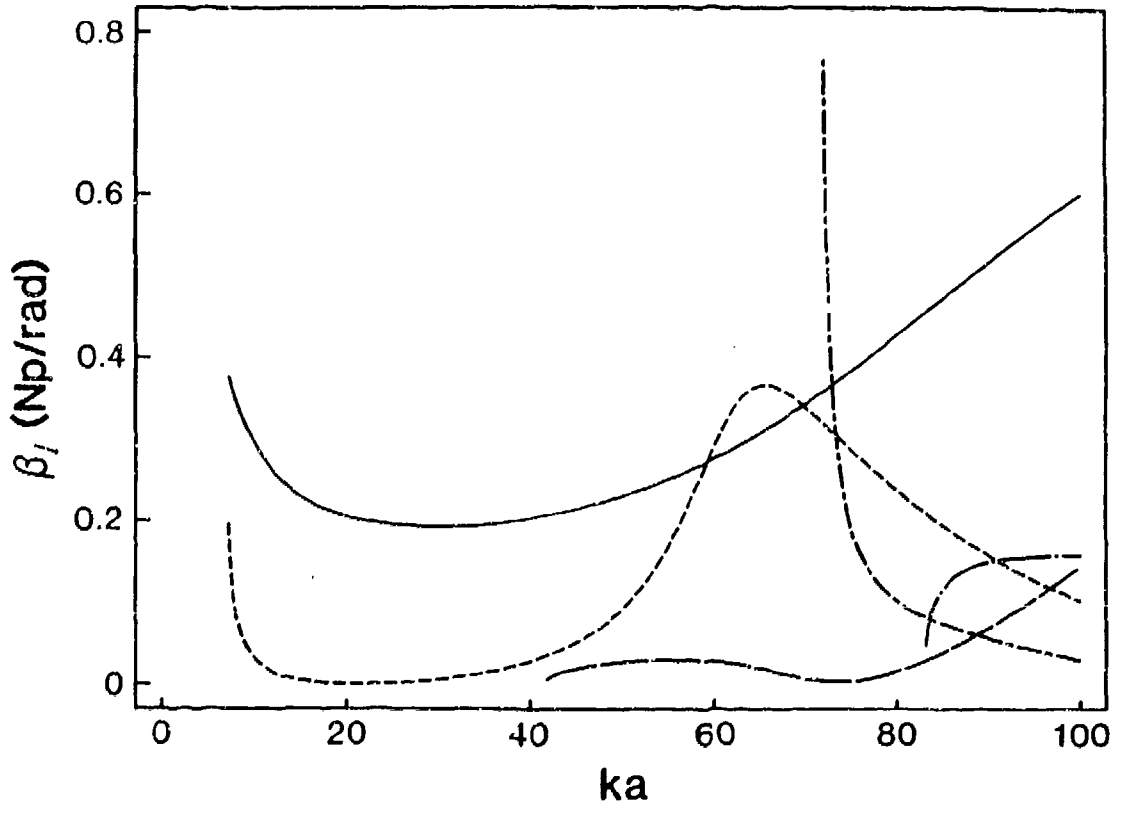

Fig. A1 The radiation damping parameters for the various leaky Lamb waves employed in $|f_{ray}|$ for the stainless steel shell considered. Each leaky Lamb wave is associated with the following line: a_0 solid; s_0 short-dashed; a_1 long-dashed; s_1 short-long-dashed; and s_2 dot-dashed.

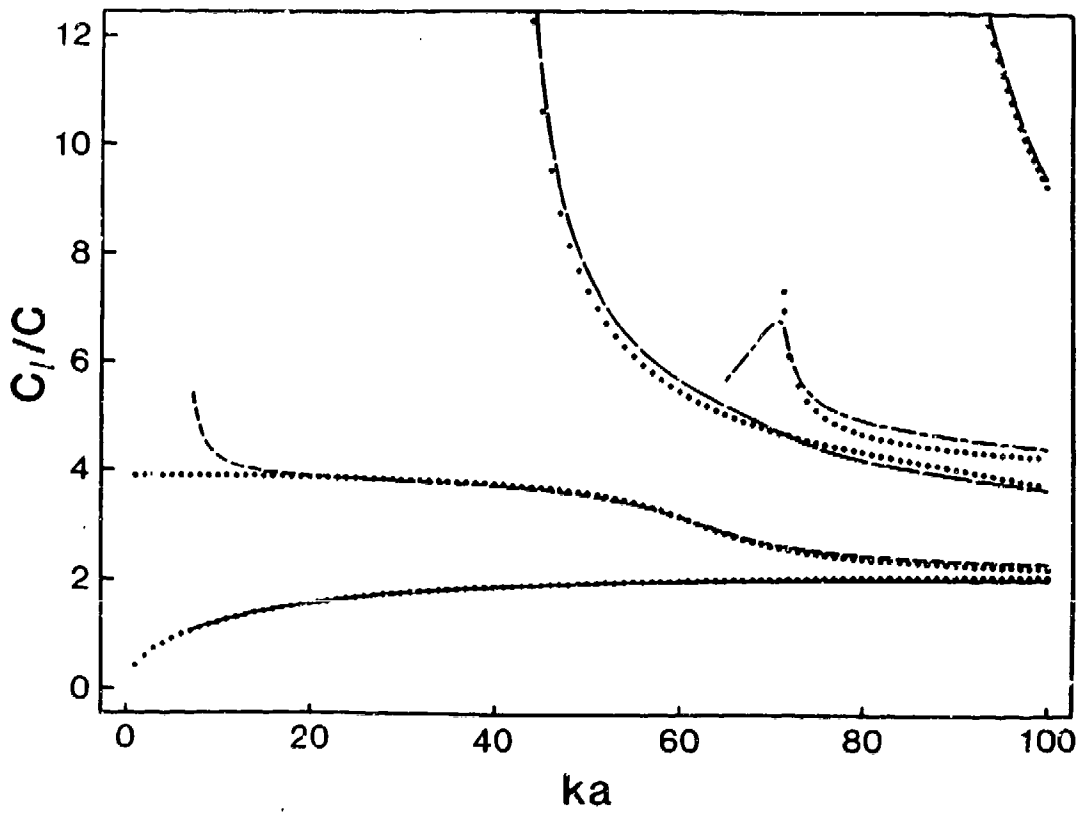

Fig. A2 The normalized dispersion curves for the various leaky Lamb waves employed in $|f_{ray}|$. Each Lamb waves is associated with the following line: a_0 solid; s_0 short-dashed; a_1 long-dashed; s_1 short-long-dashed; and s_2 dot-dashed. The dotted lines are based on corresponding mode calculations for a flat plate in a vacuum with curvature corrections as given by Marston (Ref. 17). These are included so as to confirm the classification of modes given.

cutoff frequencies. As in Fig. A1, the vertical axis has been truncated and the asymptotic behavior of these modes is not adequately represented. For example: for $l = a_1$, $c_l/c \approx 27$ at $x = 42$, and for $l = s_2$, $c_l/c \approx 32$ at $x = 85$.

The phase velocity ratio for the s_0 Lamb wave is represented by the short-dashed line in Fig. A2. Two features are observed from this dispersion curve. First, the s_0 Lamb wave is weakly dispersive in the ranges $10 < x < 40$ and $x > 80$. As discussed in Appendix B, the spacing Δx_{res} between adjacent resonance peaks in Fig. B2 is approximately equal to the normalized group velocity c_{gl}/c for weakly dispersive Lamb waves. Second, the dispersion curve appears to diverge as the frequency approaches the natural frequency ω_B of a purely radial oscillation or *breathing mode* of the shell. Such a divergence is plausible since the radial displacement of the shell at all points on the surface is in phase when $\omega = \omega_B$. In Appendix A of Ref. 15, ω_B for a thin spherical shell in vacuum is related to the *ring frequency* ω_R of an infinite cylindrical shell.[31] The estimated value of x corresponding to ω_B is $x_B = 6.3$. Furthermore, it is argued in Ref. 15 that the fluid-loading of the spherical shell will only slightly reduce x_B.

The normalized phase velocity for the s_1 Lamb wave is the final dispersion curve in Fig. A2 to be considered (the long-short dashed line). Unlike the a_1 and s_2 leaky Lamb waves, the dispersion curve for the s_1 leaky Lamb wave on the fluid-loaded shell does not approach a definite cutoff frequency. The cutoff frequency for the equivalent s_1 Lamb wave on a flat elastic plate in a vacuum corresponds to[29] $x \approx 76.8$. Near $x = 71$, the s_1 leaky Lamb wave attains a maximum value and then decreases with decreasing x. The group velocity is related to the phase velocity by[12]

$$c_{gl} = c_l\{1 - [1 - (c_l/x)(dc_l/dx)^{-1}]^{-1}\}. \qquad \text{(A4)}$$

Numerical differentiation indicates that s_1 on a fluid-loaded shell has a negative group velocity in the region $65 < x < 71$. The normalized group and phase velocities are displayed in Fig. A3. The possibility of a wave propagating with a negative group velocity was first investigated by Lamb.[32] Hackman and Sammelmann[33] have reported that an analysis of the poles of the S-matrix in the complex k-plane produces regions of negative group velocities for some leaky Lamb waves on thin elastic spherical shells. Finally, the dispersion curve has been truncated below $x = 65$ because the numerical algorithm implemented in the determination of c_l/c becomes inaccurate.

Without resorting to the above numerical differentiation, the sign of the group velocity for a leaky Lamb wave on a fluid-loaded shell can be determined from the slope of $\alpha_l(x)$. If Eq. (A3) is differentiated with respect to x, then the result is

$$\alpha_l'(x) = \frac{d\alpha_l}{dx} = \frac{c}{c_l}\left(1 - \frac{x}{c_l}\frac{dc_l}{dx}\right). \tag{A5}$$

Equation (A4) relating c_{gl} and c_l can be inverted to obtain an expression for the second term in Eq. (A5). Substituting this result into Eq. (A5) gives the simple result $\alpha_l'(x) = c/c_{gl}$. Although a plot of $\alpha_l(x)$ is not presented here, it has been verified that $\alpha_l(x)$ has a positive slope for $x > 71$, attains a local minimum near $x = 71$, and has a negative slope for $x < 71$.

Appendix B. Fabry-Perot expression for f_l

In this appendix, the a_0 and s_0 leaky Lamb wave contributions to the backscattering amplitude are isolated and examined. By considering an individual contribution, the resonant nature of Eq. (6) is demonstrated and the similarity between Eq. (6) and a Fabry-Perot resonator is illustrated. Figure B1 is $|f_l|$ where $l = a_0$ and Fig. B2 corresponds to $|f_l|$ for the s_0 leaky Lamb wave. The width of any given resonance peak from the a_0 Lamb wave contribution in Fig. B1 is representative of relatively low Q

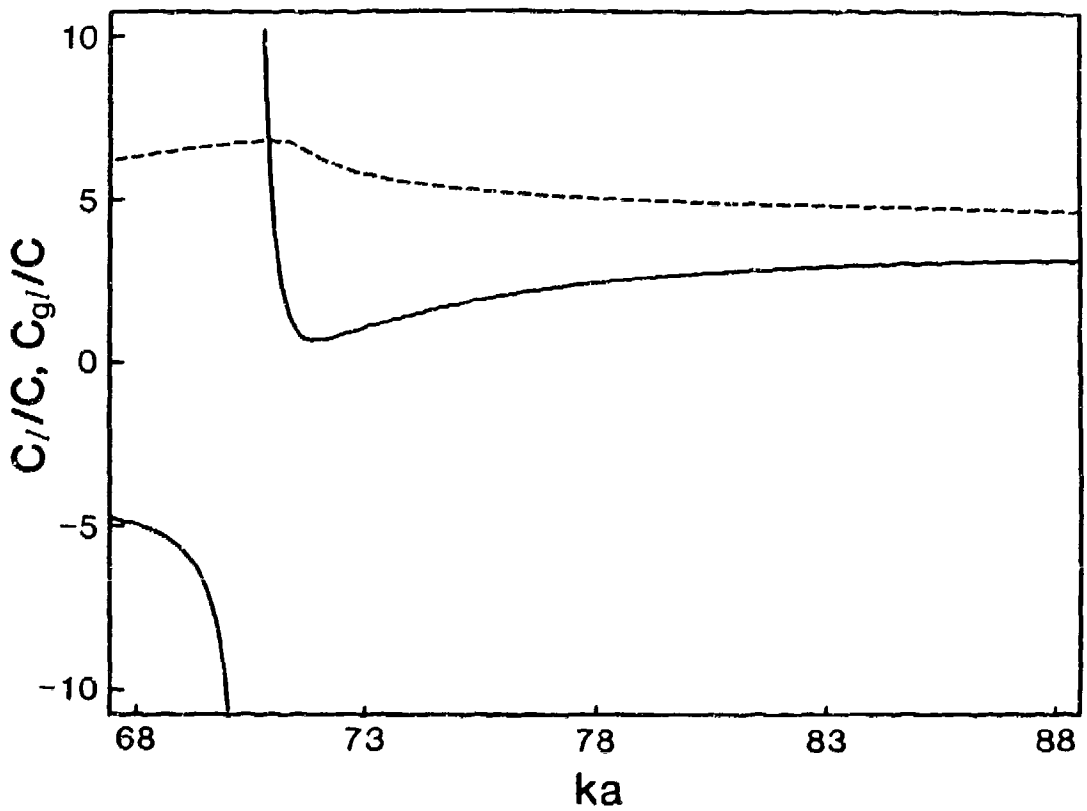

Fig. A3 The normalized phase (dashed) and group velocity (solid) for the s_1 leaky Lamb wave in the vicinity of the anomaly near $x = 71$ and longitudinal resonance at $x_{LR} \approx 76.8$. The small oscillations in the group velocity ($x > 73$) are a result of numerical differentiation.

resonances while Fig. B2 for s_0 contains both high Q resonances ($x \leq 40$) and low Q resonances ($x > 40$). Ordinarily, the increment in x for these calculations of $|f_l|$ ($l = a_0, s_0$) is $\Delta x = 0.015875$. In Fig. B2, the high Q resonances of the s_0 Lamb wave at $x \approx 17.6$, 21.3, 25.0 and 28.6 have been enhanced by sufficiently decreasing Δx to resolve the very narrow linewidths. It may be inferred from Fig. B2 and Eq. (16) that a partial-wave series calculation will be numerically intensive, since Δx must be chosen small and n_{max} exceeds x.

Consider the form of the denominator in Eq. (6). If a Lamb wave on the shell is non-dispersive, then the spacing between two adjacent resonances would be $\Delta x_{res} \approx c_l/c$. For weakly dispersive Lamb waves, it is well-known that $\Delta x_{res} \approx c_{gl}/c$. The relationship between Δx_{res} and c_{gl} can also be obtained from the form of the denominator in Eq. (6).[34] Figure A2 demonstrates that the a_0 leaky Lamb wave is weakly dispersive for $x > 50$ and $c_{gl}/c \approx 2.178$ (see Fig. 6 of Ref. 12). Inspection of Fig. B1 indicates that the spacing Δx_{res} for $x > 50$ is $\Delta x_{res} \approx 2.123$ (for comparison $1.947 < c_l/c < 2.037$, $50 < x < 100$). Again, the dispersion curve in Fig. A2 indicates the s_0 leaky Lamb wave is weakly dispersive in the regions $10 < x < 40$ and $x > 80$. The spacing between adjacent peaks in the region $10 < x < 40$ is determined from Fig. B2 to be $\Delta x_{res} \approx 3.620$ while numerical differentiation predicts $\Delta x_{res} \approx c_{gl}/c = 3.616$ (at $x = 14$, $c_l/c \approx 3.978$). A thorough investigation of the dependence of Δx_{res} on c_l/c and c_{gl}/c for dispersive leaky Lamb waves is beyond the scope of the present appendix.

Also, contained in Figs. B1 and B2 are envelops of the maximum and minimum values that $|f_l|$ can attain. From Eq. (6), $|f_l|_{max}$ and $|f_l|_{min}$ occur when $exp(i2\pi xc/c_l) = -1$ and $exp(i2\pi xc/c_l) = 1$, respectively. Inspection of Eqs. (6) and (7) demonstrates that $|f_l|_q$ ($q = min, max$) is an implicit function of x through the dependence of β_l and c_l/c on x. The importance of the lower envelop is that it describes a *smooth background* associated

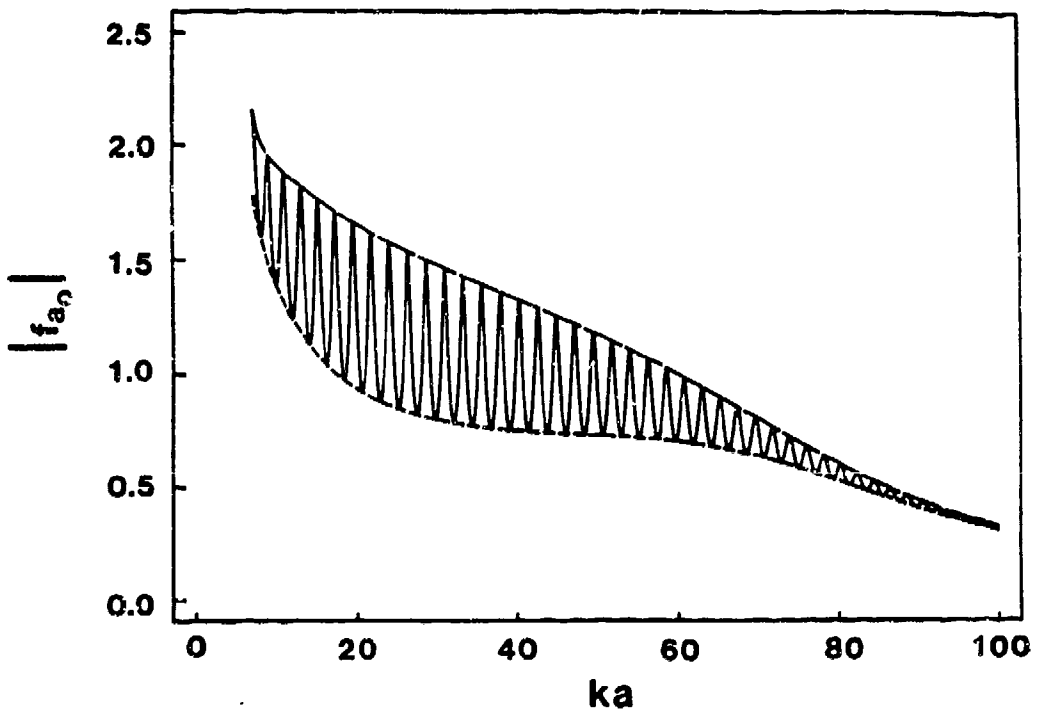

Fig. B1 The Fabry-Perot representation of the a_0 leaky Lamb wave contribution to the form function for backscattering from an evacuated elastic spherical shell. The long-dashed line is the maximum value that $|f_l|$ can attain and the short-dashed line is a minimum envelop which can be interpreted as a smooth background associated with off-resonance contributions from the a_0 Lamb wave. The widths of the resonances are representative of relatively low Q leaky Lamb wave resonances.

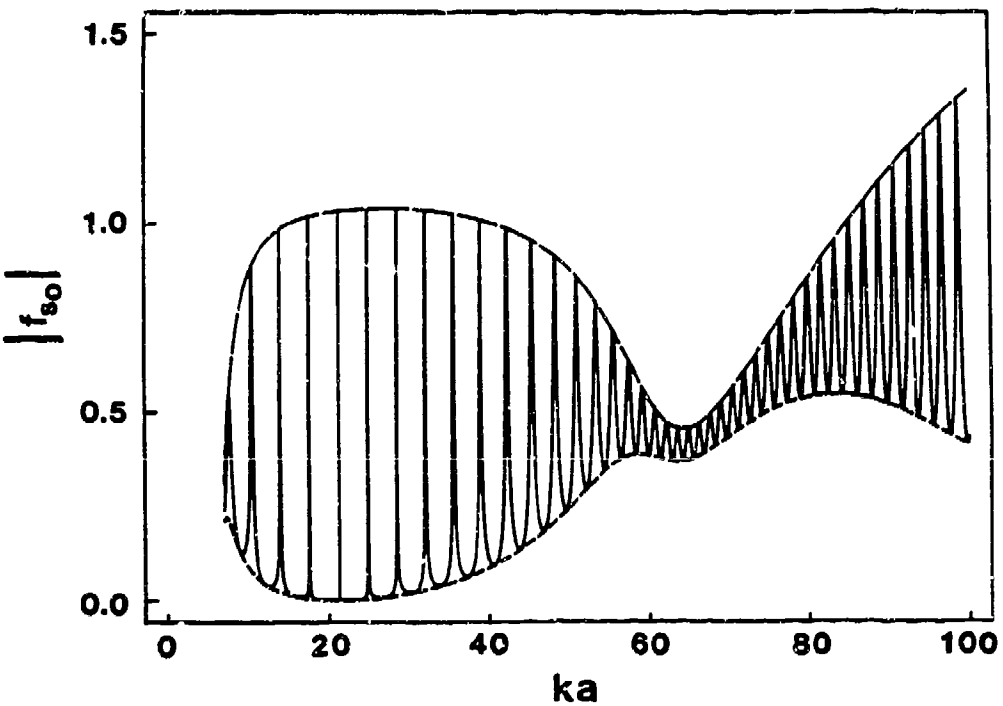

Fig. B2 The Fabry-Perot representation of the s_0 Lamb wave contribution to the form function for backscattering. The long-dashed line is the maximum value that $|f_l|$ can attain. The short-dashed line is a minimum envelop which can be interpreted as a smooth background associated with off-resonance contributions from s_0. The widths of the resonances for $x < 40$ are representative of high Q leaky Lamb wave resonances.

with the *lth* leaky Lamb wave. The resonance enhancement rises above the background. Unlike resonance scattering theory[35-37] where a suitable background contribution must be chosen to synthesis the backscattering amplitude, the Fabry-Perot form of Eq. (6) correctly accounts for a background contribution even for off-resonance values of x. That is, the resonance peaks in $|f_l|$ rise relative to $|f_l|_{min}$ which represents a off-resonance smooth background.[1]

Appendix C. Localization principle analysis of partial waves near a longitudinal resonance

The localization principle states that the *nth* partial-wave amplitude for scattering from a sphere may be associated with the contribution to the scattering from a ray having an impact parameter[14]

$$s = a(n + 1/2)/x. \tag{C1}$$

For $s > a$, rays miss the sphere, and the partial wave amplitudes typically decrease abruptly in magnitude as n increases above x. Here, we analyze the elastic response of the shell by considering the contribution of individual partial-wave amplitudes in the form function for backscattering. The elastic behavior of the shell is isolated by subtracting a rigid background. The relevant expression in the present analysis is

$$F(x,n) = f_n(x) - f_n^r(x) = \frac{2}{ix}(-1)^n(2n+1)\left(\frac{B_n(x)}{D_n(x)} + \frac{j_n'(x)}{h_n^{(1)'}(x)}\right), \tag{C2}$$

where the prime indicates differentiation with respect to the argument. The second term in Eq. (C2) represents the subtraction of an acoustically hard or rigid immovable sphere background.[37] In particular, the cause of the anomalous peak in the ray synthesis near $x =$

71 and a possible relationship between the longitudinal resonance and the s_1 leaky Lamb wave are considered below.

Figure C1 shows $|F(x,n)|$ for $x = 71.7$ which corresponds to a value of x at the center of the peak in E_2 of Fig. 7. Figure C1 illustrates the localization principle since the important contributions are the partial-wave amplitudes at $n = 8 - 11$, 15, 27, and 35. These correspond to various leaky Lamb wave contributions as well now be shown. Inspection of Fig. 1 and Eq. (4) demonstrates that the impact parameter is related to the outer radius of the shell by

$s = a\ sin(\theta_l) = ac/c_l$. It follows that a partial wave amplitude can be associated with a leaky wave contribution by

$$n = x(c/c_l) - (1/2). \qquad \text{(C3)}$$

Table CI gives the result of applying Eq. (C3). Inspection of Fig. C1 and Table CI indicate that the a_0, s_0, and a_1 leaky Lamb wave contributions are isolated and associated with a single partial wave amplitude. An interpretation of the $n = 8 - 11$ partial-wave amplitudes is that a broad bundle of rays couples to the s_1 leaky Lamb wave on the shell and and that wave contributes to backscattering. This may be consistent with the direct backscattering mechanism proposed in Sec. 4.4.

One may anticipate some relationship between the longitudinal resonance and the s_1 Lamb wave, since the resonance condition in Eq. (1a) gives $x_{LR} \approx 76.8$ which is equivalent to the cutoff frequency of s_1 on a vacuum-backed flat elastic plate. Information concerning the longitudinal resonance and the s_1 leaky Lamb wave can be obtained by studying the contributions to the form function due to individual partial waves. Figure C2 displays a sequence of partial-wave amplitudes as a function of x in the vicinity of x_{LR}. The series of large peaks starting near $x = 55$ and $n = 16$ corresponds to the s_0 mode and the set of narrow peaks is due to the a_1 leaky Lamb wave. Since an estimate of the

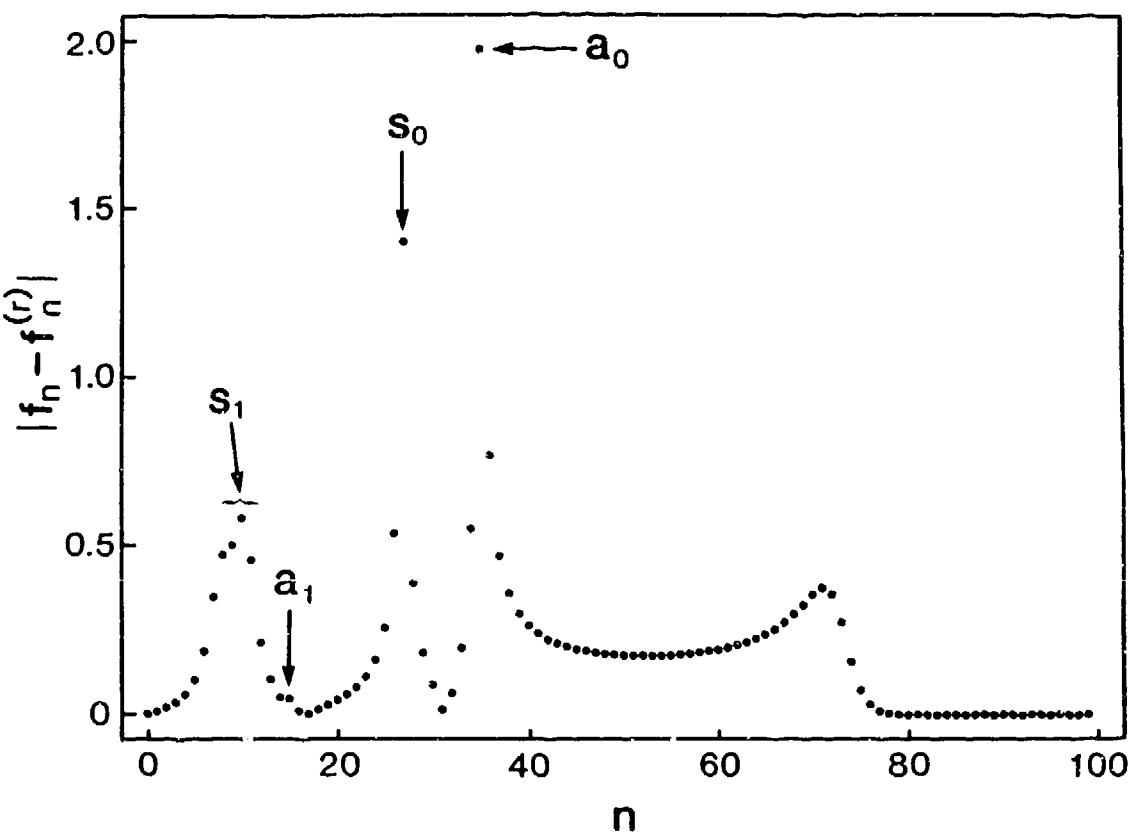

Fig. C1 Localization principle analysis of the elastic response of the shell at $x = 7\lambda.7$. Each peak is associated with a particular leaky Lamb wave contribution. A particular leaky Lamb wave can be associated with a given peak by applying Eq. (C3). (See Table C1).

TABLE CI. Localization principle identification of the partial wave amplitudes at $x = 71.7$ plotted in Fig. C1. The normalized phase velocity is given by Eq. (A3) for the stainless steel shell and n is given by Eq. (C3).

l	c_l/c	n
a_0	2.023	34.9
s_0	2.620	26.9
a_1	4.678	14.8
s_1	6.484	10.5

normalized group velocity is given by $c_{gl}/c \approx \Delta x_{res}/\Delta n$, then the s_0 and a_1 peaks demonstrate the usual behavior of positive c_{gl}/c for a surface guided elastic wave. The remaining set of peaks is primarily associated with the s_1 leaky Lamb wave. Two important feature are immediately evident. *First*, the group velocity of the s_1 Lamb wave can have either positive or negative values as demonstrated above in Appendix A. This can be seen by considering the slope, $\Delta x_{res}/\Delta n$, of a smooth curve through the peaks. However, a discrepancy between the dispersion curves from the analysis in Appendix A and the present method for estimating c_{gl}/c is also evident. The result of Eqs. (A1) - (A3) in Fig. A2 produces a single-valued function of $c_l(x)/c$. Equation (C3) and the partial-wave amplitudes in Fig. C2 would suggest, however, that $c_l(x)/c$ is a multi-valued function of x for $l = s_1$. Furthermore, the dispersion curve for s_1 in Fig. A2 is defined for $x < 71$, but Fig. C2 displays that no corresponding peaks in the partial wave amplitudes to account for this region. A *second observation* concerning these peaks is that as n tends to zero, the locus of x corresponding to these peaks appears to approach x_{LR}. The weak peak in $| F(x,0) |$ near $x = x_{LR}$ appears to be a consequence of the use of a rigid background in Eq. (C2) which does not display a longitudinal resonance. A calculation of $| F(x,n) |$ (not shown) where the rigid background has been replaced by an evacuated fluid shell background demonstrates that the peak in $| F(x,0) |$ near $x = x_{LR}$ is suppressed. This suggests that the peak in $| F(x,0) |$ displayed in Fig. C2 is associated with the longitudinal resonance.

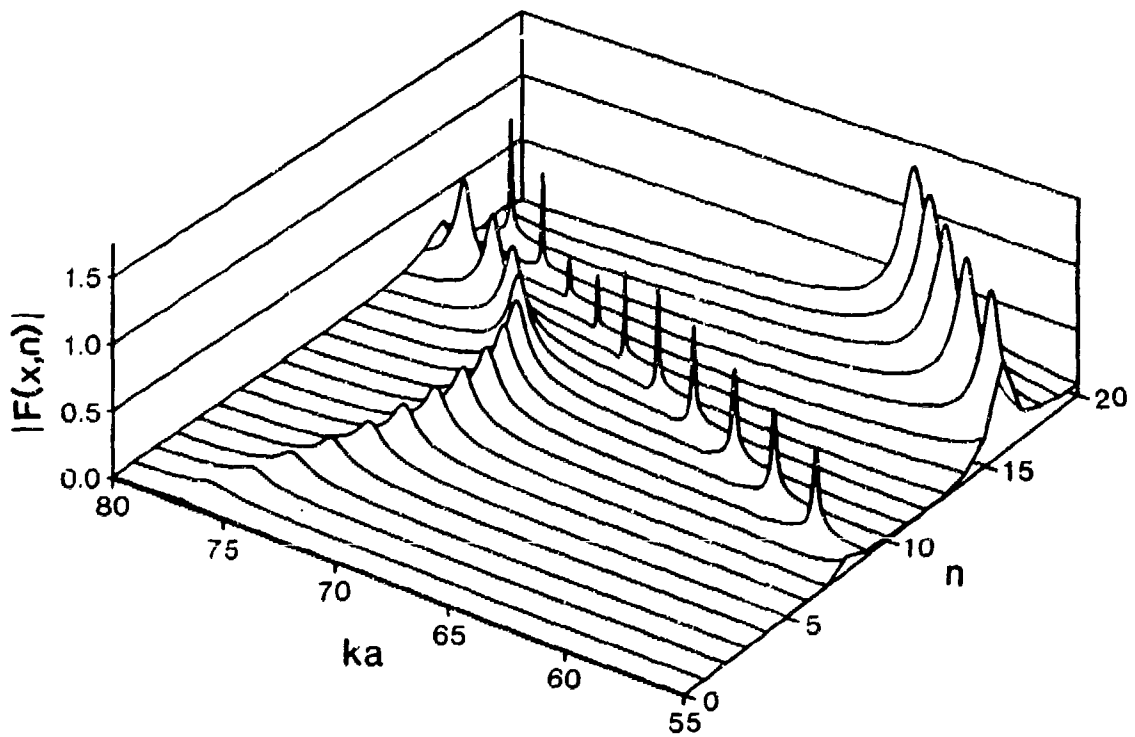

Fig. C2 A sequence of individual partial-wave amplitudes demonstrating the elastic response of the shell in the vicinity of the longitudinal resonance. The sharp peaks are due to the a_1 leaky Lamb wave and the large peaks ($n > 15$) are associated with s_0. The s_1 leaky Lamb wave peaks form the crescent shaped set.

References

1. P. L. Marston, "GTD for backscattering from elastic spheres and cylinders in water and the coupling of surface elastic waves with the acoustic field, " J. Acoust. Soc. Am. 83, 25 - 37 (1988).
2. J. M. Ho and L. B. Felsen, "New exact and ray-acoustic traveling wave formulations for source-excited fluid-loaded thin elastic spherical shells," submitted to J. Acoust. Soc. Am.
3. L. B. Felsen, J. M. Ho, and I. T. Lu, "Three-dimensional Green's function for fluid-loaded thin elastic cylindrical shell: Formulation and solution," J. Acoust. Soc. Am. 87, 543 - 553 (1990).
4. L. B. Felsen, J. M. Ho, and I. T. Lu, "Three-dimensional Green's function for fluid-loaded thin elastic cylindrical shell: Alternative representations and ray acoustic forms," J. Acoust. Soc. Am. 87, 554 - 569 (1990).
5. D. G. Crighton, "The 1988 Rayleigh medal lecture: Fluid loading — The interaction between sound and vibration," J. Sound Vib. 133, 1 - 27 (1989).
6. K. L. Williams and P. L. Marston, "Backscattering from an elastic sphere: Sommerfeld-Watson transformation and experimental confirmation," J. Acoust. Soc. Am. 78, 1093 - 1102 (1985).
7. K. L. Williams and P. L. Marston, "Synthesis of backscattering from an elastic sphere using the Sommerfeld-Watson transformation and giving a Fabry-Perot analysis of resonances," J. Acoust. Soc. Am. 79, 1702 - 1708 (1986).
8. J. B. Keller and F. C. Karal, Jr., "Geometrical theory of elastic surface-wave excitation and propagation," J. Acoust. Soc. Am. 36, 32 - 40 (1964); J. B. Keller, "Geometrical theory of diffraction," J. Opt. Soc. Am. 52, 116 - 130 (1962).

9. S. G. Kargl and P. L. Marston, "GTD synthesis of resonance amplitudes in the backscattering from an elastic spherical shell," J. Acoust. Soc. Am. Suppl. 1 85, S150 (1989).

10. P. L. Marston and S. G. Kargl, "Elastic surface wave contributions to backscattering from smooth objects described by a generalization of GTD," Oceans '89 Conference record (IEEE publication number 89CH2780-5, New York, 1989) pp. 1194 - 1198; P. L. Marston and S. G. Kargl, "Scattering from hollow shells: Quantitative ray representations of amplitudes," Proceedings of the International Congress on Recent Developments in Air- and Structure-Borne Sound and Vibration (Auburn University, Auburn, GA 1990) pp. 565 - 568.

11. P. L. Marston, S. G. Kargl, and K. L. Williams, "Rayleigh, Lamb, and Whispering Gallery wave contributions to backscattering from smooth elastic objects in water described by a generalization of GTD," in *Elastic Wave Propagation and Ultrasonic Nondestructive Evaluation*, edited by S. K. Datta, J. D. Achenback, and Y. S. Rajapakse [Elsevier Science, Amsterdam 1990] pp. 211 - 216.

12. S. G. Kargl and P. L. Marston, "Observations and modeling of the backscattering of short tone bursts from a spherical shell: Lamb wave echoes, glory, and axial reverberations," J. Acoust. Soc. Am. 85, 1014 - 1028 (1989).

13. H. C. van de Hulst, *Light Scattering by Small Particles*, (Dover, New York, 1972) pp. 208 - 209.

14. The use of the terminology *subsonic* and *supersonic* is appropriate here, since it is commonly used in structural acoustics to describe the interaction of sound and elastic structures. See for example Ref. 5 and D. G. Crighton, "Free and forced waves on a fluid-loaded elastic plate," J. Sound Vib. 63, 225 - 235 (1979).

15. S. G. Kargl and P. L. Marston, "Ray synthesis of Lamb wave contributions to the total scattering cross section for an elastic spherical shell," accepted for publication, J. Acoust. Soc. Am.

16. Y. A. Kravtsov, "Rays and caustics as physical objects," in *Progress in Optics*, edited by E. Wolf [Elsevier, Amsterdam, 1988] Vol. XXVI pp. 227 - 348.

17. P. L. Marston, "Phase velocity of Lamb waves on a spherical shell: Approximate dependence on curvature from kinematics," J. Acoust. Soc. Am. 85, 2663 - 2665 (1989).

18. P. L. Marston and K. L. Williams, "GTD for backscattering from elastic objects in water: Phase of the coupling coefficient and a simplified synthesis of the form function," J. Acoust. Soc. Am. Suppl. 83, 94 (1988).

19. K. L. Williams and P. L. Marston, "Axially focused (glory) scattering due to surface waves generated on spheres: Model and experimental confirmation using tungsten carbide spheres," J. Acoust. Soc. Am. 78, 722 - 728 (1985).

20. P. L. Marston, K. L. Williams, and T. J. B. Hanson, "Observation of the acoustical glory: High-frequency backscattering from an elastic sphere," J. Acoust. Soc. Am. 74, 605 - 618 (1983).

21. P. L. Marston and D. S. Langley, "Glory- and rainbow-enhanced acoustic backscattering from fluid spheres: Models for the diffracted axial focusing," J. Acoust. Soc. Am. 73, 1464 - 1475 (1983); 78, 1128 (1985).

22. W. P. Arnott and P. L. Marston, "Unfolding axial caustics of glory scattering with harmonic angular perturbations of toroidal wave fronts," J. Acoust. Soc. Am. 85, 1427 - 1440 (1989).

23. S. G. Kargl and P. L. Marston, "Longitudinal resonances in the form function for backscattering from a spherical shell: Fluid shell case," accepted for publication, J. Acoust. Soc. Am.

24. W. V. T. Rusch and O. Sorenson, "On determining if a specular point exists," IEEE Trans. Antennas Propag. AP-27, 99 - 101 (1979).

25. N. D. Veksler and V. M. Korunskii, "Analysis and synthesis of backscattering from a circular cylindrical shell," J. Acoust. Soc. Am. 87, 943 - 962 (1990).

26. V. A. Borovikov and N. D. Veksler, "Scattering of sound waves by smooth convex elastic cylindrical shells," Wave Motion 7, 143 - 152 (1985).

27. H. Lamb, "On waves in an elastic plate," Proc. R. Soc. London Ser. A 93, 114 - 128 (1917).

28. I. A. Viktorov, *Rayleigh and Lamb Waves: Physical Theory and Applications* (Plenum, New York, 1967) pp. 70 - 71.

29. For a flat plate in vacuum both the a_0 and s_0 Lamb waves can be excited in the plate for all frequencies. The propagation of a higher Lamb wave in a plate is analogous to a mode propagating in a waveguide. Each higher Lamb wave on a plate in vacuum has a well defined cutoff frequency. Viktorov[28] relates the *critical thickness* of a plate to the longitudinal and shear velocities. These relationships can be expressed in terms of x and an estimate of the cutoff frequency can be obtained. For the s_1 Lamb wave in a plate Viktorov gives the condition $h = \lambda_L/2$ which can be rewritten in the form $x = \pi(c_L/c)[1 - b/a]^{-1}$.

30. G. S. Sammelmann, D. H. Trivett, and R. H. Hackman, "The acoustic scattering by a submerged, spherical shell. I: The bifurcation of the dispersion curve for the spherical antisymmetric Lamb wave," J. Acoust. Soc. Am. 85, 114 - 124 (1989). Sammelmann et al. denote the supersonic branch as a_{0+} and the subsonic branch as

a_{0-} for the bifurcation of the first antisymmetric Lamb on a fluid-loaded shell. The term bifurcation refers to the behavior of the two branches. For values of x where the vacuum dispersion curve is supersonic, the a_{0+} branch replicates the vacuum dispersion curve. As the value of x decreases towards the transition region, the a_{0+} branch starts to deviate from the vacuum dispersion curve and the a_{0-} branch begins to replicate the subsonic portion of the vacuum curve. It is noted that for the shell parameters considered in this article a subsonic wave has been identified , but its radiation damping parameter appears to be fairly large over the range of x investigated. This implies that the contribution of a subsonic branch may not contribute significantly to the form function for backscattering at high-frequencies.

31. M. C. Junger and D. Feit, *Sound Structures and Their Interaction* (MIT Press, Cambridge, 1986) 2nd. ed., Sec. 6.5, 7.16, 7.18, and 9.2.

32. H. Lamb, "On group-velocity," Proc. Lond. Math. Soc., (2)1, 473 - 479 (1903 - 1904).

33. R. H. Hackman and G. S. Sammelmann, "The acoustic scattering by a submerged, elastic spherical shell: High-frequency limit," J. Acoust. Soc Am. Suppl. 85, 95 (1989).

34. S. G. Kargl and P. L. Marston, "Quasiperiod of variations in the backscattering and total cross sections of spherical shells," J. Acoust. Soc. Am. Suppl. 86, 5 (1989).

35. L. Flax, G. C. Gaunaurd, and H. Uberall, "Theory of resonance scattering," in *Physical Acoustics*, edited by W. P. Mason and R. N. Thurston (Academic, New York, 1981), Vol. 15, pp. 191 - 294.

36. G. C. Gaunaurd and H. Uberall, "RST analysis of monostatic and bistatic acoustic echoes from elastic spheres," J. Acoust. Soc. Am. 73, 1 -12 (1983).

37. G. C. Gaunaurd and M. F. Werby, "Lamb and creeping waves around submerged spherical shells resonantly excited by sound scattering," J. Acoust. Soc. Am. 82, 2021 - 2033 (1987).

Appendix I

A. Complex coupling coefficient: Approximation and an apparent exact expression

In the development of the ray methods presented in the preceding chapters, a complex coupling coefficient is defined and denoted as G_l. This coefficient describes the efficiency of the coupling of the incident acoustic wavefield in water with a surface guided elastic wave excited on the elastic spherical object during the scattering process. For the case of backscattering from a solid elastic sphere, a Sommerfeld-Watson transformation of the exact partial wave series representation of the form function f gives a virtually exact expression[1,2]

$$G_l(x) = 8\pi(c/c_l)\left(1 + \frac{ic_l\beta_l}{cx}\right)\left(\frac{i\mathcal{D}^-_{\nu_l}(x)}{2\dot{\mathcal{D}}^+_{\nu_l}(x)}\right). \qquad (1)$$

The radiation damping of the surface guided elastic wave is β_l (in *Np/rad*) and $x = ka$ is a dimensionless size parameter where k is the wavenumber in the surrounding water and a is the radius of the sphere. The normalized phase velocity of the surface guided elastic wave is c_l/c. The functions $\mathcal{D}^+$ and $\mathcal{D}^-$ are extremely complicated expressions involving combinations of spherical Bessel and Neumann functions of complex order ν_l and real argument. The functions $\mathcal{D}^+$ and $\mathcal{D}^-$ for a solid elastic sphere are given in Refs. 1 and 2. The dot above $\mathcal{D}^+$ indicates differentiation with respect to ν and this derivative is to be evaluated at ν_l where ν_l satisfies the relationships

$$\mathcal{D}^+_{\nu_l}(x) = 0, \qquad \nu_l = \alpha_l + i\beta_l, \qquad c_l(x)/c = x/[\alpha_l + 1/2]. \qquad (2a,b,c)$$

Equation (2) is a result of the above mentioned Sommerfeld-Watson transformation. [The ν_l that satisfy Eq. (2) also satisfy $D_\nu(x) = 0$ where D_ν is the denominator of the *nth partial-wave amplitude*,[1-4] $f_n(x) = (-1)^n(2n+1)(2/ix)[B_n(x)/D_n(x)]$, with the integer index n

replaced by v.] The complicated form of G_l in Eq. (1) obfuscates the dependence of G_l on the relevant surface guided elastic wave parameters β_l and c_l/c. A simple approximation for Eq. (1) would facilitate computations of forward or backwards scattering by the quantitative ray methods previously developed.

Marston developed a simple approximation for $|G_l|$ by comparing the results of resonance scattering theory[5,6] and a generalization (based on Watson transform methods) of the geometrical theory of diffraction.[2] A short summary of this analysis follows and it is restricted to the backscattering direction. In resonance scattering theory at the location of an isolated resonance, f_n is split into an appropriate background term and a surface elastic wave contribution f_{nl}. The contribution f_{nl} is usually expressed in a Breit-Wigner form

$$f_{nl}(x) \approx \frac{(2n+1)}{x}(-1)^n e^{i2\xi_n}\left(\frac{\Gamma_{nl}}{x_{nl} - x - (i/2)\Gamma_{nl}}\right), \tag{3}$$

where x_{nl} is the location of an isolated resonance and the width of the resonance can be related to Γ_{nl}. Define the *scattering function* $S_n(x) = \{[2B_n(x)/D_n(x)] - 1\}$. The denominator of $S_n(x)$ can be written so as to contain the information about the resonance location and damping; x_{nl} is the real root of the real part of that denominator. Equation (3) is a result of applying a Taylor Series expansion to the denominator of $S_n(x)$ about $x = x_{nl}$ and separating f_{nl} from a background contribution. For high-frequency backscattering from a solid elastic sphere, f_n for a rigid or immovable sphere is a suitable choice of background. It can be shown that $Re\{D_n(x = x_{nl})\} = 0$ where D_n is the denominator of f_n. The subscripts n and l imply that the isolated resonance occurs in f_n and it is classified as the *lth* type of surface elastic wave resonance (Rayleigh, Lamb, Franz, etc.). From the ray synthesis, a surface elastic wave contribution to backscattering has the following Fabry-Perot form[7]

$$f_l(x) = [- G_l e^{i\eta_l} e^{-2(\pi - \theta_l)\beta_l}]/[1 - e^{-2\pi\beta_l} e^{i2\pi\alpha_l}], \qquad (4)$$

where η_l is a propagation phase delay. The basic premise[2] leading to an approximation for G_l is that if both Eq. (3) and Eq. (4) describe the resonance contribution of a surface elastic wave, then *locally* near the isolated resonance $f_l(x) \approx f_{nl}(x)$. The remainder of the analysis involves applying Taylor series expansions to $\beta_l(x)$ and $\alpha_l(x)$ about $x = X_{nl}$. Here, X_{nl} is a real value of x such that $\alpha_l(X_{nl}) = n$ and the denominator in Eq. (4) attains a local minimum. With these expansions, Eq. (4) can be cast into a form similar to Eq. (3)

$$f_l(x) \approx \frac{- G_l e^{i\eta_l}}{i4\pi\beta_{nl}} \left(\frac{\gamma_{nl} + i2\delta_{nl}}{(X_{nl} + \delta_{nl}) - x - (i/2)\gamma_{nl}} \right), \qquad (5)$$

where

$$\delta_{nl} = - \beta_{nl}\beta'_{nl} / [\, \alpha'^{2}_{nl} + \beta'^{2}_{nl} \,], \qquad \gamma_{nl} = 2\beta_{nl}\alpha'_{nl} / [\, \alpha'^{2}_{nl} + \beta'^{2}_{nl} \,]. \qquad (6a,b)$$

The prime in Eq. (6) indicates differentiation of $\alpha_l(x)$ and $\beta_l(x)$ with respect to x evaluated at $x = X_{nl}$ and $\beta_{nl} = \beta_l(X_{nl})$.

Inspection of Eqs. (3) and (5) demonstrates that the location of poles in the complex x-plane for f_{nl} and f_l coincide if $x_{nl} = X_{nl} + \delta_{nl}$ and $\Gamma_{nl} = \gamma_{nl}$. Numerical computations for tungsten carbide and aluminum spheres indicate $| \delta_{nl} | << 1$, which suggests the following conditions $| \delta_{nl} | << \gamma_{nl}$ and $(d\beta_l/dx) << (d\alpha_l/dx)$. With these conditions and pole locations, comparison of Eqs. (3) and (5) reduces $| G_l |$ at an isolated resonance to the approximate form

$$| G_l(x = X_{nl}) | = \frac{(n+1/2)8\pi\beta_{nl}}{X_{nl}}. \qquad (7)$$

The form of Eq. (2c) and the identification of $[(n + 1/2)/X_{nl}] = [(\alpha_l(X_{nl}) + 1/2)/X_{nl}]$ suggests the following *smooth continuation* of Eq. (7)

$$| G_l(x) | = 8\pi\beta_l(x)c/c_l(x). \qquad (8)$$

Equation (8) is a simple approximation for $|G_l|$ which explicitly exhibits the dependence of $|G_l|$ on the relevant surface guided elastic wave parameters.

While this analysis gives a simple approximation for $|G_l|$, it was initially deemed too complicated to construct an approximation for the phase of G_l from the above analysis. However, Williams and Marston have subsequently demonstrated that $arg(G_l) \approx 0$ for surface guided elastic wave contributions to backscattering from solid or hollow elastic spheres.[8,9] Recently, Ho and Felsen have confirmed Eq. (8) with $arg(G_l) \approx 0$ for backscattering from *thin* elastic spherical shells.[10,11] It is noteworthy that their analysis is based on thin shell equations while the above results are from an analysis starting from the *exact* partial wave series for backscattering from elastic spheres.

A Watson transformation of the exact partial wave series representation of the form function for backscattering from an elastic spherical shell has not been performed. From the geometric similarity of the sphere and shell, it can be argued that the complex coupling coefficient for the shell will have the same form as Eq. (1). The shell and sphere coupling coefficients should only differ in the definitions of $\mathcal{D}^+$ and $\mathcal{D}^-$ in Eq. (1). The appropriate expressions are

$$\mathcal{D}_\nu^+(x) = z_\nu^{(1)}(x) - F_\nu(x), \qquad \mathcal{D}_\nu^-(x) = z_\nu^{(2)}(x) - F_\nu(x), \tag{9a}$$

$$z_\nu^{(1)}(x) = x h_\nu^{(1)'}(x)/h_\nu^{(1)}(x), \qquad z_\nu^{(2)}(x) = x h_\nu^{(2)'}(x)/h_\nu^{(2)}(x), \tag{9b}$$

$$F_\nu(x) = -x_t^2 \rho D_\nu^{(1)}(x)/\rho_e D_\nu^{(2)}(x). \tag{9c}$$

In Eq. (9b), the h_ν are spherical Hankel functions of the first and second kind of complex order and real argument and the prime denotes differentiation with respect to the argument. In Eq. (9c), $x_t = xc/c_t$ where c_t is the transverse velocity of the shell's material and $D^{(1)}$ and $D^{(2)}$ are the cofactor expansions with respect to the elements d_{11} and d_{21} of D_n from f_n

with n replaced by ν. For solid spheres, $D^{(1)}$ and $D^{(2)}$ are 2×2 determinants while for evacuated shells $D^{(1)}$ and $D^{(2)}$ would be 4×4 determinants (see Refs.1 and 3 for the elements of the determinants). This suggests that the approximation in Eq. (8) can be applied to shells for certain classes of surface guided elastic waves.

The remainder of this section compares the consequences of using Eq. (8) with $arg(G_l) = 0$ instead of Eq. (1) for an elastic spherical shell. The material of the shell is 440c stainless steel with the following parameters: longitudinal sound speed $c_L = 5.854 km/s$, transverse sound speed $c_t = 3.150 km/s$, density $\rho_e = 7.84 g/cm^3$ and inner-to-outer radii ratio $b/a = 0.838$. The parameters for water are $c = 1.479 km/s$ and $\rho = 1.00 g/cm^3$. For these parameters and the frequency range $0 < x < 100$, the relevant surface guided elastic wave contributions are the a_0 and a_1 antisymmetric (or flexural) leaky Lamb waves and the s_0, s_1, and s_2 symmetric (or dilatational) leaky Lamb waves. [The present ray synthesis is implicitly supersonic through the use of the phase velocity trace-matching condition $sin(\theta_l) = c/c_l$. Since the a_0 leaky Lamb wave becomes subsonic for $x < 7$, the actual range investigated is $7 < x < 100$. Also, for $x < 10$ contributions from Franz-type creeping waves may contribute significantly to backscattering.] Finally, partial lists of the relevant leaky Lamb wave parameters are contained in tables in Appendix II. More detailed discussions of these leaky Lamb wave parameters are contained in Appendix A of chapters 2 and 4.

Comparisons of $| G_l |$ as computed from Eqs. (1) and (8) are displayed in Figs. 1a - 4a. These figures correspond to the a_0, s_0, a_1, and s_2 leaky Lamb waves, respectively. The solid line represents the exact $| G_l |$ while the dashed line corresponds to the approximation. It is immediately evident that the two curves for $| G_l |$ are barely distinguishable for these leaky Lamb waves. Hence, Eq. (8) appears to be an excellent approximation of $| G_l |$ for these leaky Lamb waves. The phases of the exact coupling

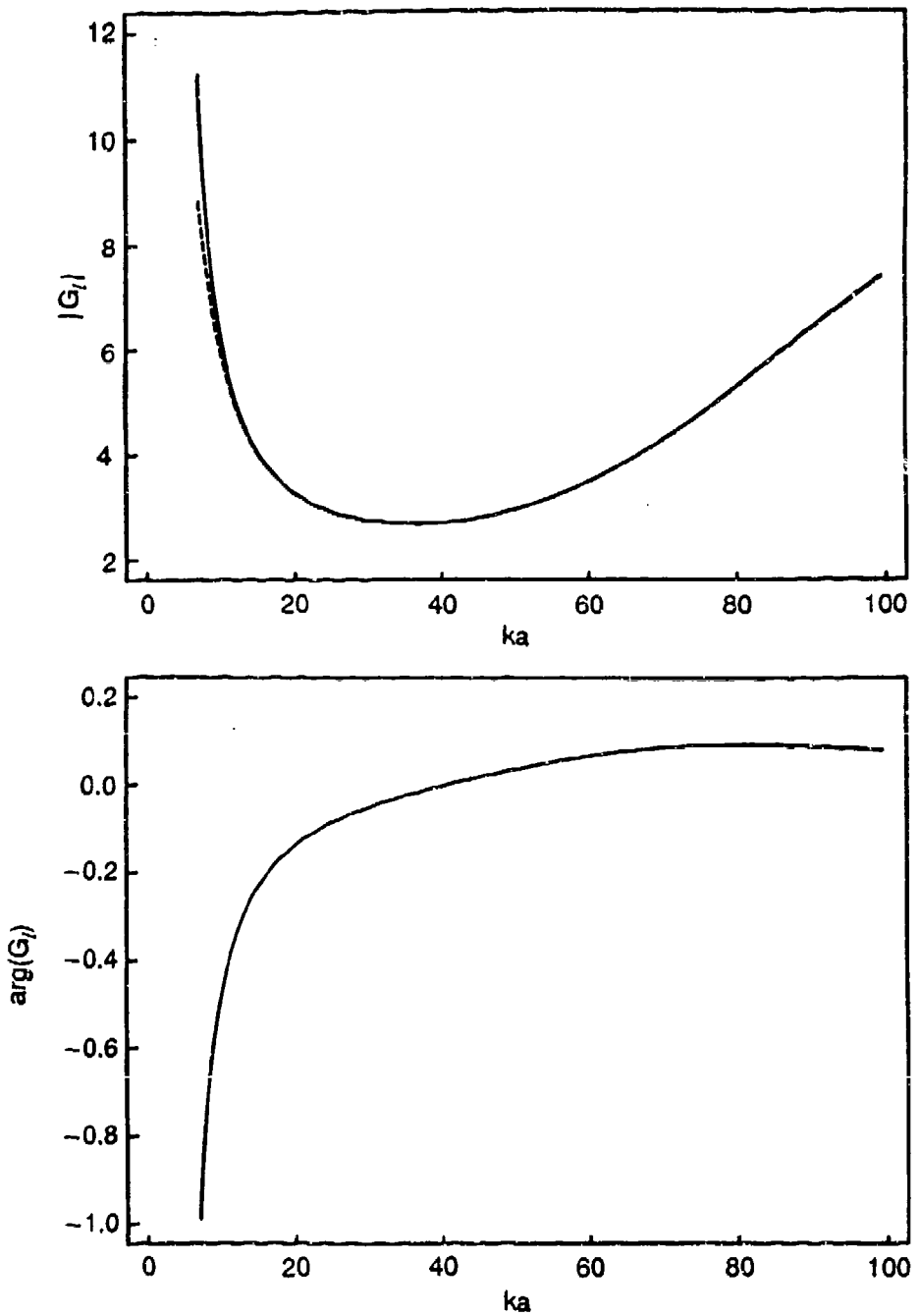

Fig. 1 In (a) the exact $|G_l|$ from Eq. (1) for $l = a_0$ is the solid line and the approximation from Eq. (8) is the dashed line. The agreement between Eqs. (1) and (8) is excellent. The phase of the exact G_l is shown in (b) and verifies the assumption $arg(G_l) \approx 0$. The material of the shell is 440c stainless steel with radii ratio $b/a = 0.838$.

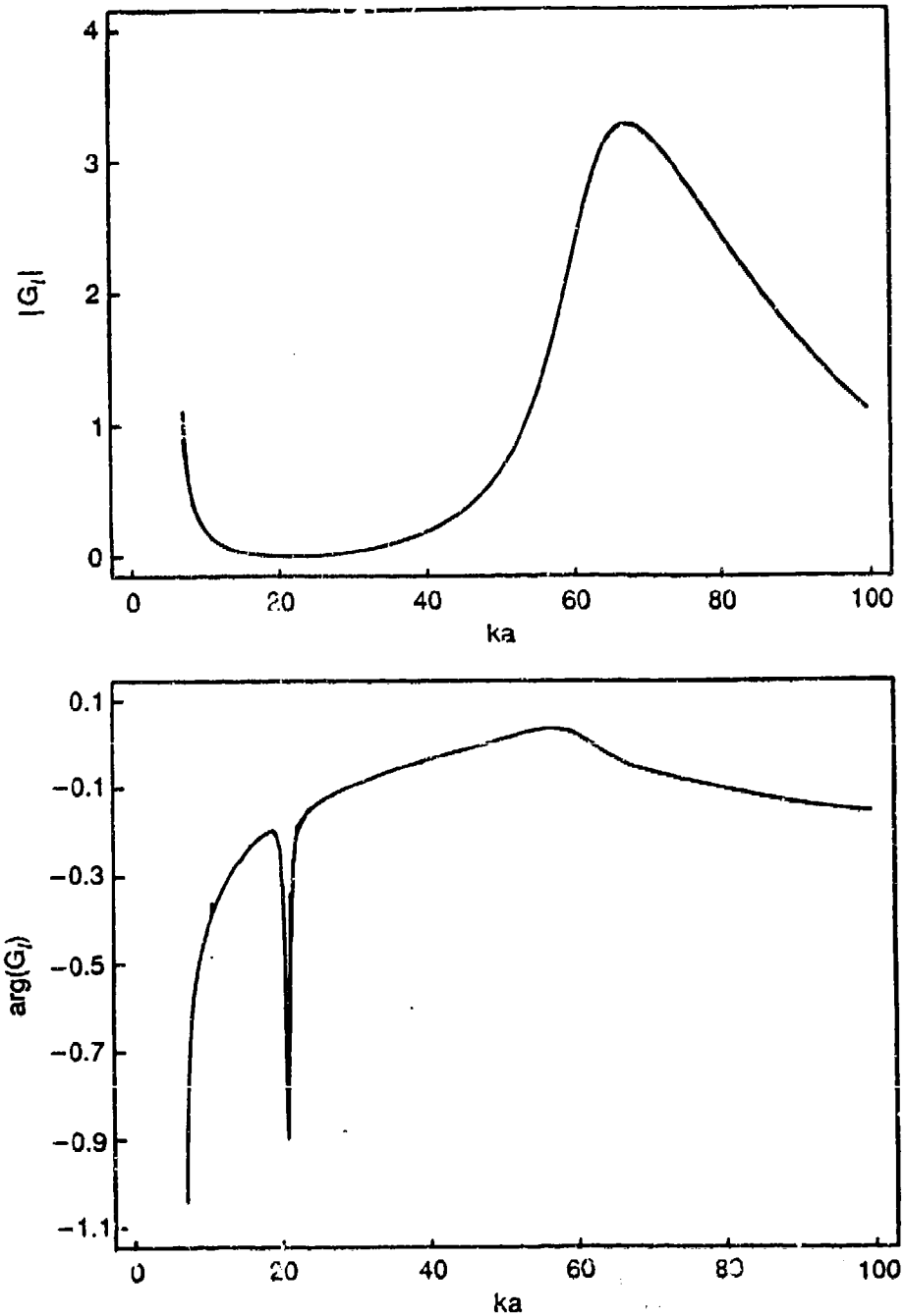

Fig. 2 In (a) the exact $|G_l|$ from Eq. (1) for $l = s_0$ is the solid line and the approximation from Eq. (8) is the dashed line. The agreement between Eqs. (1) and (8) is excellent. The phase of the exact G_l is shown in (b) and verifies the assumption $arg(G_l) \approx 0$. The material of the shell is 440c stainless steel with radii ratio $b/a = 0.838$.

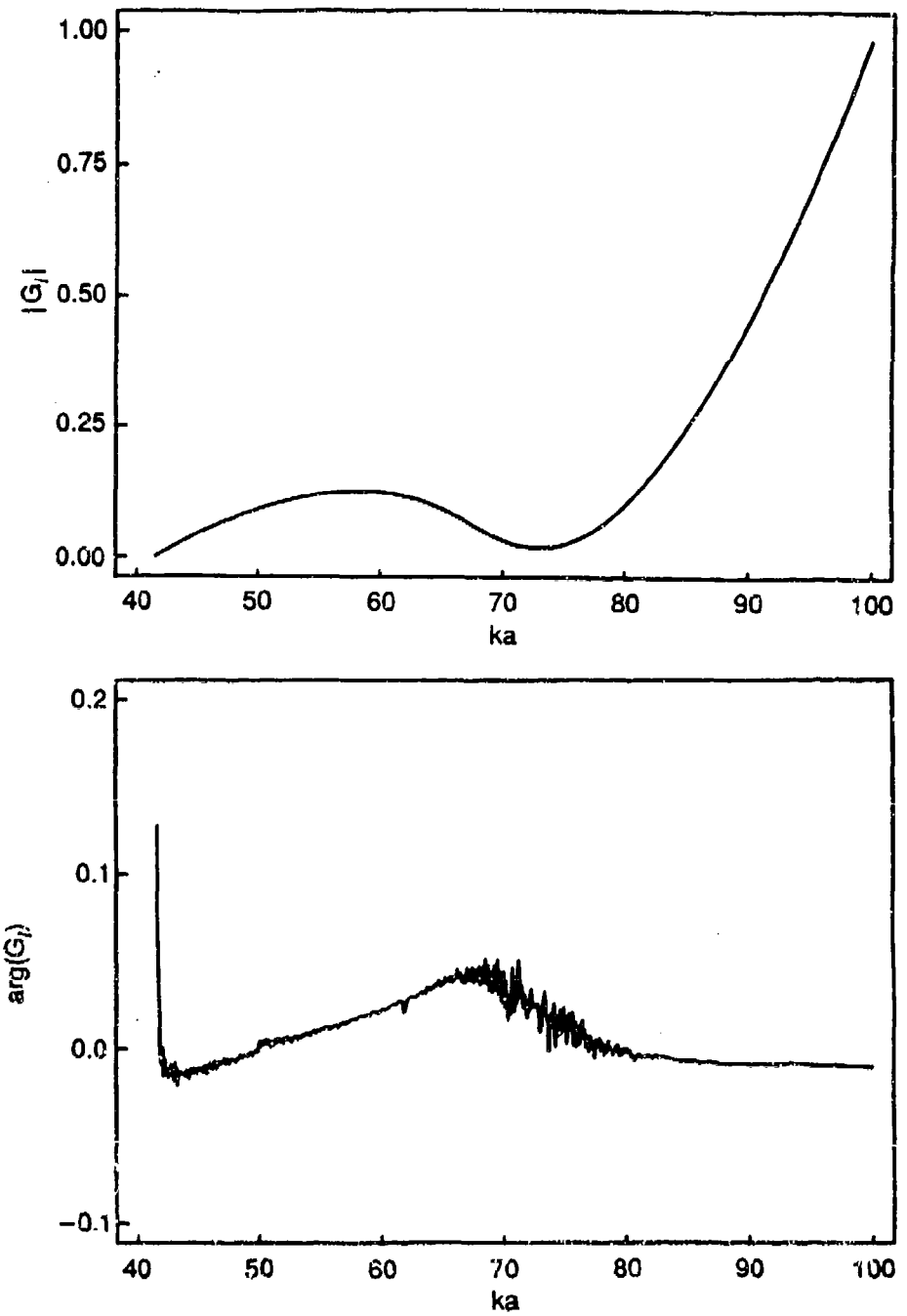

Fig. 3 In (a) the exact $|G_l|$ from Eq. (1) for $t = a_1$ is the solid line and the approximation from Eq. (8) is the dashed line. The agreement between Eqs. (1) and (8) is excellent. The phase of the exact G_l is shown in (b). The fine structure evident in $arg(G_l)$ is attributed to the method of calculation of the derivative in Eq.(1). The material of the shell is 440c stainless steel with radii ratio $b/a = 0.838$.

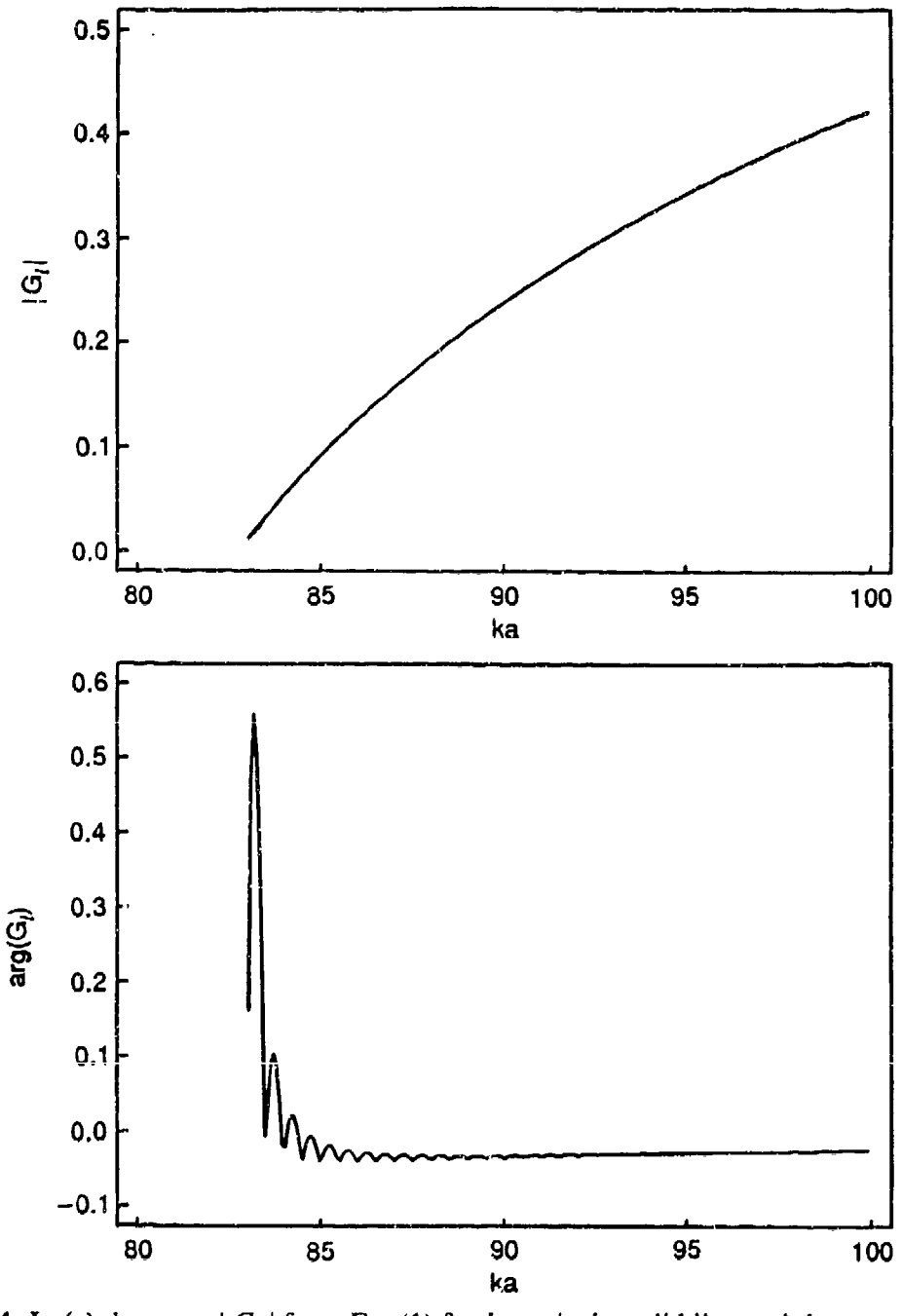

Fig. 4 In (a) the exact $|G_l|$ from Eq. (1) for $l = s_2$ is the solid line and the approximation from Eq. (8) is the dashed line. The agreement between Eqs. (1) and (8) is excellent. The phase of the exact G_l is shown in (b). The structure in $arg(G_l)$ may be associated with the fluid-loading of the shell. The material of the shell is 440c stainless steel with radii ratio b/a = 0.838.

coefficients, $arg(G_l) = tan^{-1}[Im\{G_l\}/Re\{G_l\}]$, for these Lamb waves are presented in Figs. 1b - 4b. These figures indicate that the assumption $arg(G_l) \approx 0$ ($l = a_0, s_0, a_1$, and s_2) is acceptable for the ray synthesis calculations. The apparent deviation in Figs. 1b and 2b from $arg(G_l) \approx 0$ ($l = a_0, s_0$) for $x < 20$ might be anticipated since the Watson transformation is an asymptotic analysis. The effects of the fluid loading of the shell are a plausible cause for the structure evident in $arg(G_l)$, $l = s_2$, since near a cutoff frequency the fluid loading may significantly affect the behavior of the leaky Lamb wave.[12] The rapid variation in $arg(G_l)$, $l = a_1$, is attributed to the method used in computing the derivative of $\mathcal{D}^+$ with respect to ν. However, inspection of the ray synthesis of the form function for backscattering in chapter 4 and the total scattering cross section in chapter 2 demonstrates the usefulness of Eq. (8) with $arg(G_l) = 0$.

The s_1 leaky Lamb wave contribution to backscattering demonstrates behavior that merits a more detailed discussion. Figure 5 displays $|G_l|$ calculated using Eqs. (1) and (8). In Fig. 5, the dashed line is the approximation and the solid curve is the exact $|G_l|$. Inspection of Fig. 5 indicates that Eq. (8) is an excellent approximation for $|G_l|$ when $x > 72$, but it appears to diverge from the exact coupling coefficient for $x \leq 72$. The resolution in the region of the divergence is enhanced in Fig. 5b to give greater detail of the maximum in the exact $|G_l|$. Furthermore, the phase of the exact G_l in Fig. 6 supports the assumption $arg(G_l) \approx 0$ for $x > 72$, but $arg(G_l)$ appears to have a $-\pi/2$ phase shift in the vicinity of $x = 72$. The apparent divergence of Eq. (8) from the exact $|G_l|$ and the $-\pi/2$ phase shift are related to the negative group velocity of the s_1 leaky Lamb wave. In Appendices A and C of chapter 4, this leaky Lamb wave is shown to have a negative group velocity for $x < 72$. Hence, the approximation in Eq. (8) for $|G_l|$ with $arg(G_l) = 0$ appears to be applicable for those surface guided elastic wave that have positive group velocity and seems to breakdown when the group velocity becomes negative.

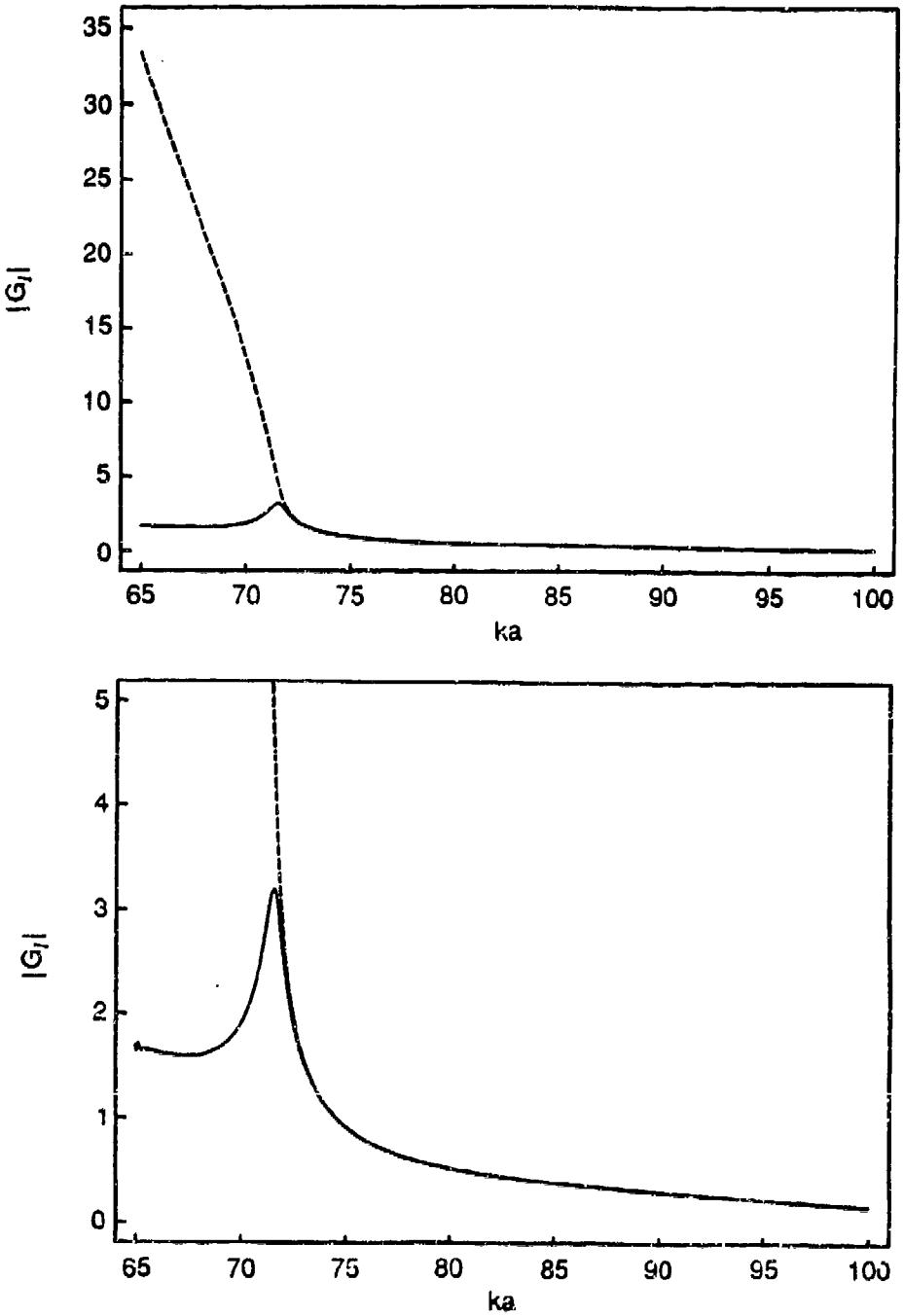

Fig. 5 A comparison of the exact $|G_l|$, $l = s_1$, from Eq. (1) (solid line) and the approximation from Eq. (8) (dashed line). Figure 5a demonstrates the apparent divergence of the approximation from the exact $|G_l|$ while Fig. 5b enhances the resolution near the maximum in $|G_l|$ at $x \approx 72$.

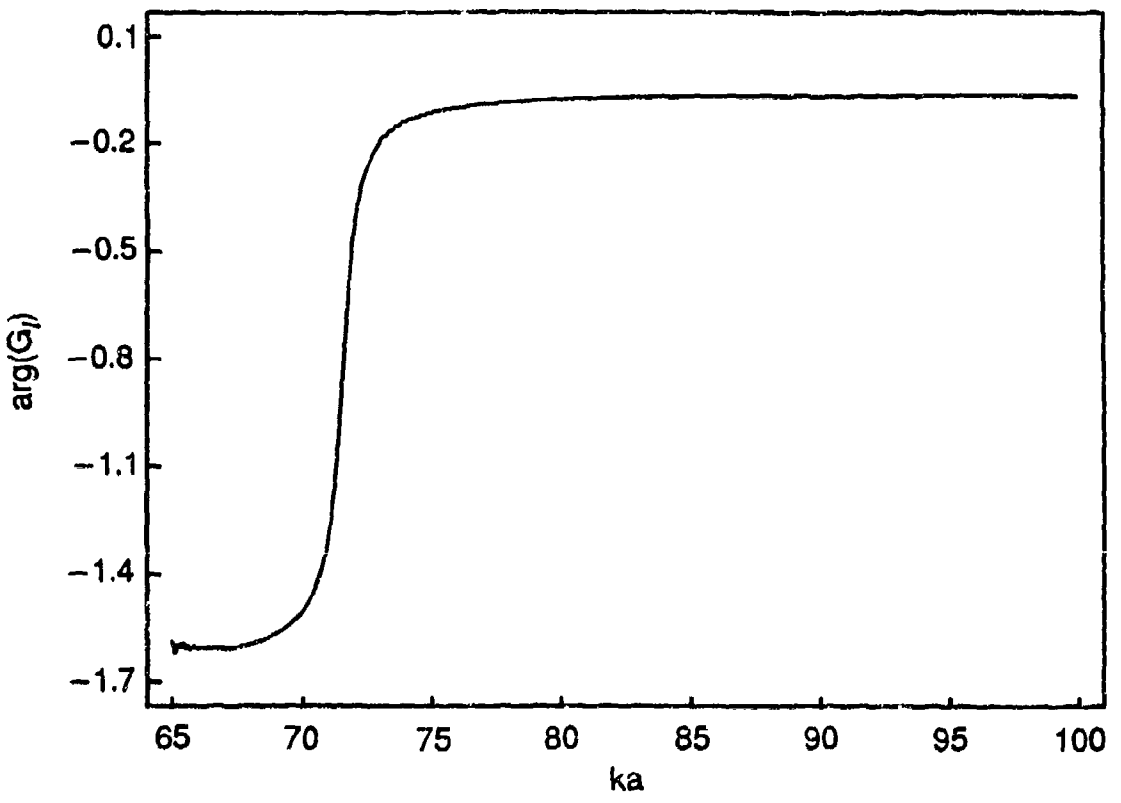

Fig. 6 The phase of the exact G_l, $arg(G_l) = tan^{-1}[Im(G_l)/Re(G_l)]$. When $x > 72$, the assumption $arg(G_l) = 0$ is applicable. But, near $x = 72$ $arg(G_l)$ has a $-\pi/2$ phase shift. This shift is attributed to the negative group velocity of the $l = s_1$ leaky Lamb wave for $x < 72$.

Two important numerical techniques used in the determination of the exact G_l are noted. First, the derivative, $d\mathcal{D}^+/d\nu$, evaluated at the *lth* leaky Lamb wave pole $\nu = \nu_l$ is performed by a contour integration. The theory of residues from complex analysis gives

$$\left(\frac{d\mathcal{D}_\nu^+(x)}{d\nu}\right)_{\nu=\nu_l} = \frac{1}{2\pi i}\oint_C \frac{\mathcal{D}_\nu^+(x)}{(\nu-\nu_l)^2}\,d\nu, \tag{10}$$

where $\mathcal{D}^+$ is assumed analytic everywhere within and on the contour C and ν_l is contained within C. For the numerical algorithm implemented, C is chosen so as to isolate the residue of the pole at $\nu = \nu_l$ from any other possible residue contribution. While Eq. (10) appears to be a good method for the evaluation of $d\mathcal{D}^+/d\nu$ at $\nu = \nu_l$, there seems to be regions where numerical round-off may corrupt the result from Eq. (10). To minimize this type of possible numerical error, a three-point sliding average was implemented on $|\,G_l\,|$ and $arg(G_l)$. This sliding average tends to smooth any fluctuations in $|\,G_l\,|$ or $arg(G_l)$ introduced from implementation of Eq. (10).

B. Significance of the group velocity and its sign

To better understand the breakdown of Eq. (8), it is first necessary to review the relationship between the group and phase velocities and the spacing between adjacent resonances. The group velocity for the *lth* leaky Lamb wave c_{gl} is defined by $c_{gl} = d\omega/dk_l$ where ω is the angular frequency and k_l is the wavenumber of the Lamb wave propagating on the shell. The phase velocity of the *lth* leaky Lamb wave is $c_l = \omega/k_l$ and the phase velocity of the incident wave is $c = \omega/k$. The group and phase velocities for the *lth* leaky Lamb wave are related by

$$c_{gl} = c_l\{1 - [1 - (c_l/x)(dc_l/dx)^{-1}]^{-1}\}. \tag{11}$$

It is generally accepted that for a weakly dispersive surface guided elastic wave the spacing between adjacent resonance peaks is $\Delta x_{res} \approx c_{gl}/c$. If the leaky Lamb wave propagates without dispersion, then Eq. (11) reduces to the expected result $c_{gl} = c_l$.

The simple relationship $\Delta x_{res} \approx c_{gl}/c$ can be established from the Fabry-Perot form of a leaky Lamb wave contribution to backscattering. If $x = x_m$, $(m = 1,2)$, correspond to different resonances in f_l, then x_1 and x_2 are adjacent resonance if the phase $\Phi(x) = 2\pi\alpha_l(x)$ in the denominator of Eq. (4) changes by 2π as $x = x_1$ is increased to x_2. The condition for adjacent resonances becomes $[\alpha_l(x_2) - \alpha_l(x_1)] = 1$ where $\Delta x_{res} = x_2 - x_1$. A two term Taylor series expansion of $\alpha_l(x_2)$ about $x = x_1$ gives the expression $\Delta x_{res} \approx [\alpha'_l(x = x_1)]^{-1}$ where terms of order $(\Delta x_{res})^2$ and higher can be neglected for weakly dispersive leaky Lamb waves. The function $\alpha'_l(x)$ can be evaluated from Eqs. (2c) and (11). Differentiation of Eq. (2c) gives $\alpha'_l(x) = (c/c_l)[1 - (x/c_l)(dc_l/dx)]$. From Eq. (11), the second term in $\alpha'_l(x)$ becomes $(x/c_l)(dc_l/dx) = (c_{gl} - c_l)/c_l$. Combining these results gives the simple expressions

$$\alpha'_l(x) = c/c_{gl}\,, \qquad \Delta x_{res} \approx c_{gl}/c. \tag{12a,b}$$

Equation (12b) has been verified in Appendix A of chapter 4 for regions of x where the a_0 and s_0 leaky Lamb waves demonstrate weak dispersion.

The relevance of Eq. (12a) to the s_1 leaky Lamb wave contribution to backscattering and the breakdown of Eq. (8) for the coupling coefficient may be found by examining $\alpha_l(x)$. The instantaneous slope of $\alpha_l(x)$ is $\alpha'_l(x)$ which implies that the group velocity of a leaky Lamb wave can be directly obtained from the Watson transformation without the use of Eq. (11). Figures 7a and 7b are $\alpha_l(x)$ and $\beta_l(x)$ determined by a Watson methodology. Figure 7a shows that $\alpha'_l(x)$ is positive for $x > 72$, goes through zero near $x = 72$, and is negative for $x < 72$. As x approaches $x \approx 72$ from above c_{gl}/c divergences to $+\infty$ and

divergences to $-\infty$ as x approaches 72 from below. Hence, Fig. 7a confirms the group velocity calculation displayed in Fig. A.3 of chapter 4 for the s_1 leaky Lamb wave. The radiation damping parameter β_l, $l = s_1$ is shown in Fig. 7b for completeness. Inspection of Fig. 7b and Eq. (4) demonstrates that for $x < 72$ contribution from circumnavigation of the s_1 Lamb wave about shell is negligible. The locus of s_1 leaky Lamb wave roots $\nu_l(x)$, $l = s_1$ is displayed in Fig. 8.

Finally, the width of an isolated resonances is related to Γ_{nl} in Eq. (3). With the assumed coincidence of the poles of $f_{nl}(x)$ and $f_l(x)$ in the complex x-plane Γ_{nl} becomes γ_{nl} as noted below Eq. (6). Inspection of Eq. (6b) suggests, however, that γ_{nl} would go to zero near $x = 72$ as $\alpha'_l(x)$ vanishes. Furthermore, since $\alpha'_l(x)$ becomes negative for $x < 72$, then γ_{nl} would be negative for any resonances in this region. That is, *the width of leaky Lamb wave resonances would appear to be negative for a leaky Lamb wave with negative group velocity if the resonance is assumed isolated having the form of Eq. (3).* When c_{gl}/c is negative, however, the argument breaks down since the resonance spacing from Eq. (12b) is predicted to be negative. It would appear that the derivation that $\gamma_{nl} < 0$ also breaks down. Finally, when $c_{gl}/c < 0$, it may also be argued that the combined result of Eqs. (4) and (8) with $arg(G_l) = 0$ is incomplete.

One caveat is noted. From Fig. (7b), it is observed that the s_1 leaky Lamb wave has a rather large radiation damping parameter. In Ref. 2, the assumption $2\pi\beta_l << 1$ was used in deriving Eq. (8). Subsequently, this condition was determined to be too restrictive and Eq. (8) has been shown to give fairly good agreement with the exact $|G_l|$ even when $2\pi\beta_l << 1$ is not satisfied.[2] [Whether the group velocity is positive or negative for the relevant surface elastic waves in those comparison was not pursued.] Furthermore, the $exp[-2(\pi - \theta_l)\beta_l]$ factor in Eq. (4) indicates that the s_1 leaky Lamb wave contribution in

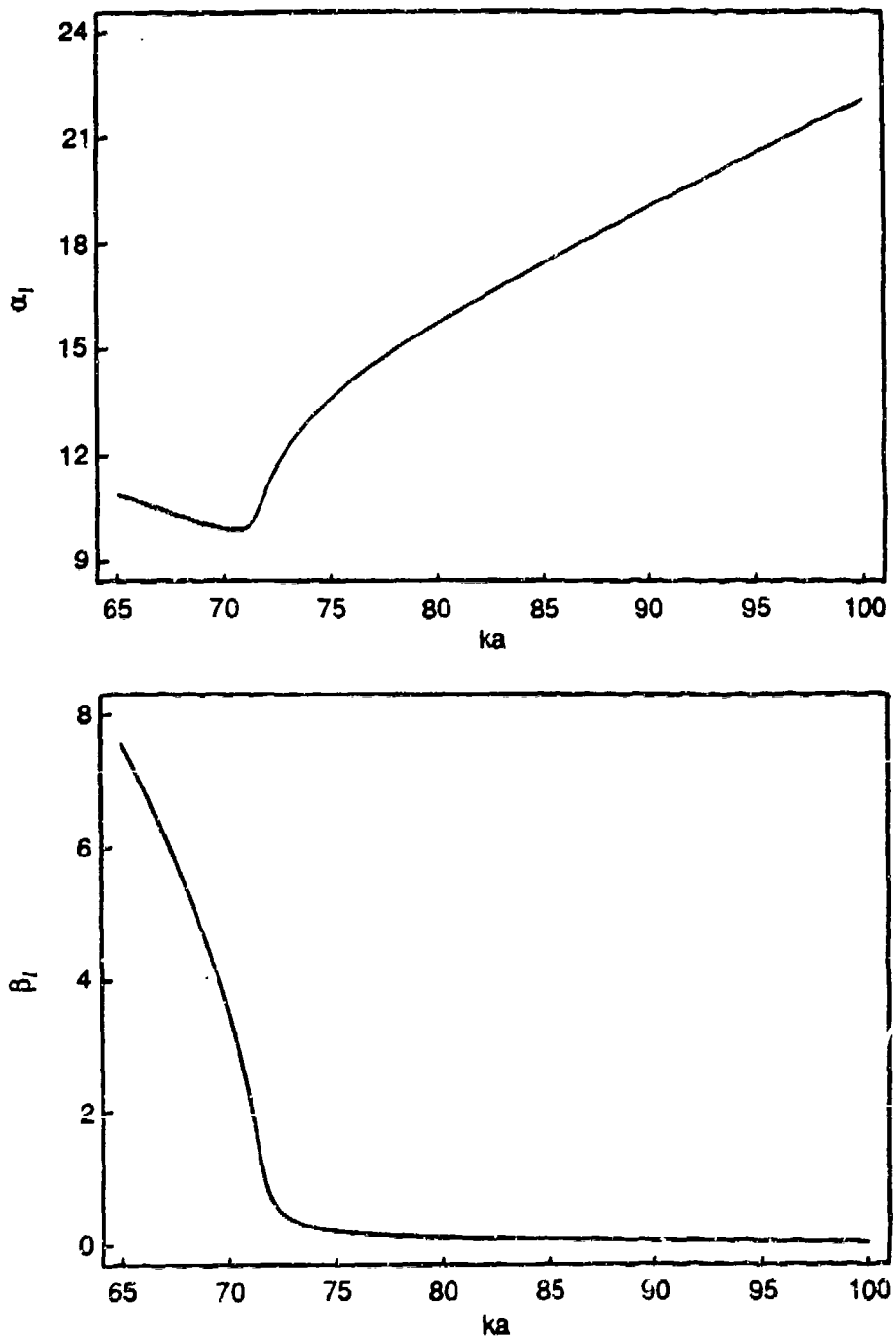

Fig. 7 The $l = s_1$ leaky Lamb wave parameters: (a) $\alpha_l(x)$ and (b) $\beta_l(x)$. The instantaneous slope of $\alpha_l(x)$ is related to the normalized group velocity through Eq.(11). When the group velocity becomes negative, the derivation leading to Eq. (8) may breakdown. From (b), the radiation damping of the s_1 leaky Lamb wave is observed to be extremely large.

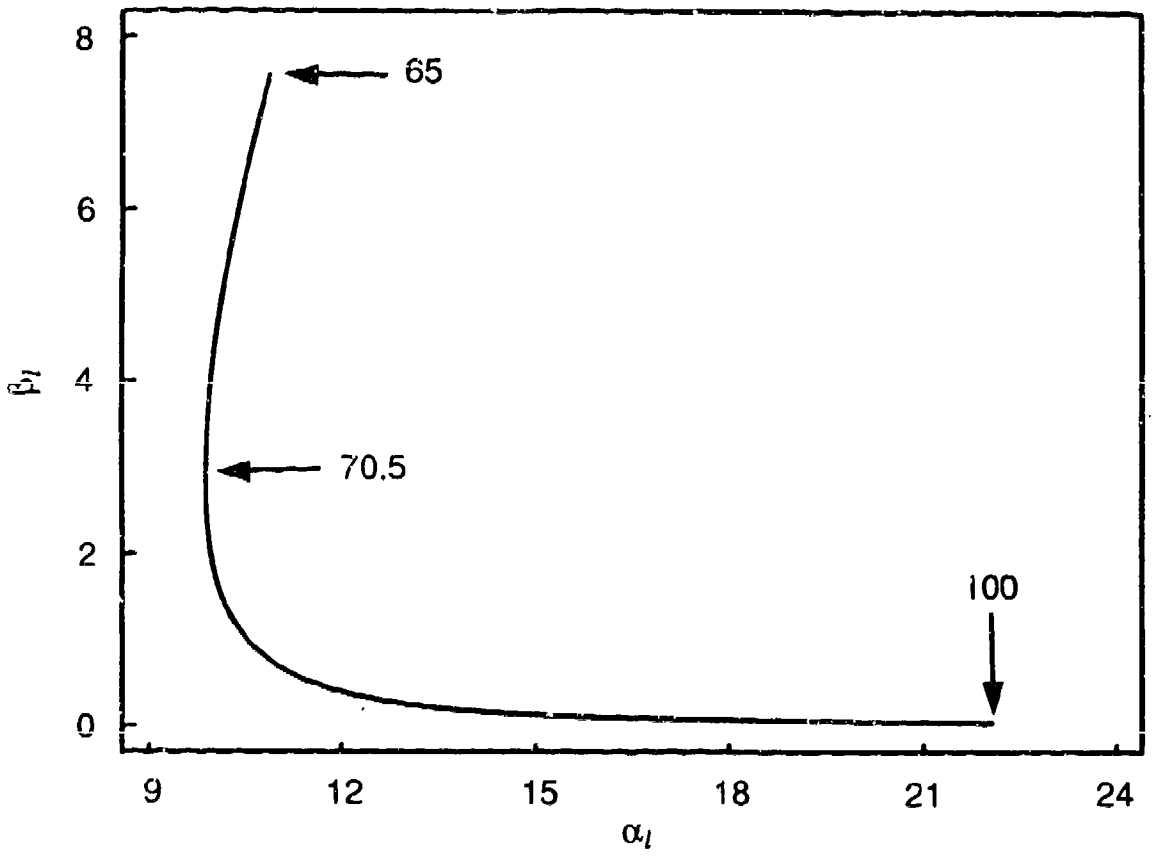

Fig. 8 The locus of the s_1 leaky Lamb wave roots from the Watson methodology. The *ka* for the upper and lower roots $\nu_l(x)$ are indicated in the figure. The *ka* of the inflection point in $\nu_l(x)$ is also indicated.

the ray synthesis for the ray path assumed in Eq. (4) is negligible for $x < 72$ since β_l is large.

Finally, the present level of ray synthesis appears to be incomplete. The current ray model includes contributions from a specular reflection and leaky Lamb waves which circumnavigate the elastic spherical shell. The generalized specular reflection contains the ordinary specular ray and rays associated with repeated internal reflections from the inner surface of the shell at $r = b$ (see Sec. 2 of Chapter 4). The inclusion of these internal rays seems to correctly describe the manifestation of longitudinal resonances in the form function for backscattering. The ray synthesis of the *lth* leaky Lamb wave contribution giving a Fabry-Perot form accounts for the propagation of the leaky Lamb wave around the shell, but negiects the possibility of a direct ray contribution. A direct contribution from a leaky Lamb wave is briefly discussed in Sec. 4 of Chapter 4 and is illustrated by ray $B''A''$ in Fig. 1 of Chapter 4 (where $\theta_l \rightarrow 0$). The results of a Sommerfeld-Watson transformation of the form function for backscattering from an elastic sphere,[1] which are extended to the shell, are based on the assumption $\alpha_l >> \beta_l$. This assumption may omit direct ray contributions associated with a leaky Lamb wave when $\beta_l \sim \alpha_l$. Furthermore, the negative group velocity may be in some way associated with of large radiation damping.[8] It is noteworthy that the use of the revised coupling coefficient shown in Figs. 5 and 6 does not remove the anomaly near $x = 71$ in Fig. 7 of Chapter 4. That is because $|f_l|$ is small since β_l is large ($\beta_l \geq 2$) near this anomaly.

References

1. K. L. Williams and P. L. Marston, "Backscattering from an elastic sphere:Sommerfeld-Watson transformation and experimental confirmation," J. Acoust.Soc. Am. 78, 1093 - 1102 (1985).
2. P. L. Marston, "GTD for backscattering from elastic spheres and cylinders in water and the coupling of surface elastic waves with the acoustic field, " J. Acoust. Soc.Am. 83, 25 - 37 (1988).
3. S. G. Kargl and P. L. Marston, "Observations and modeling of the backscattering of short tone bursts from a spherical shell: Lamb wave echoes, glory, and axial reverberations," J. Acoust. Soc. Am. 85, 1014 - 1028 (1989).
4. S. G. Kargl and P. L. Marston, "Ray synthesis of Lamb wave contributions to the total scattering cross section for an elastic spherical shell," accepted for publication, J. Acoust. Soc. Am.
5. L. Flax, L. R. Dragonette, and H. Uberall, "Theory of elastic resonance excitation by sound scattering," J. Acoust. Soc. Am. 63, 723 - 731 (1978).
6. L. Flax, G. C. Gaunaurd, and H. Uberall, "Theory of resonance scattering," in *Physical Acoustics*, edited by W. P. Mason and R. N. Thurston (Academic, New York, 1981), Vol. 15, pp. 191 - 294.
7. K. L. Williams and P. L. Marston, "Synthesis of backscattering from an elastic sphere using the Sommerfeld-Watson transformation and giving a Fabry-Perot analysis of resonances," J. Acoust. Soc. Am. 79, 1702 - 1708 (1986).
8. P. L. Marston, S. G. Kargl, and K. L. Williams, "Rayleigh, Lamb, and Whispering Gallery wave contributions to backscattering from smooth elastic objects in water described by a generalization of GTD," in *Elastic Wave Propagation and Ultrasonic Nondestructive Evaluation*, edited by S. K. Datta, J. D.

Achenback, and Y. S. Rajapakse [Elsevier Science, Amsterdam 1990] pp. 211 - 216.

9. P. L. Marston and K. L. Williams, "GTD for backscattering from elastic objects in water: Phase of the coupling coefficient and a simplified synthesis of the form function," J. Acoust. Soc. Am. Suppl. 83, 94 (1988).

10. J. M. Ho and L. B. Felsen, "New exact and ray-acoustic traveling wave formulations for source-excited fluid-loaded thin elastic spherical shells," accepted for publication in J. Acoust. Soc. Am.

11. L. B. Felsen and J. M. Ho, "Rigorous spectral theory for azimuthally dependent source-excited fields in a fluid in the presence of a thin elastic spherical shell: Formulation and high-frequency asymptotics," J. Acoust. Soc. Am. Suppl. 1 87, S53 (1990); J. M. Ho and L. B. Felsen, "Rigorous spectral theory for azimuthally dependent source-excited fields in a fluid in the presence of a thin elastic spherical shell: Ray parameterization and high-frequency results," J. Acoust. Soc. Am. Suppl. 1 87, S53 (1990).

12. S. G. Kargl and P. L. Marston, "Ray synthesis of the form function for backscattering from an elastic spherical shell: Leaky Lamb waves and longitudinal resonances," submitted to J. Acoust. Soc. Am.

Appendix II

Leaky Lamb wave parameters

The contents of this appendix are five tables containing the parameters used in the ray synthesis calculations presented in Chapters 2 and 4 and Appendix I. The method employed in determining these parameters ' 'line in Appendix A of Chapter 2 or 4. The format of each table is four columns of numbers for the dimensionless size parameter ka, normalized phase velocity of the leaky Lamb wave c_l/c, the radiation damping parameter β_l, and $\alpha_l = Re(\nu_l)$ from the Watson transform methodology. These tables are for a 440c stainless steel shell with inner-to-outer radii ratio $b/a = 0.838$. The material parameters for 440c stainless steel are given in Sec. 5 of chapter 2.

The computer code used in determining ν_l for the *lth* leaky Lamb wave at a fixed x is essentially the same as the FORTRAN program ZNU implemented by Williams[1] for solid elastic spheres. This program is based on the winding number theory from complex analysis which is discussed by Williams. Two modifications were made to ZNU for the computation of ν_l for the evacuated spherical shell. First, the external function $F(\nu)$ is the determinant $D_n(x)$ in the denominator of the partial-wave coefficient where the integer index n is replaced everywhere by complex ν. For spheres, $D_\nu(x)$ is a 3×3 determinant and for evacuated shells $D_\nu(x)$ becomes a 5×5 determinant. The elements of $D_n(x)$ for a shell are listed in Appendix A of Ref. 2. Second, the routine OLVER that is employed for the computation of Bessel and Neumann functions of real argument and complex order has been slightly rewritten. Previously, this routine returned single precision values, but since all other computations in ZNU (and in OLVER) are double precision OLVER was modified to return double precision values. One other modification to OLVER consisted of the rewriting of portions of the code that are in FORTRAN IV in standard FORTRAN 77.

Once a root ν_l at a fixed x for the *lth* leaky Lamb wave was determined, it was inserted into a second computer code that tracked the locus $\nu_l(x)$. A discussion of the necessary mathematical theory is given in Appendix B of Ref. 2. The algorithm assumed that $\nu_l(x)$ is a well-behaved function of x (see Fig. A1 of Chapter 2) and that $\nu_l(x)$ was approximately the value of ν_l at $x+\Delta x$ where $\Delta x << 1$. A square contour was centered about $\nu_l(x)$, x was increased (or decreased) by Δx and then the winding number was determined from numerical integration of Eq. (B1) in Ref. 2. If the winding number is equal to one (an isolated zero, $\nu = \nu_l$, of $D_\nu(x)$ is enclosed within the contour), then Eq. (B2) from Ref. 2 was integrated about the same contour. This recursive procedure was implemented for the determination of the parameters given in Tables II.1 - II.5.

References

1. K. L. Williams, Ph. D. dissertation, Washington State University (1985); available from the Defense Technical Information Center (Cameron Station, Alexandria, VA), Accession number AD-A158884.
2. S. G. Kargl and P. L. Marston, "Observations and modeling of the backscattering of short tone bursts from a spherical shell: Lamb wave echoes, glory, and axial reverberation," J. Acoust. Soc. Am. 85, 1014 - 1028 (1989).

Table II.1 The a_0 leaky Lamb wave parameters

ka	c_l/c	α_l	β_l	ka	c_l/c	α_l	β_l
7.00	1.084072	5.057134	0.383446	8.00	1.145666	6.482839	0.349988
9.00	1.199730	7.001686	0.319891	10.0	1.248506	7.509575	0.295577
11.0	1.293156	8.006322	0.276207	12.0	1.334342	8.493196	0.260708
13.0	1.372558	8.971365	0.248181	14.0	1.408150	9.442120	0.237946
15.0	1.441409	9.906483	0.229505	16.0	1.472554	10.365476	0.222498
17.0	1.501791	10.81982	0.216644	18.0	1.529290	11.27017	0.211732
19.0	1.555182	11.71722	0.207613	20.0	1.579610	12.16135	0.204157
21.0	1.602686	12.60301	0.201267	22.0	1.624505	13.04259	0.198866
23.0	1.645162	13.48039	0.196897	24.0	1.664737	13.91669	0.195304
25.0	1.683309	14.35170	0.194052	26.0	1.700941	14.78566	0.193103
27.0	1.717691	15.21878	0.192434	28.0	1.733624	15.65114	0.192022
29.0	1.748780	16.08299	0.191845	30.0	1.763213	16.51439	0.191896
31.0	1.776967	16.94545	0.192153	32.0	1.790076	17.37634	0.192609
33.0	1.802577	17.80712	0.193257	34.0	1.814507	18.23787	0.194087
35.0	1.825891	18.66873	0.195096	36.0	1.836764	19.09969	0.196279
37.0	1.847151	19.53084	0.197632	38.0	1.857077	19.96226	0.199153
39.0	1.866561	20.39404	0.200840	40.0	1.875630	20.82616	0.202694
41.0	1.884300	21.25874	0.204714	42.0	1.892595	21.69176	0.206898
43.0	1.900525	22.12533	0.209249	44.0	1.908108	22.55949	0.211769
45.0	1.915362	22.99425	0.214458	46.0	1.922300	23.42967	0.217318
47.0	1.928935	23.86577	0.220342	48.0	1.935281	24.30260	0.223548
49.0	1.941352	24.74014	0.226932	50.0	1.947150	25.17855	0.230503
51.0	1.952696	25.61774	0.234247	52.0	1.957989	26.05786	0.238197

53.0	1.963046	26.49886	0.242336	54.0	1.967873	26.94079	0.246672
55.0	1.972478	27.38371	0.251207	56.0	1.976872	27.82759	0.255943
57.0	1.981057	28.27252	0.260883	58.0	1.985041	28.71854	0.266031
59.0	1.988834	29.16563	0.271386	60.0	1.992438	29.61386	0.276951
61.0	1.995861	30.06326	0.282730	62.0	1.999109	30.51382	0.288721
63.0	2.002189	30.96557	0.294924	64.0	2.005101	31.41859	0.301338
65.0	2.007853	31.87290	0.307964	66.0	2.010449	32.32848	0.314796
67.0	2.012896	32.78538	0.321832	68.0	2.015195	33.24363	0.329068
69.0	2.017353	33.70323	0.336501	70.0	2.019376	34.16418	0.344117
71.0	2.021263	34.62655	0.351917	72.0	2.023021	35.09033	0.359887
73.0	2.024654	35.55553	0.368019	74.0	2.026168	36.02214	0.376265
75.0	2.027564	36.49020	0.384720	76.0	2.028849	36.95966	0.393266
77.0	2.030026	37.43055	0.401925	78.0	2.031099	37.90285	0.410681
79.0	2.032071	38.37660	0.419523	80.0	2.032949	38.85170	0.428427
81.0	2.033733	39.32823	0.437391	82.0	2.034432	39.80610	0.446391
83.0	2.035046	40.28531	0.455415	84.0	2.035585	40.76577	0.464444
85.0	2.036046	41.24758	0.473471	86.0	2.036436	41.73064	0.482477
87.0	2.036762	42.21485	0.491445	88.0	2.037024	42.70028	0.500374
89.0	2.037226	43.18685	0.509245	90.0	2.037374	43.67450	0.518053
91.0	2.037473	44.16318	0.526782	92.0	2.037521	44.65290	0.535432
93.0	2.037526	45.14359	0.543993	94.0	2.037491	45.63517	0.552456
95.0	2.037417	46.12766	0.560822	96.0	2.037309	46.62099	0.569089
97.0	2.037169	47.11510	0.577247	98.0	2.037001	47.60994	0.585298
99.0	2.036806	48.10551	0.593243	100.0	2.036586	48.60179	0.601084

Table II.2 The s_0 leaky Lamb wave parameters

ka	c_l/c	α_l	β_l	*ka*	c_l/c	α_l	β_l
7.0	5.672502	0.734023	0.257460	8.0	4.768751	1.177588	9.36004e-02
9.0	4.411582	1.540085	5.16725e-02	10.0	4.235214	1.861156	3.24039e-02
11.0	4.131961	2.162174	2.14516e-02	12.0	4.065046	2.451996	1.45435e-02
13.0	4.018514	2.735027	9.91413e-03	14.0	3.984383	3.013719	6.69481e-03
15.0	3.958239	3.289564	4.40952e-03	16.0	3.937482	3.563510	2.77951e-03
17.0	3.920461	3.836225	1.62705e-03	18.0	3.906104	4.108173	8.40220e-04
19.0	3.893684	4.379697	3.42250e-04	20.0	3.882687	4.651071	7.97300e-05
21.0	3.872742	4.922514	1.59100e-05	22.0	3.863574	5.194210	1.24970e-04
23.0	3.854973	5.466319	3.89240e-04	24.0	3.846779	5.738986	7.96640e-04
25.0	3.838863	6.012345	1.33805e-03	26.0	3.831120	6.286527	2.01034e-03
27.0	3.823465	6.561658	2.81140e-03	28.0	3.815824	6.837864	3.74218e-03
29.0	3.808135	7.115277	4.80525e-03	30.0	3.800339	7.394032	6.00586e-03
31.0	3.792385	7.674275	7.35021e-03	32.0	3.784225	7.956158	8.84729e-03
33.0	3.775811	8.239845	1.05080e-02	34.0	3.767098	8.525516	1.23452e-02
35.0	3.758041	8.813362	1.43745e-02	36.0	3.748588	9.103615	1.66137e-02
37.0	3.738693	9.396507	1.90834e-02	38.0	3.728302	9.692308	2.18088e-02
39.0	3.717362	9.991310	2.48179e-02	40.0	3.705806	10.293874	2.81443e-02
41.0	3.693569	10.60038	3.18271e-02	42.0	3.680577	10.91125	3.59108e-02
43.0	3.666747	11.22702	4.04499e-02	44.0	3.651984	11.54825	4.55070e-02
45.0	3.636183	11.87561	5.11561e-02	46.0	3.619230	12.20989	5.74824e-02
47.0	3.600981	12.55200	6.45916e-02	48.0	3.581286	12.90301	7.26029e-02
49.0	3.559972	13.26416	8.16586e-02	50.0	3.536840	13.63691	9.19230e-02
51.0	3.511670	14.02301	0.103584	52.0	3.484216	14.42445	0.116846

53.0	3.454221	14.84355	0.131937	54.0	3.421392	15.28305	0.149076
55.0	3.385458	15.74595	0.168431	56.0	3.346179	16.23551	0.190073
57.0	3.303382	16.75504	0.213881	58.0	3.257042	17.30757	0.239423
59.0	3.207344	17.89528	0.265850	60.0	3.154775	18.51879	0.291861
61.0	3.100104	19.17676	0.315840	62.0	3.044410	19.86520	0.336147
63.0	2.988909	20.57793	0.351540	64.0	2.934767	21.30753	0.361481
65.0	2.882956	22.04630	0.366147	66.0	2.834155	22.78737	0.366245
67.0	2.788750	23.52510	0.362730	68.0	2.746857	24.25557	0.356537
69.0	2.708440	24.97592	0.348488	70.0	2.673345	25.68442	0.339227
71.0	2.641345	26.38025	0.329233	72.0	2.612192	27.06305	0.318843
73.0	2.585635	27.73292	0.308290	74.0	2.561434	28.39007	0.297732
75.0	2.539353	29.03508	0.287265	76.0	2.519193	29.66839	0.276955
77.0	2.500764	30.29058	0.266844	78.0	2.483897	30.90227	0.256955
79.0	2.468440	31.50402	0.247305	80.0	2.454265	32.09632	0.237902
81.0	2.441245	32.67980	0.228745	82.0	2.429277	33.25490	0.219838
83.0	2.418263	33.82216	0.211181	84.0	2.408122	34.38195	0.202775
85.0	2.398775	34.93475	0.194616	86.0	2.390154	35.48094	0.186707
87.0	2.382201	36.02085	0.179049	88.0	2.374851	36.55495	0.171636
89.0	2.368062	37.08347	0.164468	90.0	2.361786	37.60675	0.157544
91.0	2.355984	38.12505	0.150864	92.0	2.350614	38.63871	0.144424
93.0	2.345643	39.14797	0.138224	94.0	2.341044	39.65302	0.132259
95.0	2.336785	40.15415	0.126526	96.0	2.332840	40.65155	0.121020
97.0	2.329188	41.14542	0.115739	98.0	2.325805	41.63594	0.110679
99.0	2.322670	42.12336	0.105831	100.0	2.319769	42.60775	0.101101

Table II.3 The a_1 leaky Lamb wave parameters

ka	c_l/c	α_l	β_l	*ka*	c_l/c	α_l	β_l
42.0	28.71326	0.962739	6.85368e-03	43.0	16.73859	2.068915	1.28650e-02
44.0	13.12078	2.853460	1.66242e-02	45.0	11.22238	3.509846	1.94656e-02
46.0	10.014726	4.093236	2.17523e-02	47.0	9.164049	4.628737	2.36409e-02
48.0	8.525793	5.129975	2.52179e-02	49.0	8.025656	5.605420	2.65350e-02
50.0	7.621105	6.060729	2.76363e-02	51.0	7.285776	6.499941	2.85153e-02
52.0	7.002441	6.925982	2.92020e-02	53.0	6.759251	7.341106	2.97018e-02
54.0	6.547668	7.747211	3.00173e-02	55.0	6.361508	8.145749	3.01466e-02
56.0	6.196069	8.537988	3.00869e-02	57.0	6.047717	8.925045	2.98301e-02
58.0	5.913572	9.307947	2.93676e-02	59.0	5.791311	9.687675	2.86860e-02
60.0	5.679032	10.065181	2.77712e-02	61.0	5.575073	10.441560	2.66050e-02
62.0	5.478043	10.81791	2.51732e-02	63.0	5.386673	11.19553	2.34563e-02
64.0	5.299794	11.57594	2.14448e-02	65.0	5.216276	11.96100	1.91423e-02
66.0	5.135036	12.35288	1.65774e-02	67.0	5.055015	12.75416	1.38237e-02
68.0	4.975240	13.16768	1.10206e-02	69.0	4.895021	13.59595	8.38266e-03
70.0	4.814225	14.04024	6.16345e-03	71.0	4.733506	14.49945	4.56789e-03
72.0	4.654351	14.96940	3.66768e-03	73.0	4.578581	15.44380	3.41507e-03
74.0	4.507755	15.91615	3.75392e-03	75.0	4.442661	16.38177	4.63919e-03
76.0	4.383449	16.83795	6.06924e-03	77.0	4.329773	17.28384	8.03265e-03
78.0	4.281067	17.71976	1.05131e-02	79.0	4.236684	18.14666	1.34778e-02
80.0	4.196021	18.56568	1.68916e-02	81.0	4.158494	18.97820	2.07165e-02
82.0	4.123652	19.38538	2.49176e-02	83.0	4.091011	19.78839	2.94636e-02
84.0	4.060276	20.18825	3.43295e-02	85.0	4.031121	20.58595	3.94923e-02
86.0	4.003290	20.98233	4.49350e-02	87.0	3.976569	21.37816	5.06404e-02

88.0	3.950755	21.77423	5.65988e-02	89.0	3.925690	22.17118	6.27988e-02
90.0	3.901231	22.56964	6.92314e-02	91.0	3.877255	22.97021	7.58885e-02
92.0	3.853650	23.37347	8.27627e-02	93.0	3.830321	23.77995	8.98488e-02
94.0	3.807183	24.19017	9.71307e-02	95.0	3.784153	24.60469	0.104604
96.0	3.761164	25.02401	0.112258	97.0	3.738158	25.44861	0.120075
98.0	3.715079	25.87898	0.128037	99.0	3.691880	26.31561	0.136129
100.0	3.668520	26.75895	0.144322				

Table II.4 The s_1 leaky Lamb wave parameters

ka	c_l/c	α_l	β_l	ka	c_l/c	α_l	β_l
65.0	5.709630	10.88427	7.561313	66.0	5.907279	10.67266	6.900472
67.0	6.116464	10.454041	6.191272	68.0	6.327767	10.246286	5.421073
69.0	6.536299	10.056432	4.554775	70.0	6.723228	9.911665	3.525174
71.0	6.797864	9.944458	2.161037	72.0	6.254679	11.01138	0.693661
73.0	5.758624	12.17664	0.355892	74.0	5.498012	12.95941	0.248617
75.0	5.331644	13.56695	0.194698	76.0	5.213098	14.07866	0.162056
77.0	5.122361	14.53213	0.140130	78.0	5.049325	14.94761	0.124354
79.0	4.988286	15.33710	0.112390	80.0	4.935832	15.70801	0.102943
81.0	4.889747	16.06528	9.52149e-02	82.0	4.848589	16.41214	8.87058e-02
83.0	4.811332	16.75094	8.30929e-02	84.0	4.777253	17.08333	7.81386e-02
85.0	4.745802	17.41056	7.36876e-02	86.0	4.716574	17.73357	6.96259e-02
87.0	4.689251	18.05307	6.58708e-02	88.0	4.663565	18.36968	6.23565e-02
89.0	4.639316	18.68386	5.90374e-02	90.0	4.616330	18.99601	5.58780e-02
91.0	4.594466	19.30643	5.28498e-02	92.0	4.573600	19.61545	4.99315e-02
93.0	4.553627	19.92328	4.71072e-02	94.0	4.534459	20.23015	4.43636e-02
95.0	4.516011	20.53626	4.16917e-02	96.0	4.498212	20.84181	3.90837e-02
97.0	4.481001	21.14695	3.65346e-02	98.0	4.464319	21.45184	3.40403e-02
99.0	4.448117	21.75661	3.15994e-02	100.0	4.432345	22.06142	2.92110e-02

Table II.5 The s_2 leaky Lamb wave parameters

ka	c_l/c	α_l	β_l	ka	c_l/c	α_l	β_l
83.0	87.25604	0.451224	4.12350e-02	84.0	43.13697	1.447286	9.23560e-02
85.0	31.51721	2.196939	0.114933	86.0	25.57552	2.862591	0.128295
87.0	21.84771	3.482111	0.137002	88.0	19.25171	4.071021	0.142974
89.0	17.32399	4.637385	0.147201	90.0	15.82827	5.186030	0.150257
91.0	14.62990	5.720140	0.152495	92.0	13.64587	6.241966	0.154148
93.0	12.82195	6.753189	0.155372	94.0	12.12103	7.255115	0.156276
95.0	11.51684	7.748792	0.156940	96.0	10.99016	8.235086	0.157418
97.0	10.526631	8.714724	0.157755	98.0	10.115261	9.188332	0.157981
99.0	9.747499	9.656452	0.158121	100.0	9.416545	10.119606	0.157979

TECHNICAL REPORT DISTRIBUTION, UNCLASSIFIED CONTRACT

Defense Technical Information Center Comeron Station Alexandria, VA 22314	2 one-sided copies
L. E. Hargrove Physics Division, Code 1112 Office of Naval Research 800 N. Quincy Street Arlington, VA 22217-5000	1 two-sided copy
S. G. Kargl Naval Coastal Systems Center Physical Acoustics Branch Code 2120 Panama City, FL 32407	1 two-sided copy